UNIVERSITY OF THE FREE STATE
UNIVERSITEIT VAN DIE VRYSTAAT
YUNIVESITHI YA FREISTATA

UFS
NATURAL AND AGRICULTURAL SCIENCES
CHEMISTRY

EN ROUTE: OPTIMISATION OF REACTION CONDITIONS AND CO-CATALYST EMPLOYMENT TO FAVOUR GRUBBS SECOND GENERATION CATALYST MEDIATED CROSS-METATHESIS

A dissertation submitted in accordance with the requirements for the degree

Doctor of Philosophy in Chemistry

In the

Department of Chemistry

Faculty of Natural and Agricultural Sciences

at the

University of the Free State

by

Olufemi Abiola Odewole

Supervisor: Prof. E. Erasmus

Co-Supervisor: Dr. M.R Swart

November 2024

Dedication

I, Olufemi Abiola Odewole, hereby declare that the content disclosed in this thesis is, under the guidance and direction of Prof. E. Erasmus (supervisor) and Dr M.R. Swart (co-supervisor), my own work, and it has not been previously submitted to/at another University or Faculty. Permission was obtained from the relevant copyright holders to use publication content for this thesis where necessary.

19 November 2024

_____ _____

Olufemi Abiola Odewole Date

Acknowledgements

It is with utmost joy and excitement I give my unreserved appreciation to God, from whom all blessings flow for the gift of life, motivation, and opportunity to undertake and complete this study.

To my exceptional supervisor and academic mentor, Prof. Lizette Erasmus, thank you immensely for your guidance, funding, and empathy throughout the course of this degree. You are simply God's gift to me, and I have learnt excellence, compassion and dedication from you.

To my inspiring Co-supervisor, Dr Marthinus R. Swart, thank you for your words of encouragement, timely assistance, guidance, and training on NMR instruments. You are simply amazing.

To my delectable wife and sons, Olatoun, Richard and Raymond; thank you for your patience, commitment, support, love and prayers. Your companionship has made me a better man.

To my parents, Olusegun and Mosunmola Odewole, and my father-in-law and mother-in-law, Abiodun and Adekemi Oladoyin, thank you for your unconditional love and encouragement to accomplish this feat.

To my siblings, Oludare, Babajide and Anuoluwapo, thank you for believing in me.

To my colleague and friend, Dr. Akpokovo Godfrey Akpomie; thank you for the significant role you played getting me to the University of the Free State.

To my fellow postgraduate students in the Physical Chemistry group, thank you for creating a fun, conducive and healthy environment. You guys are the best.

To the Chemistry Department and the University of the Free State, thank you for providing all the necessary equipment, resources and financial support.

To TETFUND, University of Nigeria, Nigeria; thank you for the study leave and financial support.

Table of Contents

Dedication i
Acknowledgements ii
List of Tables vi
List of Figures viii
List of Schemes xi
Abstract xiii
List of Abbreviations xv
CHAPTER 1 INTRODUCTION 1
1.1 Introduction 1
1.2 Problem Statement 2
1.3 Previous Research 3
1.4 Objective 3
1.5 Chapter Layout 4
References 6
CHAPTER 2 LITERATURE REVIEW 8
2.1 Introduction 8
2.1.1 Overview 8
2.2 Types of Olefin metathesis reactions 10
2.3 Metathesis mechanism 13
2.4 Catalyst for metathesis reactions 14
2.4.1 Schrock catalyst 14
2.5 Grubbs' Catalysts 17
2.6 Additives effects on metathesis reactions 22
2.6.1 Types of additives as co-catalyst 22
2.6.2 Additives to Grubbs' catalysts 22
2.6.2.1 Salts 22
2.6.2.2 Phenols and alcohols 27
2.6.2.3 Phosphines 33
2.6.2.4 Others 36
2.6.3 Additives to Schrock's catalysts 42
2.7 Conclusion 46

References 47
CHAPTER 3 EN ROUTE INVESTIGATION OF REACTION CONDITIONS' INFLUENCE ON CROSS-METATHESIS YIELDS EMPLOYING GRUBBS SECOND GENERATION -*p*-CRESOL CATALYST DERIVATIVE 55
3.1 Abstract 55
3.2 Introduction 56
3.3 Results and Discussion 58
3.4 Materials and methods 66
3.4.1 General 66
3.4.2 ^{1}H NMR Spectroscopy 66
3.4.3 Influence of *p*-cresol equivalent to GII on metathesis reaction between 1 and 2 67
3.4.4 Influence of mole ratio of 1 on the metathesis reaction catalysed by *p*-cresol/GII 67
3.4.5 Monitoring of the metathesis 68
3.5 Conclusion 68
References 70
CHAPTER 4 SPECTROSCOPIC EXPLORATION OF CATALYST DYNAMICS AND ELECTROCHEMICAL PROPERTIES OF GRUBBS SECOND GENERATION IN DIFFERENT SOLVENTS 72
4.1 Abstract 72
4.2 Introduction 73
4.3 Results and Discussion 75
4.4 Experimental section 83
4.5 Conclusion 85
References 86
CHAPTER 5 UNVEILING THE POWER OF ADDITIVES: ENHANCING GRUBBS' CATALYST PERFORMANCE WITH PHENOL DERIVATIVES 88
5.1 Abstract 88
5.2 Introduction 89
5.3 Results and Discussion 91
5.3.1 Experimental section 103
5.4 Conclusion 104
References 106
CHAPTER 6 CRITICAL EVALUATION OF THIS STUDY AND FUTURE WORK 109

6.1 Critical Evaluation of this study 109
6.2 Future Perspective 111
CHAPTER 7 PUBLICATIONS AND CONFERENCE CONTRIBUTIONS 112
7.1 Publications 112
7.1.1 Metathesis reactions: Effect of additives as co-catalysts to Grubbs' or Schrock's catalyst . 112
7.1.2 En route investigation of reaction conditions' influence on cross-metathesis yields employing Grubbs 2nd generation–*p*-cresol catalyst derivative 112
7.1.3 Spectroscopic Exploration of Catalyst Dynamics and Electrochemical Properties of Grubbs Second Generation in Different solvent. 113
7.1.4 Unveiling the power of additives: Enhancing Grubbs' catalyst performance with phenol derivatives 113
7.2 Conferences 114
7.2.1 Oral Presentations 114
7.2.2 Poster Presentations 114
APPENDICES 115
APPENDIX A: SUPPLEMENTARY INFORMATION FOR CHAPTER 3 115
APPENDIX B: SUPPLEMENTARY INFORMATION FOR CHAPTER 4 119
APPENDIX C: SUPPLEMENTARY INFORMATION FOR CHAPTER 5 122

List of Tables

Table 2.1: Conversion and selectivity towards the formation 7-tetradecene after 6 h under different conditions 24
Table 2.2: Optimizing reaction conditions 25
Table 2.3: Comparisons of NaI *vs* CuI as additive in **GII** catalysed olefin cross-metathesis. 26
Table 2.4: The effect of additives on product distribution from the same starting materials 27
Table 2.5: Series of CM reactions catalysed by **GII** with and without an additive (*p*-cresol) 28
Table 2.6: Screening of alcohol additives effect on dienyl isomerization catalysed by **GII** for the reaction displayed in Scheme 2.23, using 0.05 M of the diene in toluene. % Conversion and ^{1}H NMR yield vs mesitylene as an internal standard is reported. 29
Table 2.7: Summarised data for phenol resins enhancement of the productivity of **GII** for CM of *trans*-1-methoxy-4-(1-propenyl)benzene (TA) and 2-ethylhexyl acrylate (EHA) as demonstrated in scheme 23[a] 31
Table 2.8: Metathesis reaction of α,β-carbonyl compounds **19** and trans-β-methyl styrene **20** catalysed by **GII**[a] 32
Table 2.9: Screening of catalyst for reaction selectivity[a] 33
Table 2.10: Influence of the additives on the reaction selectivity and isolated yield of the desired product **25C** 34
Table 2.11: Polymerization of *t*CO with **GI** and increasing amounts of PPh_3 36
Table 2.12: Catalyst screening and additive effect on RCM of monostyrylated products. 37
Table 2.13: Screening of various catalyst and additives to obtain the maximum efficiency and selectivity. 39
Table 2.14: Investigation of cross-metathesis between α-methylene-γ-butyrolactone, **30A**, and 1-acetoxy-9-decene, **30B**, using 5 mol % of the catalyst. 40
Table 2.15: Results obtained for the different ruthenium-catalysed reactions of 1-allyl-3-(phenyl)urea **31A** 42
Table 2.16: Comparison of ROMP of norbornene catalysed by different catalyst/co-catalyst system[a] 43
Table 2.17: Comparison of efficiency of different co-catalyst in the self metathesis of 4-decyne[a] 45
Table 3.1: Summarised data results of the *p*-cresol equivalent (vs **GII** eq.), resulting the isolated product yield of the cross-metathesis (for the reaction refluxed in CH_2Cl_2 under Ar and X1 = 0.33) 62
Table 3.2: Table showing moles of reagent, mole fraction of 1, mole ratios, cross-metathesis yield, and self-metathesis yield 62
Table 4.1: Summary of the FTIR and UV-vis data of **GII** in different solvents 76

Table 4.2: The observed kinetic rate constant k_{obs}, for the transformation of 0.10 mM **GII** determined λ_{max} for the different solvents at 25 °C followed by UV-Vis spectroscopy under Ar. The C-P stretching frequency as measure by FTIR in the different solvent (from Table 4.1) is also shown 77

Table 4.3. Peak anodic potentials, E_{pa}, peak potential difference ΔE_p, formal reduction potentials, E°, peak anodic current, i_{pa}, and current ratios i_{pc}/i_{pa} for 0.8mM solution of **GII** in DCM, DCE, CLF, and TOL containing 0.08M $[N(^nBu)_4[PF_6]$ as supporting electrolyte at 25°C for indicated scan rates of the Ru^{II}/Ru^{III} redox couples. 81

Table 4.4: Solvent studies of the metathesis reaction between trans-1-methoxy-4-(1-propenyl) benzene (**1**) and 2-ethylhexyl acrylate (**2**) catalysed by p-cresol/**GII.** 83

Table 5.1: Summary of the ATR-FTIR and UV-vis data of GII and the GII-phenol adducts 92

Table 5.3: Peak anodic and cathodic potentials, E_{pa} and E_{pc}, peak potential difference ΔE_p, formal reduction potentials, E°, (vs ferrocene) peak currents, $i_{pa\ or\ pc}$, and current ratios i_{pc}/i_{pa} for 0.8mM solution of **GII** and the **GII**-phenol adducts containing 0.08M $[N(^nBu)_4[PF_6]$ as supporting electrolyte at 25°C for indicated scan rates of the Ru^{II}/Ru^{III} redox couples. 101

List of Figures

Figure 2.1: Commercially available Schrock's metathesis catalyst 17
Figure 2.2: Series of ruthenium-carbene olefin metathesis catalysts, indicating the order of increasing activity for the derivatives 18
Figure 2.3: Some of the commercially available Ruthenium metathesis catalysts 21
Figure 2.4: Graph of diene concentration against time. Red-without CuCl, Black-with CuCl 23
Figure 2.5: Some aryloxy- and siloxyl-based co-catalyst. 44
Figure 3.1: (a) Grubbs' second generation catalysts (**GII**) and an intermediate ruthenacyclobutane (**Ru-1**), (b) the formation of hydrogen bonds between phenols and the chloride ligands of the catalyst [23–25]. 57
Figure 3.2: The reaction scheme showing the cross-metathesis (CM) and self-metathesis (SM) reactions pathways catalysed by *p*-cresol/GII between *trans*-1-methoxy-4-(1-propenyl)benzene (1) and 2- ethylhexyl acrylate (**2**) to form (E)-1,2-bis(4-methoxyphenyl)ethene (**3**), butene (**4**), (*E*)-2-ethylhexyl-3-(4-methoxyphenyl)acrylate (**5**), propene (**6**), bis(2-ethylhexyl) maleate (**7**), and ethene (**8**) 59
Figure 3.3: The graphs showing the relationship between (A) the *p*-cresol:**GII** ratio and the isolated % yield of CM product, 5, (for the reaction refluxed in CH_2Cl_2 under Ar and X1 = 0.33) and (B) shows the CM product, 5, in terms of mole fraction of 1. [mole fraction of 1. [mole fraction: $X_1 = (n_1)/(n_1 + n_2)$, where n is the mol of the reactants used] 61
Figure 3.4: The assigned resonances used for the kinetic data belonging to 1, 2, 3, and 5 are indicated by blue, red, green, and purple respectively, ★ shows the assigned ^{1}H NMR resonances used as characteristics compounds indicators. The time dependent ^{1}H NMR of the metathesis reaction mixture between trans-1-methoxy-4-(1-propenyl) benzene and 2-ethylhexyl acrylate in the presence of *p*-cresol/**GII** (100:1 ratio) at (B) 25 °C and (C) 35 °C in CD_2Cl_2. The spectra at times t = 0 min. (1), t = 3 mins. (2), t = 11 mins. (3), t = 30 mins. (4), t = 77 mins. (5), t = 162 mins. (6), t = 262 mins. (7), t = 392 mins. (8), t = 702 mins. (9) and t = 722 mins. (10) are shown 65
Figure 3.5: The time trace of the metathesis reaction between 1 and 2 catalysed by *p*-cresol/**GII** adduct at (A) 25 °C and (B) 35 °C in CD_2Cl_2 under Ar and X_1 = 0.33, following the appearance of the *in situ* metathesis product formation, SM (3, green), and CM (5, purple). 66
Figure 4.1: Optimised 3D structure of Grubbs' second generation catalyst 73
Figure 4.2: UV–Vis spectra of 0.10 mM solutions of **GII** in dry dichloromethane (grey), chloroform (yellow), dichloroethane (blue), tetrahydrofuran (green), and toluene (red). Insert: Expanded sections between 300-400 nm and 400-600nm. Color can be seen in the online version. 75

Figure 4.3: UV–Vis spectra measured over time for the dissociation of PCy_3 from a 0.10 mM **GII**, in dry (A) chloroform, (B) DCM, (C) DCE, (D) toluene, and (E) THF under Ar. 1st Insert: Absorbance *vs* time graph at λ_{max}. 2nd Insert: A first order kinetic plot of data for the process compiled from the data of the 1st insert; the slope gives the observed rate constant, k_{obs}. (F) The relationship between the k_{obs} and the C-P stretching frequency. 77

Figure 4.4: Comparative cyclic voltammograms of 0.8 mM **GII** in DCM, DCE, CLF, and THF at 25 °C using 0.08 M $[N(^nBu)_4][PF_6]$ as the electrolyte on a glassy carbon working electrode at a scan rate of 50 mV s^{-1}, under a blanket of argon. 79

Figure 4.5: Cyclic voltammogram of a 0.8 mM solution of **GII** in the presence of 0.08 M $[N(^nBu)_4][PF_6]$ as supporting electrolyte at 25 °C at scan rates ranging from 50-1000 mV s^{-1} in (A) DCM, (B) DCE, (C) CLF, and (D) THF 80

Figure 4.6: (A) The relationship between the % yield of the CM product for the **GII** catalysed metathesis reaction between **1** and **2**, and the Gutmann donor number of the different solvents. (B) The relationship between the k_{obs} (for the dissociation of $PCy_3$from **GII**) and the% yield of the CM product for the **GII** catalysed metathesis reaction between **1** and **2**. 83

Figure 5.1: Grubbs' second generation catalyst (**GII**) 90

Figure 5.2: Comparative UV-Vis spectra of 0.10 mM solutions of **GII** and **GII**-phenol adducts in dry dichloromethane. Insert: Expanded sections between 300-400 nm and 400-600 nm. 92

Figure 5.3: UV–Vis spectra measured over time for the dissociation of PCy3 from the 0.10 mM **GII**-phenol adducts and GII in dry DCM under Ar. (A) **GII**-PP, (B) **GII**-2MP, (C) **GII**-4MP, (D) **GII**-TBP, (E) **GII**-3MP, (F) **GII**-MOP, (G) **GII**-P, (H) **GII**-BP, (I) **GII**-TFP, (J) **GII**-NP, and (K) **GII**. 1st Insert: Absorbance *vs* time graph at λ_{max}. 2nd Insert: A first order kinetic plot of data for the process compiled from the data of the 1st insert; the slope gives the observed catalyst transformation rate constant, k'_{obs}. 95

Figure 5.4: Relationship between the observed catalyst transformation rate constant (k'_{obs}) for the for the dissociation/decomposition of the PCy_3 from the GII-phenol adducts vs (A) the Hammett constant (σ_R), and (C) the pK_a of the phenols additives. The relationship between (B) the Hammett constant (σ_R) or (D) the isolated %CM product (of the reaction trans-1-methoxy-4-(1-propenyl) benzene and 2-ethylhexyl acrylate, catalysed by **GII**-phenol adducts) and the pK_a of the phenol additives. 97

Figure 5.5: ^{31}P NMR of **GII** at time 5 min (1), **GII** at time 60 min (2), **GII-NP** at time 5 min (3), **GII-NP** at time 60 min (4), **GII-3MP** at time 5 min (5), and **GII**-3MP at time 60 min (6) in CD_2Cl_2 at 25 °C. 98

Figure 5.6: Comparative cyclic voltammogram of a 0.8 mM solution of **GII** and the **GII**-phenol adducts in the presence of 0.08 M $[N(^nBu)_4][PF_6]$ as supporting electrolyte at 25 °C at 100 mV s^{-1}, referenced vs ferrocene, but decamethylferrocene (Fc*) was used as internal reference. 100

Figure 5.7: The cyclic voltammograms of a 0.8 mM solution of (A) **GII** in the presence of 0.08 M $[N(^{n}Bu)_4[PF_6]$ as supporting electrolyte at 25 °C at scan rates ranging from 50-1000 mV s^{-1}. (B) The relationships between i_{pc}/i_{pa} and scan rates at 25 °C for the Ru^{II}/Ru^{III} process for **GII**. Insert: Schematic representation of the E_rC_r mechanism for **GII**. 101

List of Schemes

Scheme 2.1: Schematic representation of an olefin metathesis reaction 8
Scheme 2.2: Representation of self-metathesis reaction 10
Scheme 2.3: Representation of a cross-metathesis reaction 11
Scheme 2.4: Representation of ring closing metathesis reaction 11
Scheme 2.5: Representation of acyclic diene metathesis reaction 12
Scheme 2.6: Representation of ring opening metathesis polymerization (ROMP) 12
Scheme 2.7: Representation of ene-yne metathesis reaction 13
Scheme 2.8: Chauvin's proposed metathesis mechanism 14
Scheme 2.9: Synthesis of the first stable metal carbene 15
Scheme 2.10: Synthesis of an electron deficient tantalum-neopentylidene catalyst 16
Scheme 2.11: Synthesis of Tungsten-oxo-neopentylidene complex (L = PEt_3, etc.) 16
Scheme 2.12: Synthesis of the first well-defined ruthenium carbene catalyst 18
Scheme 2.13: Initial synthesis of Hoveyda-Grubbs first generation catalyst 19
Scheme 2.14: An example of ring closing metathesis catalysed by **HGI** 20
Scheme 2.15: Synthesis of Hoveyda-Grubbs second generation catalyst 20
Scheme 2.16: Synthesis of series of bispyridine complexes 21
Scheme 2.17: Self metathesis of 1-octene to give 7-tetradecene and ethene (R = $(CH_2)_5CH_3$) 24
Scheme 2.18: Cross-metathesis between TBS-protected allylphenol and MVK for additives effect 24
Scheme 2.19: Comparisons of NaI vs CuI as additive in **GII** catalysed olefin cross-metathesis 25
Scheme 2.20: Enyne metathesis of diphenyl acetylene mediated by **GII** (DMAD = dimethyl acetylenedicarboxylate) 26
Scheme 2.21: Proposed mechanism for the formation of hydrogen bonds between phenols and the chloride ligands of the catalyst [37,107,108]. 28
Scheme 2.22: An example of dienyl isomerization catalysed by **GII** with an alcohol as additive (R = H or $CO(CH_3)$) 29
Scheme 2.23: Cross-metathesis of *trans*-1-methoxy-4-(1-propenyl)benzene and 2-ethylhexyl acrylate catalysed by GII in the presence of poly(vinyl phenol) resins as an additi 30
Scheme 2.24: Metathesis reaction of α,β-carbonyl compounds 24A-F and trans-β-methyl styrene **24I-IV** catalysed by **GII** 32
Scheme 2.25: Cross-metathesis between 25A and 25B for catalyst screening 33
Scheme 2.26: Cross-metathesis between 25A and 25B for additives effect 34

Scheme 2.27: ROMP of *trans*-Cyclooctene 35
Scheme 2.28: RCM of monostyrylated products catalysed by **HGII** with 1,6-heptadiene as the additive 37
Scheme 2.29: Cyclopolymerization (CP) of 1,6-heptadiyne 38
Scheme 2.30: Cross-metathesis of α-methylene-γ-butyrolactone, **30A**, and 1-acetoxy-9-decene, **30B** 40
Scheme 2.31: Reactions showing isomerization against metathesis for 1-allyl-3-(phenyl)urea **31A** 41
Scheme 2.32: ROMP of norbornene with Molybdenum complexes 32A-D 43
Scheme 2.33: Self metathesis of 4-decyne catalysed by $Mo(CO)_6$ /additives 45
Scheme 4.1: An illustration of the phosphine dissociation/association equilibrium of **GII**, producing the active catalytic species, and other potential side reactions such as phosphine oxidation and decomposition of the active catalytic species 76
Scheme 4.2: Schematic representation of the E_rC_r electrochemical mechanism for **GII** in chlorinated solvents. 80
Scheme 4.3: The metathesis reaction between *trans*-1-methoxy-4-(1-propenyl)benzene (**1**) and 2-ethylhexyl acrylate (**2**) catalysed by **GII**. 82
Scheme 5.1: An illustration depicting the phosphine dissociation/association equilibrium of **GII**-phenol adducts, producing the active catalytic species (**GII**^{A}), the phenol-stabilized active catalytic species (**GII**^{AS}), alongside other potential side reactions, including phosphine oxidation and decomposition of the active catalytic species. 94
Scheme 5.2: The metathesis reaction between trans-1-methoxy-4-(1-propenyl) benzene, 1, and 2-ethylhexyl acrylate, 2, catalysed by **GII**-phenols. 102

Abstract

The use of additives in olefin cross-metathesis reactions which employs the commercially available Grubbs' second generation catalyst, **GII**, has resulted in better catalyst performance, catalyst stability, suppression of other non-metathetic reactions like olefin isomerization, self-metathesis and improved desired metathesis product yield. The addition of *p*-cresol to **GII** enhances selectivity for cross-metathesis over self-metathesis, with 100 equivalents of *p*-cresol ensuring optimal catalyst performance. Optimisation of the metathesis reaction conditions were performed between *trans*-1-methoxy-4-(1-propenyl)benzene and 2-ethylhexyl acrylate, varying *trans*-1-methoxy-4-(1-propenyl)benzene mole fractions from approximately 0.09 to 0.91 suggesting that the CM pathway is kinetically more favourable. The ^{31}P NMR study between **GII** and *p*-cresol showed that the cresol binds to the tricyclohexylphosphine oxide preventing the oxide from decomposing the active catalyst.

The reaction progress was monitored using ^{1}H NMR spectroscopy at 25 °C and 35 °C in CD_2Cl_2 solvent over 722 minutes, maintaining a constant *p*-cresol/**GII** ratio (100:1, X_1 = 0.33). The reaction setup followed previous protocols with slight adjustments for time-trace analysis. Results revealed an induction period at both temperatures, significantly shorter at 35 °C (4 minutes vs. 40 minutes at 25 °C). The elevated temperature notably favours the selectivity of the *p*-cresol/**GII** catalyst. Reaction kinetics showed the cross-metathesis rate with the modified catalyst was approximately 1.5 times faster than self-metathesis, with k'_{obs} values of 0.0575 min^{-1} (25 °C) and 0.68 min^{-1} (35 °C) for cross-metathesis compared to 0.033 min^{-1} and 0.41 min^{-1} for self-metathesis, respectively. Further optimisation was carried using different solvents in the metathesis reaction between *trans*-1-methoxy-4-(1-propenyl)benzene and 2-ethylhexyl acrylate. The UV-Vis kinetics revealed that the phosphine (PCy_3) ligand dissociation equilibrium from Grubbs second generation catalyst (**GII**) in different solvents (dichloromethane, dichloroethane, chloroform, tetrahydrofuran, and toluene) were determined to be pseudo first order with k'_{obs} = 4.8 - 15.6 x 10^{-3} min^{-1}.

According to an electrochemical study using Cyclic Voltammetry (CV) in the different solvents, an electrochemically reversible behaviour was observed for **GII** dissolved in the chlorinated solvents (DCM, DCE, and CLF). The formal reduction potentials, $E°'$, of **GII** in the different chlorinated solvents increased as the polarity index of the solvent became larger. In THF, however,

only the oxidation of **GII** could be detected. Upon oxidation of **GII**, THF (with a lone pair electron on the oxygen) which is highly coordinative solvent, nucleophilically attach to the electrochemically produced $Ru^{\bullet+}$, resulting in a redox inactive THF associated compound. A correlation was established between the ease of **GII** oxidation in the different solvents and the rate of PCy_3 dissociation in that solvent. The % yield of the cross-metathesis product in the different solvents at 40 °C catalysed by **GII** exponentially increased as the Gutmann donor number of the solvent increased, with DCM showing highest yield. In THF, no metathesis could be detected, agreeing the electrochemical data, that THF coordinate to the positively charged or active **GII** rending it inactive.

Non-structural modification of Grubbs' second generation catalyst involving the use of additives such as phenol derivatives (4-nitrophenol (**NP**), 4-(trifluoromethyl)phenol (**TFP**), 4-bromophenol (**BP**), phenol (**P**), 4-methoxyphenol (**MOP**), 4-tertbutylphenol (**TBP**), 3-methylphenol (**3MP**, *m*-cresol), 4-methylphenol (**4MP**, *p*-cresol), 2-methylphenol (**2MP**, *o*-cresol) and 4-propylphenol (**PP**) are investigated. The catalyst behaviour and interactions between **GII** and the different phenol derivatives were characterised using UV-Vis spectroscopy, attenuated total reflection Fourier transformed infrared (ATR-FTIR), and CV. The ATR-FTIR spectra revealed distinct C-N and C-P stretching frequencies from the **GII**-phenol adducts, alongside phenol-associated O-H and C=C stretching bands. UV-Vis spectra displayed strong absorption bands at 335 nm and weaker bands between 503-509 nm, linked to metal-ligand charge transfer. CV showed electrochemical reversibility for most **GII**-phenol adducts, except those with electron-withdrawing groups. Metathesis reactions were performed between *trans*-1-methoxy-4-(1-propenyl)benzene and 2-ethylhexyl acrylate, revealing a correlation between electron-donating phenol groups and higher cross-metathesis (CM) yield. While phenol derivatives influenced catalyst activation rates, no direct correlation was found between activation rates and catalytic selectivity. The study highlights the significance of electron-donating phenol derivatives in enhancing catalytic efficiency by increasing Ru centre electrophilicity.

KEYWORDS: Grubbs 2nd generation catalyst; *p*-cresol; self-metathesis; cross-metathesis, UV-Vis, electrochemistry, phenol derivatives, solvent influence, electrophilicity, catalyst-additive interaction.

List of Abbreviations

2MP	2-methylphenol
3MP	3-methylphenol
4MP	4-methylphenol
ATR	Attenuated Total Reflection
BP	4-bromophenol
Ci	Chemically irreversible
CM	Cross-metathesis
Cr	Chemically reversible
CV	Cyclic Voltammetry
DFT	Density functional theory
DMAD	Dimethyactylenedicarboxylate
Er	Electrochemically reversible
FcH	Ferrocene
FcH*	Decamethyl ferrocene
FTIR	Fourier Transform Infrared
GI	Grubbs first generation catalyst
GII	Grubbs second generation catalyst
GIII	Grubbs third generation catalyst
HGI	Hoveyda-Grubbs first generation catalyst
HGII	Hoveyda-Grubbs second generation catalyst
MLCT	Metal to ligand charge transfer
MOP	4-methoxylphenol
MVK	Methyl Vinyl Ketone
NMR	Nuclear magnetic resonance
NP	4-nitropheno
OMC	Octyl methoxycinnamate
P	Phenol
PCy_3	Tricyclohexylphosphine

PP	4-propylphenol
PTLC	Preparative Thin Layer Chromatography
RCM	Ring-closing metathesis
ROM	Ring-opening metathesis
RRM	Ring-rearrangement metathesis
SM	Self-metathesis
TBP	4-tertbutylphenol
TFP	4-(trifluoromethyl)phenol
TLC	Thin-layer chromatography
TMS	Tetramethylsilane
TOF	Turnover frequency
UV–Vis	Ultraviolet–Visible light

CHAPTER 1
INTRODUCTION

1.1 Introduction

Olefin metathesis has been used to solve a range of organic synthesis difficulties because it makes it straightforward to produce carbon-carbon double bonds in one step when other synthetic methods require multiple steps [1–3]. These are only a few of the many applications for olefin metathesis; cross-metathesis, self-metathesis, ene-yne metathesis, ring-opening metathesis, ring-closing metathesis and ring-rearrangement metathesis [4–9]. In 2001, Gladysz came up with the concept of an "ideal catalyst" whose intention is to prompt the curiosity of researchers all over the world to develop a catalyst for an ideal synthesis [10,11]. Highly active olefin metathesis catalysts have been developed over the past few decades because of tailored research for the reduction of synthetic steps to achieve a desirable product in organic and polymer chemistry [12–16]. Among the active ruthenium-based catalysts that exhibits greater selectivity, with greater functional group tolerance and higher moisture and atmospheric oxygen stability is the Grubbs' second-generation catalyst, **GII**, which makes it the most widely used homogenous olefin metathesis catalyst [17]. On the other hand, cross-metathesis is a practical synthetic method for the formation of the desired product by adding a molecular fragment to a simple olefin, frequently containing a functional group [6,18]. In a typical cross-metathesis (CM) reaction, one of two product formation pathways can be followed: these being the CM and SM product pathways. It is possible however to favour one of these pathways above the other though tailoring the substrate ratio, having one substrate in excess, based on its steric or electronic effect [19]. Prior to the invention of **GII**, it was challenging to create substituted olefins with an electron-withdrawing functionality, such as α, β-unsaturated carbonyl compounds through cross-metathesis with terminal olefins [20].

Although the Grubbs' second-generation catalyst has shown success in acrylate metathesis, its limitations include the necessary dissociation of the PCy_3 ligand, which can lead to unwanted side reactions and catalyst deactivation [21–23]. To address this, phosphine-free and Hoveyda-type catalysts have been explored as alternatives, with several reports demonstrating their efficiency in cross-metathesis reactions with acrylates [24–26]. However, the widespread use and cost-

effectiveness of the Grubbs catalyst have motivated researchers to seek solutions to mitigate its limitations other than the alternative catalysts. In 2005, Forman and Tooze [27] pioneered the use of phenol as a phosphine scavenger, proposing that it captures released PCy_3 to form an adduct, $(PhOH)_nPCy_3$. Building on this work, Santos *et al*. and Swart *et al*. [21,28] investigated the scavenging potential of phenol derivatives, such as *p*-cresol, in acrylate metathesis, achieving significant improvements in catalyst performance. Notably, phenol and phenol-functionalized resin were found to enhance the selectivity of cross-metathesis products, favouring the formation of the desired product over self-metathesis in quantitative yields compared to reactions without these additives [27].

Despite efforts to enhance catalyst efficiency, the current methodology remains unsatisfactory for economically viable processes, which require a turnover number of over 50,000 for homogeneous metathesis catalysts [29]. To improve the yield of the desired cross-metathesis product, researchers have explored various strategies, including modifying the electronic and steric properties of metathesis partners by introducing electron-donating and electron-withdrawing groups [28,30]. Other approaches include optimizing the ratio of **GII** catalyst to co-catalyst/additives [21,31], varying catalyst loading [24,32], and identifying the ideal catalyst composition [33–35]. It was found that reducing the electrophilicity of the acrylate moiety and decreasing the electron density on the α,β-carbonyl compound, catalysed by **GII** in the presence of excess phenol, led to increased cross-metathesis yields [28]. In contrast, Fogg's group observed that the beneficial effect of catalyst loading is offset by the rate of catalyst decomposition, as these parameters are interconnected [23]. However, the group achieved a breakthrough by using **GII** with poly (vinylphenol) resin as a PCy_3 stabilizer in acrylate cross-metathesis, resulting in catalyst efficiency comparable to the more expensive Hoveyda-Grubbs second-generation catalyst [21].

1.2 Problem Statement

Since the second-generation Grubbs catalyst (**GII**) with phenol has emerged as a preferred choice for α,β-unsaturated carbonyl compounds via cross-metathesis reactions involving for α,β-unsaturated carbonyl compounds and olefins [22,24,26], it has motivated researchers to seek a non-structural modification to mitigate its limitations other than the conventional structural modification of the catalysts. Numerous studies have reported the use of non-structural

modifications, involving the addition of chemical species such as salts, alcohols, and metal halides as co-catalysts or additives to Grubbs catalyst, to enhance its activity, selectivity and stability through a simple and effortless method [21,36–42]. To optimise Grubbs catalyst performance in metathesis reactions, it is essential to understand the interactions between additives and the catalyst. Investigating the effects of additives can provide valuable insights into the mechanisms of catalytic reactions, enabling the design and development of more effective catalysts or modifications to existing ones. However, there is a limited understanding of the characterization of the Grubbs catalyst-additive interaction, which is crucial to substantiate the beneficial effects of additives on **GII** and promote non-structural modification of commercially available metathesis catalysts.

1.3 Previous Research

Previous research conducted suggested the formation of *p*-cresol adduct with hydrogen bonds to one or both of the chloride ligands of the catalyst, thereby favouring cross-metathesis over self-metathesis in the reaction between electron deficient α,β- carbonyl compounds and prop-1-en-1-ylbenzene [28]. Employing UV-Vis spectroscopic kinetic study and 31P NMR for stability studies indicated that the second-generation Grubbs catalyst **GII** is more stable than the first-generation Grubbs catalyst **GI**. The electrochemical behaviour of these catalysts was investigated, and the cyclic voltammetry revealed that both catalysts followed a one-electron transfer Ru^{II}/Ru^{III} process. The first-generation Grubbs catalyst follows an ErCi (Electrochemically reversible and chemically irreversible) mechanism, and the second-generation Grubbs catalyst follows an E_rC_r (Electrochemically reversible and chemically reversible). Furthermore, the second-generation Grubbs catalyst oxidises at much lower potentials and is chemically more stable than the first-generation counterpart [43,44].

1.4 Objective

To determine how additives affect the Grubbs second-generation catalyst and to understand the interactions between the additives and the catalyst. Therefore, this study focused on the following:

1. The determination of the ideal *p*-cresol to Grubbs second-generation catalyst ratio to improve cross-metathesis product yield of the reaction between 2-ethylhexyl acrylate and *trans*-1-methoxy-4-(1-propenyl)benzene .
2. ^{1}H NMR kinetic studies are used to monitor the metathesis reaction and the product distribution evaluated at various temperatures, times, and the *p*-cresol/catalyst ratios.
3. ^{31}P NMR was used to investigate the interaction between Grubbs second generation and *p*-cresol and ascertain the hydrogen bond interaction between *p*-cresol/catalyst adduct.
4. Solvent studies to determine the most suitable solvent for better catalyst behaviour and gain insight into the solvation of the system.
5. UV-Visible kinetics study to gain insight into the *p*-cresol/catalyst adduct stability in different solvents and the catalyst with different phenol derivatives.
6. Cyclic voltammetry to determine the electrochemical behaviour and propose an electrochemical mechanism for *p*-cresol/catalyst adduct in different solvents and the catalyst with different phenol derivatives.

1.5 Chapter Layout

Chapter 1 provides a concise introduction to olefin metathesis and the catalyst commonly used for it, emphasising the effect of additives. It equally provides a problem statement, a summary of previous research conducted and the objective of this study. Finally, it provides a brief layout of the chapters in this thesis.

Chapter 2 provides a literature review on metathesis reactions, types of metathesis reactions, development of catalysts for metathesis reaction, metathesis mechanism and additives effect on metathesis reactions.

Chapter 3 presents the comparative studies of varying reaction conditions, substrate ratio and *p*-cresol/second-generation Grubbs catalyst ratio for the metathesis reaction between trans-1-methoxy-4-(1-propenyl) benzene and 2-ethylhexyl acrylate employing Nuclear Magnetic Resonance spectroscopy, Attenuated Total Reflection Fourier Infrared spectroscopy (ATR-FTIR), Preparative Thin-layer Chromatography (PTLC), Ultraviolet-Visible light Spectroscopy (UV-Vis).

Chapter 4 presents a spectroscopic investigation, and electrochemical properties of second-generation Grubbs catalyst/*p*-cresol adduct in different solvents employing Attenuated Total Reflection Fourier Infrared spectroscopy (ATR-FTIR), Ultraviolet-Visible light Spectroscopy (UV-Vis), and Cyclic voltammetry (CV).

Chapter 5 presents the results obtained from the metathesis reaction between trans-1-methoxy-4-(1-propenyl) benzene and 2-ethylhexyl acrylate catalysed by the second-generation Grubbs catalyst and different phenol derivatives as additives/co-catalyst. The spectroscopic investigation and electrochemical properties of second-generation Grubbs catalyst and different phenol derivatives employing Attenuated Total Reflection Fourier Infrared spectroscopy (ATR-FTIR), Ultraviolet-Visible light Spectroscopy (UV-Vis), and Cyclic voltammetry (CV).

Chapter 6 critically evaluates the results obtained in this study, along with the enumeration of possible future research.

Chapter 7 summarizes the research outputs of this study in terms of publications and conference contributions.

References

[1] F. C. Courchay, T. W. Baughman, K. B. Wagener, *J Organomet Chem* **2006**, *691*, 585–594.

[2] F. B. Hamad, T. Sun, S. Xiao, F. Verpoort, *Coord Chem Rev* **2013**, *257*, 2274–2292.

[3] J. W. Morzycki, *Steroids* **2011**, *76*, 949–966.

[4] M. Renom Carrasco, C. Nikitine, M. Hamou, C. de Bellefon, C. Thieuleux, V. Meille, *Catalysts* **2020**, *10*, 435.

[5] C. Guo, X. Li, X. Zhu, W. Chu, S. Liu, Y. Wang, P. Zeng, S. Guo, L. Xu, *Chinese J. Catal.* **2018**, *39*, 37–46.

[6] X. Meng, J. B. Matson, K. J. Edgar, *Polym Chem* **2014**, *5*, 7021–7033.

[7] G. S. Sankaran, *Open Access J. Agric. Res.* **2018**, *3*.

[8] I. Mandal, A. F. M. Kilbinger, *JACS Au* **2022**, *2*, 2800–2808.

[9] E. Jecs, S. T. Diver, *Org Lett* **2015**, *17*, 3510–3513.

[10] J. A. Gladysz, *Pure Appl Chem* **2001**, *73*, 1319–1324.

[11] A. Michrowska, K. Grela, *Pure Appl Chem* **2008**, *80*, 31–43.

[12] P. Schwab, R. H. Grubbs, J. W. Ziller, *J Am Chem Soc* **1996**, *118*, 100–108.

[13] M. Scholl, S. Ding, C. W. Lee, R. H. Grubbs, *Org Lett* **1999**, *1*, 953–956.

[14] S. Gessler, S. Randl, S. Blechert, *Tetrahedron Lett* **2000**, *41*, 9973–9976.

[15] M. S. Sanford, M. Ulman, R. H. Grubbs, *J Am Chem Soc* **2001**, *123*, 749–750.

[16] R. R. Schrock, *Angew Chem Int Ed* **2006**, *45*, 3748–3759.

[17] R. H. Grubbs, *Angew Chem Int Ed* **2006**, *45*, 3760–3765.

[18] R. Palkovits, D. Arlt, H. Stepowska, F. Schüth, *Micropor Mesopor Mat.* **2010**, *132*, 319–327.

[19] O. A. Odewole, M. R. Swart, E. Erasmus, *Tetrahedron* **2024**, *162*, 134105.

[20] A. K. Chatterjee, T.-L. Choi, D. P. Sanders, R. H. Grubbs, *J Am Chem Soc* **2003**, *125*, 11360–11370.

[21] A. G. Santos, G. A. Bailey, E. N. dos Santos, D. E. Fogg, *ACS Catal* **2017**, *7*, 3181–3189.

[22] G. A. Bailey, D. E. Fogg, *J Am Chem Soc* **2015**, *137*, 7318–7321.

[23] W. L. McClennan, S. A. Rufh, J. A. M. Lummiss, D. E. Fogg, *J Am Chem Soc* **2016**, *138*, 14668–14677.

[24] K. Kaczanowska, B. Trzaskowski, A. Peszczyńska, A. Tracz, R. Gawin, T. K. Olszewski, K. Skowerski, *ChemCatChem* **2020**, *12*, 6366–6374.

[25] K. Lafaye, L. Nicolas, A. Guérinot, S. Reymond, J. Cossy, *Org Lett* **2014**, *16*, 4972–4975.

[26] D. Schweitzer, K. D. Snell, *Org Process Res Dev* **2015**, *19*, 715–720.

[27] G. S. Forman, R. P. Tooze, *J Organomet Chem* **2005**, *690*, 5863–5866.

[28] M. R. Swart, L. Twigge, E. Erasmus, C. Marais, B. C. B. Bezuidenhoudt, *Eur J Inorg Chem* **2021**, 1752–1762.

[29] K. A. Burdett, L. D. Harris, P. Margl, B. R. Maughon, T. Mokhtar-Zadeh, P. C. Saucier, E. P. Wasserman, *Organometallics* **2004**, *23*, 2027–2047.

[30] M. R. Swart, C. Marais, E. Erasmus, *Catalyst* **2021**, *11*, 1483.

[31] Odewole O.A, Swart M.R, Erasmus E, *Eur J Inorg Chem* **2024**.

[32] J. I. Yun, D. Kim, J. Lee, *Tetrahedron Lett* **2011**, *52*, 1928–1930.

[33] K. Żukowska, A. Szadkowska, A. E. Pazio, K. Woźniak, K. Grela, *Organometallics* **2012**, *31*, 462–469.

[34] J. P. Martínez, B. Trzaskowski, *J Phys Chem A* **2022**, *126*, 720–732.

[35] A. Michrowska, R. Bujok, S. Harutyunyan, V. Sashuk, G. Dolgonos, K. Grela, *J Am Chem Soc* **2004**, *126*, 9318–9325.

[36] G. S. Forman, A. E. McConnell, R. P. Tooze, W. Janse Van Rensburg, W. H. Meyer, M. M. Kirk, C. L. Dwyer, D. W. Serfontein, *Organometallics* **2005**, *24*, 4528–4542.

[37] E. L. Dias, S. T. Nguyen, R. H. Grubbs, *J Am Chem Soc* **1997**, *119*, 3887–3897.

[38] W. H. Meyer, A. E. McConnell, G. S. Forman, C. L. Dwyer, M. M. Kirk, E. L. Ngidi, A. Blignaut, D. Saku, A. M. Z. Slawin, *Inorganica Chim Acta* **2006**, *359*, 2910–2917.

[39] M. Abbas, A. Leitgeb, C. Slugovc, *Synlett* **2013**, *24*, 1193–1196.

[40] C. Feng, X. Wang, B.-Q. Wang, K.-Q. Zhao, P. Hu, Z.-J. Shi, *Chem. Commun.* **2012**, *48*, 356–358.

[41] B. J. Ireland, B. T. Dobigny, D. E. Fogg, *ACS Catal* **2015**, *5*, 4690–4698.

[42] M. Rivard, S. Blechert, *European J Org Chem* **2003**, *2003*, 2225–2228.

[43] M. R. Swart, B. C. B. Bezuidenhoudt, C. Marais, E. Erasmus, *Inorganica Chim Acta* **2021**, *514*, 120001.

[44] M. R. Swart, C. Marais, E. Erasmus, *ACS Omega* **2021**, *6*, 28642–28653.

CHAPTER 2

LITERATURE REVIEW

Metathesis reactions: Effect of additives as co-catalysts to Grubbs' or Schrock's catalyst

2.1 Introduction

2.1.1 Overview

One of the most powerful and widely used synthetic methods in modern organic chemistry is the formation of alkene carbon-carbon double bonds. This is often achieved through Wittig reactions, Heck coupling, Stille coupling, and Peterson olefination to name but a few [1]. One of the more desirable alkene formation reactions is olefin metathesis as alkenes itself act as the reactive functional groups [2–4]. It is a metal catalysed transformation that involves the interconversion of olefins into new olefins (Scheme **2.1**: Schematic representation of an olefin metathesis reaction 2.1) by the rearrangement of substituents through a metallocyclic intermediate [5,6]. Olefin metathesis is a chemical reaction where carbon-carbon double bonds (olefins) are rearranged using metal catalysts to create new carbon-carbon double bonds with different partner molecules.

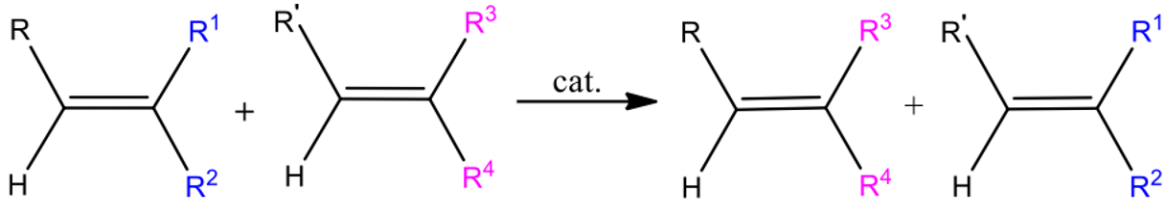

Scheme 2.1: Schematic representation of an olefin metathesis reaction

The groundwork for metathesis reactions was laid by numerous researchers [7–11] in the field after the first instance of transition-metal catalysed metathesis was discovered in 1957 [12]. Among the several researchers that focused their investigations on olefin metathesis, were Robert H. Grubbs, Yves Chauvin, and Richard R. Schrock, who's immense contributions to the field of olefin metathesis, led them to share the 2005 Nobel Prize in Chemistry. With the elucidation of the reaction mechanism by Chauvin and the focused design of transition metal-based metathesis

catalysts by Schrock and Grubbs, these reactions were finally made possible for industrial uses, ranging from the synthesis of polymers to pharmaceuticals [13,14]. Schrock had prepared the first well-defined highly active metathesis catalysts (high oxidation state tantalum (Ta) and tungsten (W) carbene complexes) [13,15]; Robert Grubbs, on the other hand, provided synthetic chemists with active catalysts that exhibits greater selectivity, with greater functional group tolerance and higher moisture and atmospheric oxygen stability relative to those of the tantalum and tungsten system [16]. He accomplished this by employing one of the platinum group metals, ruthenium (Ru). The Ru metal centre is surrounded by two neutral electron-donating entities (e.g. tricyclohexylphosphine or *N*-heterocyclic carbenes), two mono anionic groups (e.g. chlorides), and one alkylidene moiety. These catalysts were developed from Robert Grubbs' rigorous research to develop a more selective, more stable ruthenium-based metathesis catalyst [15,17]

Hoveyda *et al*., after investigating the Schrock catalyst, focused their research on improving the commercially viable Grubbs' catalysts [18–20]. Their research found that replacement of one of the phosphine ligands with a chelating benzylidine ether ligand produced an exceptionally air and moisture stable metathesis active catalyst [21]. Although it has slightly varied substrate specificities, these complex exhibits efficiencies comparable to those of the Grubbs systems. It is a significantly efficient catalyst for metatheses involving electron-deficient substrates such as acrylonitrile and halogenated alkenes especially fluorinated alkenes [22,23]. Research in the field of olefin metathesis has witnessed tremendous success as it has led to the development of several metathesis transformations: for example, ring opening metathesis polymerization (ROMP), ring closing metathesis (RCM), cross-metathesis (CM), acyclic diene metathesis polymerization (ADMET), en-yne metathesis (EYM) and many others. The catalysts for these transformations are now commercially available (see Figure 2.8) for the structure of these catalysts) and has subsequently led to various studies and investigations to improve the commercially available catalysts with regards to thermal and functional groups stability, selectivity, catalyst recyclability and catalyst lifetime [16,24,25]. These studies include density functional theory (DFT) investigations [26–31], catalyst modification via ligand exchange research [16,32–34], nuclear magnetic resonance (NMR) investigations [6,35–37] and mechanistic studies [38–41]. However, despite these achievements, these catalysts decompose during the reaction studied by Grubbs and Fogg [42–44], to alleviate this problem, additive were added to the reaction mixture. To the best of our knowledge there are very few reviews focusing on the investigation of the effect of additives on the current commercially

available Grubbs catalyst. Investigating the effects of additives on metathesis catalysts, such as Grubbs catalyst, is crucial for catalysis advancement. This optimises the catalyst's performance by enhancing its catalytic activity, improving reaction conditions, and influencing factors such as temperature, pressure, and solvent choice. Understanding the interaction between additives and the Grubbs catalyst is important for fine-tuning its selectivity and yield in specific chemical reactions. Research into the effects of additives can significantly contribute to a better understanding of the mechanisms involved in catalytic reactions, paving the way for the design and development of even more efficient catalysts or modifications to existing ones. Investigating the effect of additives on the Grubbs catalyst is essential for catalysis to progress, as it enhances efficiency and opens up practical applications in various industries.

This review will firstly allude some types of metathesis reactions, followed by a brief overview of the Schrock and Grubbs catalysts. This review will then enumerate the influence of additives as co-catalyst on the activity and selectivity of the specified available olefin metathesis catalyst.

2.2 Types of Olefin metathesis reactions

Self-metathesis (Scheme 2.2), cross-metathesis, ring closing metathesis, acyclic diene metathesis polymerization, ring opening metathesis polymerization, and ene-yne metathesis are just a few of the more frequently studied metathesis processes explored for synthetic chemistry [45–48]. In self-metathesis (SM), symmetrical internal olefins are produced via the transformation of both internal and terminal olefins. It is a versatile synthetic method for producing a range of fatty acid derivatives and olefins with added value. Examples of this includes the SM of methyl oleate via Grubbs' catalyst second generation (**GII**) and the SM of 1-butene to ethene and hexene, facilitated by a Mo- based heterogenous catalyst [49,50].

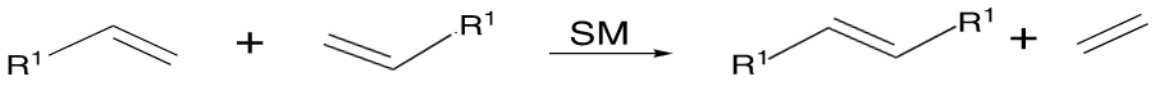

Scheme 2.2: Representation of self-metathesis reaction

Cross-metathesis is the process of fragmenting two non-identical olefins and then combining two different fragments to create new olefins (

Scheme 2.**3**). In a typical cross-metathesis (CM) reaction, one of two product formation pathways can be followed: these being the CM and SM product pathways. One of these pathways can however be favoured above the other though tailoring the substrate ratio, having one substrate in excess, based on its steric or electronic effect [51]. Usually, the CM product is the desired product, and many researchers have varied the functionality of **GII** (see Figure 2.8 for the structure) and even employed additives to improve the selectivity of **GII** to catalyse this reaction [6,52–54].

Scheme 2.3: Representation of a cross-metathesis reaction

Ring closing metathesis (RCM) is often used for synthesizing both carbocyclic and heterocyclic compounds through intramolecular metathesis of terminal dienes (examples of internal dienes are also known), a method that has improved the synthetic route to form cyclic olefins (see Scheme 2.4 for an example of RCM) [55]. In general, ring-closing metathesis is thought to be reversible like other metathesis reactions, however, because ethylene or propylene is readily released as a gaseous by-product, ring closing metathesis can be viewed as an irreversible reaction. The quest for atom economy in the advancement of green chemistry makes RCM preferred among other synthetic methods for ring formation since the only significant by-product is ethylene [56]. The uniqueness of RCM to form large ring systems has led to its application in the synthesis of epothilones, a second-generation anticancer drug, natural products e.g. dictyostatin, discodermolide and to tune polymer microstructure, macrostructure, and co-monomer composition [57–59].

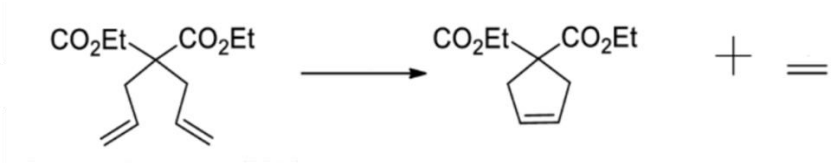

Scheme 2.4: Representation of ring closing metathesis reaction

Acyclic diene metathesis (ADMET) polymerization is an olefin metathesis step growth polycondensation reaction promoted by a suitable metathesis catalyst to prepare polymers (see Scheme 2.5 for an example of ADMET). These polymers are characterised by well-defined framework, varied functionalities, and distinctive properties [60]. The polymerization occurs when mostly terminal dienes react to form repeating cell polymers. This reaction produces growing unsaturated polymer chains that retain the functionality and symmetry of the monomer. Although the intricacy and sophistication of ADMET polymers have increased dramatically in recent years, the reaction's basic nature has not changed from when it was first successfully conducted [61,62].

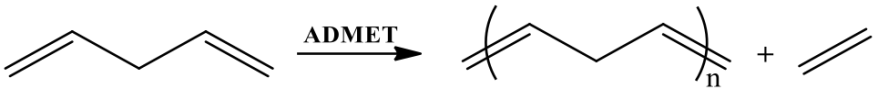

Scheme 2.5: Representation of acyclic diene metathesis reaction

Another olefin polymerization method is the ring opening metathesis polymerization (ROMP) which is a chain growth technique (see Scheme 2.6 for an example of ROMP). It involves the ring opening metathesis of a cyclic olefin resulting to repeating unit cell polymers. ROMP affords polymer chemists the luxury of producing polymers with regular chemical structure, well defined morphology, controlled molecular weight distribution and phase transition [63,64]. In 2020, Liang and co-workers adopted ROMP using low ring strain diazaphosphepine-based cyclic olefin in the synthesis of degradable polyphosphoramidate with Grubbs' catalyst third generation (**GIII**), which can be used to prepare micellar nanoparticles [65]. Other monomers, including δ-pinene [66], cyclic phosphates [67], silyl ether [68], levoglucosenol, 1,2-bis(3-thienyl)cyclopentene [69], and cyclic enol ethers [70], have been reported in the preparation of degradable polymers via ROMP.

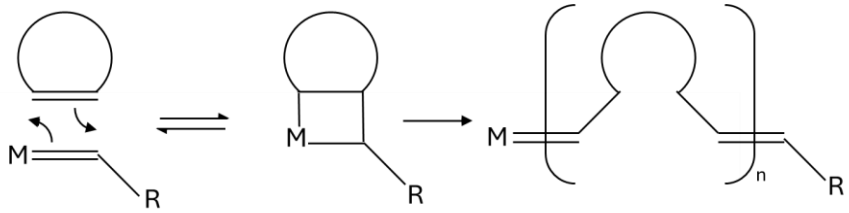

Scheme 2.6: Representation of ring opening metathesis polymerization (ROMP)

Ene-yne metathesis (EYM) has a similar mechanistic approach to alkene metathesis, although, it has received less attention by researchers compared to alkene metathesis statistically. It is a reaction that involves bond redistribution between an alkene and an alkyne to produce a 1,3-dienes (see Scheme 2.7 for an example of EYM) [71]. Atom economy is promoted in EYM because it is driven by the enthalpic stability of the formed conjugated 1,3-dienes. The fascinating part of EYM reactions is that it can be catalysed by metal carbenes especially Grubbs' – and Hoveyda-Grubbs' catalysts like other types of olefin metathesis reactions [72]. Rohde and Diver carried out a catalyst screening and optimization study between styrene and alkyne in a cross ene-yne metathesis (EYCM). Although unbranched terminal alkynes are prone to complications during cross-metathesis due to competing alkyne oligomerization. This setback is obviated when Grubbs catalyst with high steric demand was used. Subsequently, they were used for the synthesis of several terminal alkynes that usually give a low yield under standard conditions [73,74].

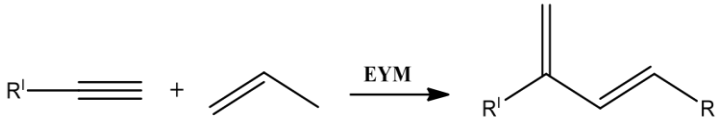

Scheme 2.7: Representation of ene-yne metathesis reaction

2.3 Metathesis mechanism

Various researchers thoroughly investigated the mechanistic route of the metathesis reactions, and their efforts significantly contributed to the success of metathesis reactions decades ago [11,75–78] and until now the generally accepted proposed mechanism involving the coordination of an olefin to a metal carbene via the metallacyclobutane intermediate which is applicable to all types of metathesis reactions is Chauvin's mechanism [7]. In this Chauvin mechanism (Scheme 2.8), the starting metal-alkylidene (**1**) react with an olefin (**2**) to form the metallacyclobutane intermediate (**3**). This intermediate can either proceed to form ethylene (**4**) and a secondary metal-alkylidene (**5**). Conversely, (**3**) can reversibly retreat to the primary metal-alkylidene (**1**) and the initial substrate olefin (**2**). The secondary metal-alkylidene (**5**) consist of the metal, its ligands (denoted by the brackets around the metal), and the alkylidene from the substrate olefin. Another olefin (**6**) can be introduced into the cycle to finally form the metathesis product (**9**) and the starting metal-alkylidene (**1**), and the cycle can start again [79]. A mixture of olefins in equilibrium gets formed while the catalytic cycle progresses, and thermodynamic parameters define the final product ratio.

To alter the equilibrium in the direction of the desired products, for example, one of the olefins (**4**) can be removed from the system if it is volatile [7].

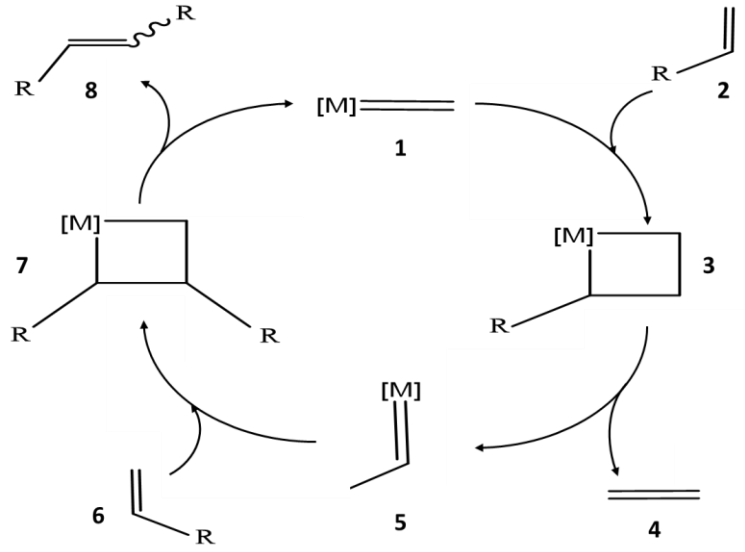

Scheme 2.8: Chauvin's proposed metathesis mechanism

2.4 Catalyst for metathesis reactions

2.4.1 Schrock catalyst

There were three thought-provoking ideas that motivated Richard Schrock to investigate and develop a suitable catalyst for metathesis reactions. Wilkinson categorically abolished the narrative that transition metal to carbon single bond is essentially weak and suggested that metal-carbon double bonds should be explored in homogenous catalysis in his shared Nobel prize lecture with E.O. Fischer in 1973 [80]. Fischer and his group's extensive research led to the discovery of transition metal carbene and carbyne complexes. At that time, there is no catalytic reaction where either of these complexes have been employed as catalyst [81]. Ultimately, Schrock's interest in organometallic chemistry, particularly with transition metal and homogenous catalysis, was affirmed when he joined DuPont De Nemours and company. This field held significant potential for applications in industry and medicine, gathering substantial attention from organic chemists. Schrock proceeded to explore the organometallic chemistry of Tantalum (Ta). Ta in its highest possible oxidation state of +V interested him due to its inherent stability. Additionally, Schrock sought to employ the neopentyl ligand (CH_2CMe_3) to investigate the extent of steric hinderances

in homoleptic d^0 tantalum pentaalkyls and the possible decomposition pathways as highlighted in Gordon Juvinall's paper [82].

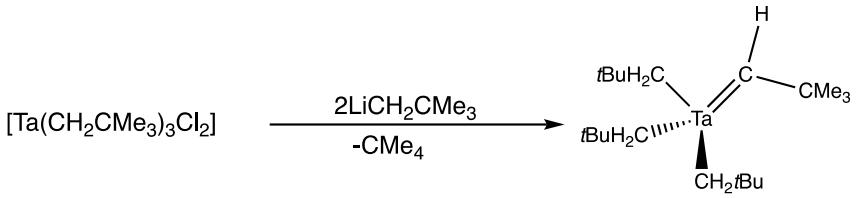

Scheme 2.9: Synthesis of the first stable metal carbene

In an experimental attempt to prepare [Ta-$(CH_2CMe_3)_5$], two equivalents of [$LiCH_2CMe_3$] was reacted with [Ta-$(CH_2CMe_3)_3Cl_2$] in an addition reaction. Contrary to the expected product [Ta-$(CH_2CMe_3)_5$], a quantitative yield of an orange, crystalline and thermally stable [$(Me_3CCH_2)_3Ta{=}CHCMe_3$] was formed. Fortunately, this tantalum neopentylidene complex is the first stable transition metal M=CHR (Scheme **2.9:** Synthesis of the first stable metal carbene

2.9) and its terminal alkylidene was produced through an α-hydrogen abstraction from an alkyl. The high thermal stability, resistance to intermolecular decomposition, and further intramolecular reactions of [$(Me_3CCH_2)_3Ta{=}CHCMe_3$] led to the emergence of other high-oxidation-state, four-coordinate species with four sterically demanding covalently bound ligands [83].

It was hypothesised that a neopentylidene ligand might be further deprotonated by an external base as an outcome of the "deprotonation" of a neopentyl ligand to produce a neopentylidene ligand. In fact, the first analogous high-oxidation-state, anionic, neopentylidyne species was formed when n-butyllithium was added to [$(Me_3CCH_2)_3Ta{=}CHCMe_3$] [84].

Schrock interest centred on the metathesis potential of alkenes and alkynes with tantalum neopentylidenes and neopentylidynes. Alongside this, he investigated the unexplored high oxidation state class of tantalum carbene and carbyne complexes driven by the absence of known "carbyne' complex capable of catalysing alkyne metathesis. Contrary to the anticipated formation of a metallacyclobutane intermediate, which was expected to form through the loss of an olefin and creation of a new alkylidene, as proposed in Chauvin's mechanism, a surprising discovery was made. It was found that when electron deficient tantalum and niobium alkylidene complexes, containing chloride ligands, reacted with olefins, they underwent a rearrangement process via β-hydride transfer. This led to the generation of several potential rearrangement products, as no

metathesis product was observed during the reaction. To address this shortcoming, Schrock employed niobium and tantalum complexes containing *tert*-butoxide ligands (Scheme **2.10:** Synthesis of an electron deficient tantalum-neopentylidene catalyst

2.10) because *tert*-butoxide ligands inhibit metal reduction and favours metathesis reactions such as *cis*-2-pentene [85].

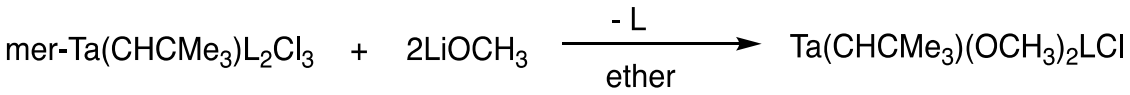

Scheme 2.10: Synthesis of an electron deficient tantalum-neopentylidene catalyst

In an unexpected outcome, Schrock and his group unintentionally produced an 18-electron oxo tungsten carbene complex while attempting to synthesize a tungsten-oxo-alkylidene complex from a tantalum neopentylidene complex and a tungsten-oxo complex (Scheme **2.11:** Synthesis of Tungsten-oxo-neopentylidene complex (L = PEt3, etc.)

2.11). This unexpected compound, formed in the presence of trace amount of $AlCl_3$, and proved to be an effective in catalysing metathesis reactions involving both internal and terminal olefins. It was proposed that the role of the $AlCl_3$ was to remove either a phosphine- or a chloride ligand from the metal, creating an empty coordination site for metathesis reactions to take place [86].

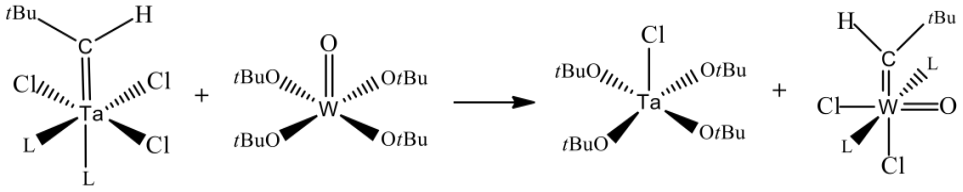

Scheme 2.11: Synthesis of Tungsten-oxo-neopentylidene complex (L = PEt3, etc.)

In other investigations of ligands with strong electron withdrawing properties, hexafluoro-*tert*-butoxide has been reported to have the highest activity; Schrock therefore focussed on synthesizing Mo analogous of this ligand $[Mo(NAr)(CHCMe_2Ph)[OCMe(CF_3)_2]_2]$ since a molybdenumcyclobutane has a better tendency to lose an olefin, preserving the Chauvin mechanism and ensuring its efficiency for metathesis reactions. The highly electron withdrawing $OCMe(CF_3)_2$ group in the Mo bisalkoxide catalyst known as Schrock's catalyst makes it

remarkably potent for a wide range of metathesis reactions [87,88]. Figure 2.1 illustrates the structures of the commercially available Schrock catalysts.

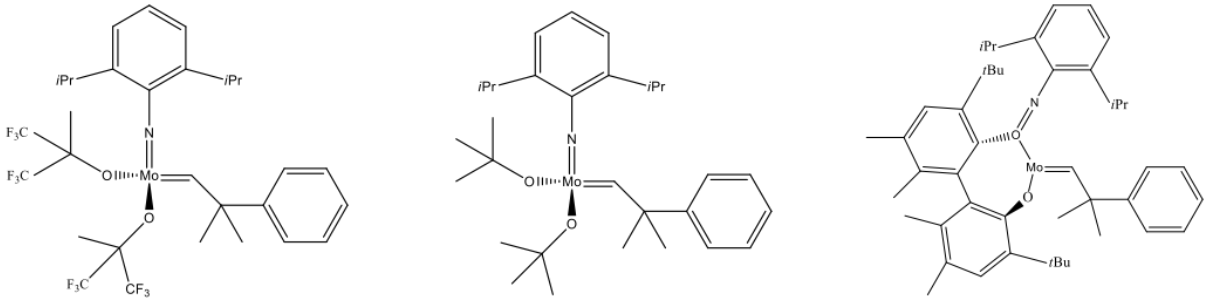

Figure 2.1: Commercially available Schrock's metathesis catalyst

2.5 Grubbs' Catalysts

Prior research conducted by various researchers in the field of metathesis catalyst development played a pivotal role in directing the research efforts of Robert Grubbs and his group. This prior work enabled them to focus their metathesis investigation on enhancing the catalyst performance in terms of activity, selectivity, stability, and the ability to tolerate a broad range of functional groups while operating under milder conditions.

One of these research investigations were that of Michelotti *et al.* who reported the use of hydrated trichlorides of ruthenium, osmium, and iridium to promote the polymerization of norbornene and its derivatives resulting in high molecular weight materials [89]. Novak and Grubbs, inspired by Michelotti's work, employed these systems to promote the formation of poly-7-oxo-norbornenes as they realized that ruthenium (II) complexes could be a better active catalyst for polymerization [90]. Their investigations produced a catalyst system with better tolerance for most functional groups and aqueous media. However, they did have a few setbacks; the catalytic intermediates are highly active with very low concentrations in their reaction mixture, characterizing them is challenging and the structure of the active catalyst is unknown which makes tweaking the catalyst impossible [89,91]. They assumed the formation of a metal carbene is requisite for olefin metathesis to occur. Hence the development of Ru carbene complexes with a well-defined structure and stability to both protic/aqueous solvents were imperative for further catalyst modification. Few years of intense investigation by Nguyen and Grubbs resulted in the first air stable carbene complex prepared from the reaction between $[RuCl_2(PPh_3)_3]$ and 3,3-

diphenylcyclopropene (Scheme **2.12:** Synthesis of the first well-defined ruthenium carbene catalyst

2.12) [91].

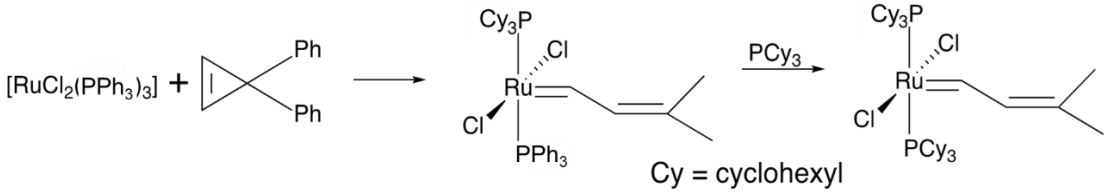

Scheme 2.12: Synthesis of the first well-defined ruthenium carbene catalyst

The metathesis activity of this ruthenium carbene catalyst (the synthesis is shown in Scheme **2.12:** Synthesis of the first well-defined ruthenium carbene catalyst

13) was restricted to the ring-opening metathesis polymerization of highly strained monomers, even though it demonstrated stability to a variety of functional groups. Further modification via ligand exchange by replacing the triphenylphosphine (PPh_3) ligands with less basic phosphine ligands, such as tricyclohexylphosphine (PCy_3), improved the activity of the catalyst for olefin metathesis and ROMP with lower strained monomers (see Figure 2.2 how the activity changes with the different ligands).

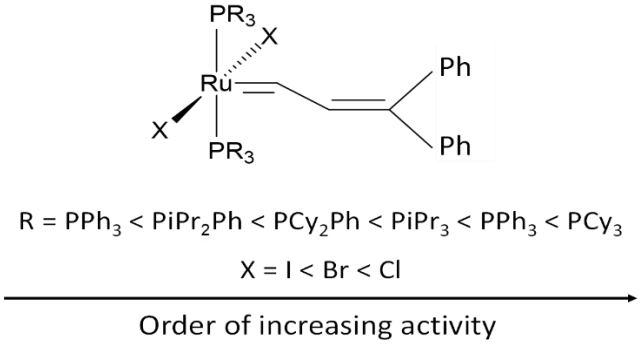

Figure 2.2: Series of ruthenium-carbene olefin metathesis catalysts, indicating the order of increasing activity for the derivatives

In 1995 Schwab, while working with Grubbs, reported a series of well-defined alkylidene Ru complexes employing diazoalkanes as an alternative carbene source [92]. Following phosphine ligand exchange of $[RuCl_2(PPh_3)_3]$, the resulting compound was reacted with phenyldiazomethane

accompanied which produced the air stable [$RuCl_2$(=CHR`)(PCy_3)$_2$], Grubbs' catalyst first generation (**GI**), known as the first-generation Grubbs' catalyst which is commercially available. **GI** has proven to be a highly active catalyst for metathesis reactions including ROMP, RCM, and metathesis of acyclic olefins [93,94]. The need for commercially available catalysts increased along with the rate of research being conducted on ruthenium catalysed metathesis. Grubbs *et al*.'s mechanistic research revealed that ruthenium interacts very differently from early transition metals [17]. One of these observations was that ruthenium, being high in d electrons, prefer strong electron-donating ligands as opposed to electron-withdrawing ligands. Further tuning of **GI** through the substitution of one of the phosphine ligands with an *N*-heterocyclic carbene (NHC) ligand resulted in a series of highly active catalysts. Among this series of catalysts is the commercially available second-generation Grubbs' catalyst, **GII**. **GII** displayed a better activity in a wide range of metathesis reactions including electron deficient and sterically demanding olefins and it showed an increased rate of catalyst turnover compared to **GI** [18].

Despite recent advancements, pursuit of creating a new, highly efficient ruthenium complex for cross-metathesis of functionalized olefins prompted the tuning of L-type ligands in [(H_2IMes)(PCy_3)(Cl_2)Ru=CHP]. This was done because the rate at which ligands dissociate are related to catalyst efficiency. During mechanistic studies of Ru-catalysed transformations, conducted by the Hoveyda group, they discovered that ROMP catalysed by **GI** was not as effective when 2-isoproposystyrene was present. They proposed that a Ru-chelate complex formed. This prompted the preparation of a new type of Ru complex that possesses an internal metal-oxygen chelate. The Hoveyda-Grubbs first generation catalyst (**HGI**) was synthesised through catalyst modification of **GI**. The tricyclohexylphosphine ligands was exchange with a bidentate styrenyl ligands to form **HGI** (Scheme **2.13:** Initial synthesis of Hoveyda-Grubbs first generation catalyst 2.13).

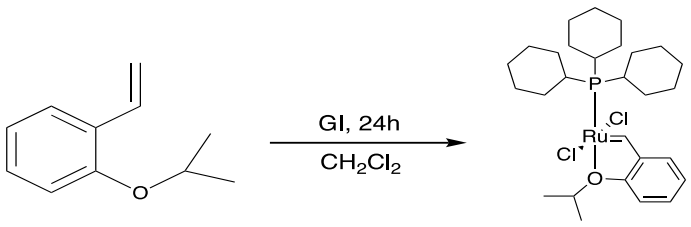

Scheme 2.13: Initial synthesis of Hoveyda-Grubbs first generation catalyst

HGI is an active metathesis catalyst especially for RCM of dienes that have double bonds. As an example, and as depicted in Scheme 2.14: An example of ring closing metathesis catalysed by HGI

2.14, Hoveyda *et al*. observed a 100% conversion for the RCM of 2-buteny-(1-phenyl) allyl ether to produce 2-phenyl-2,5-dihydrofuran catalysed by **HGI**. Additionally, it has the added practical advantage of being reusable and can be recovered in high yield by chromatography [95].

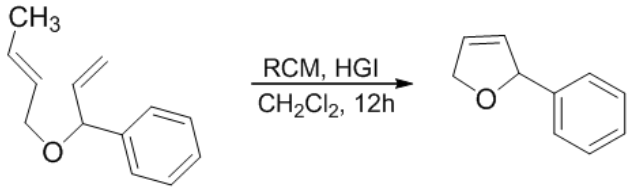

Scheme 2.14: An example of ring closing metathesis catalysed by HGI

Regardless of the advantageous attributes, **GI** and **HGI** are only efficient for substrates that contain terminal olefins and recovery of **HGI** is complicated. To enhance the catalytic activity and to address the issue of ease of recovery, Hoveyda and his group adopted a bidentate ligand, 2-isopropoxystrene, to modify **GII** (Scheme **2.15:** Synthesis of Hoveyda-Grubbs second generation catalyst

2.15). This resulted in the first recyclable metathesis catalyst which is now conventionally known as Hoveyda-Grubbs' second generation catalyst **HGII** [96].

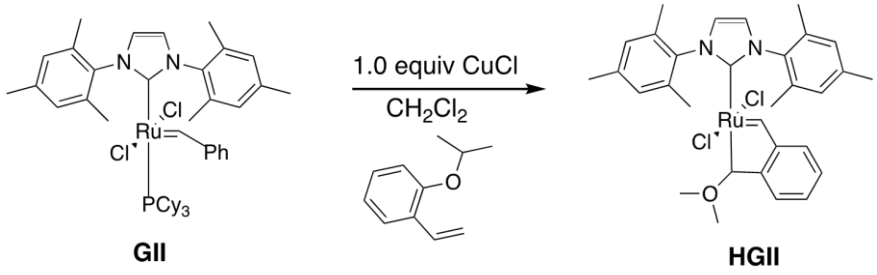

Scheme 2.15: Synthesis of Hoveyda-Grubbs second generation catalyst

Schrock's imido alkylidene catalyst and **HGII** is the only reported catalysts to successfully promote acrylonitrile cross-metathesis with slow dissociation rates. It was reported that the nature of ligands influences the rates of initiation, dissociation, and the rebinding of ligand, all related to the catalyst efficiency [87]. The Grubbs group prepared a series of bispyridine complexes by adding

an excess of appropriate pyridine to **GII** (Scheme **2.16:** Synthesis of series of bispyridine complexes

2.16), and the initiation rate of these classes of pyridine-ligated Ru alkylidene complexes was measured by both NMR spectroscopy and UV-Vis kinetic studies.

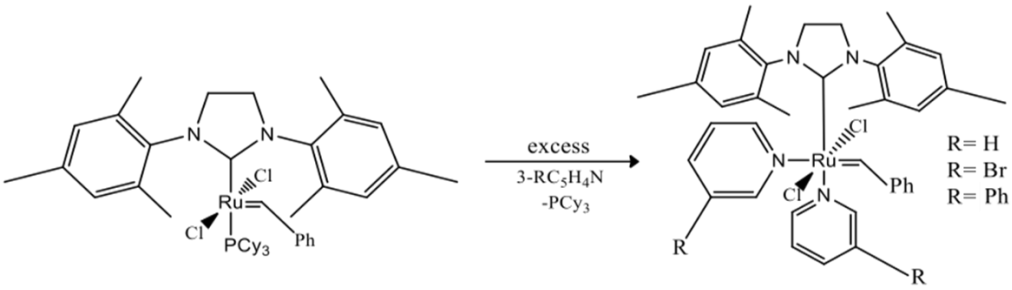

Scheme 2.16: Synthesis of series of bispyridine complexes

Comparison of the bispyridine complexes' catalytic activity to mediate CM between acrylonitrile and allylbenzene revealed that the 3-bromopyridine derivative gave the best yield. It has the best catalyst turnover because the electron deficient 3-bromopyridine dissociates very rapidly from the Ru centre and the rebinding is slow compared to others. It has been categorized as the fastest initiator of any Ru-based catalyst for the metathesis of simple olefins and conventionally known as third generation Grubbs catalyst **GIII** (see Figure 2.3) [97]

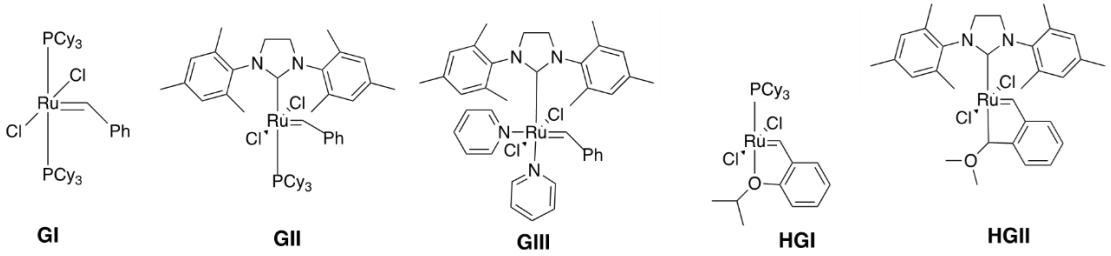

Figure 2.3: Some of the commercially available Ruthenium metathesis catalysts

Even though a myriad of research has been carried out to enhance these catalysts via structural transformation, but none of them are easily accessible and commercially viable; as a result, they are not addressed in greater detail in this review [4,32,47,97–103]. Our focus will be on the commercially available Schrock and Grubbs catalyst and the additive route is a simple and very efficient means of upgrading the performance of these catalyst.

2.6 Additives effects on metathesis reactions

2.6.1 Types of additives as co-catalyst

Continuous effort to reduce production cost of bulk chemicals, which is largely dependent on catalyst activity and lifetime, has inspired chemists to investigate ways to improve catalyst properties. To enhance the activity and lifetime of the existing commercially available ruthenium-based catalyst for olefin metathesis transformations, chemists have investigated catalyst modification or altered reaction conditions. In this review, our focus is to extensively discuss the use of additives in olefin metathesis reactions employing Grubbs' – or Schrock's catalysts.

Additives for the purpose of this review are defined as chemical species that are added to an existing (Grubbs or Schrock) catalyst to either improve its efficiency or stabilize the active catalyst specie, resulting in the extension of the life cycle of the catalyst or through suppression of other non-metathetic reactions like olefin isomerization that compete with desired metathesis product formation. Additives do not modify the catalyst through ligand displacement but rather interacts with the catalyst through van der Waals bonds or assist with ligand dissociation of the catalyst. Alcohols, salts, phosphines, and organic dienes are often used as additives in metathesis reactions.

2.6.2 Additives to Grubbs' catalysts

2.6.2.1 Salts

In 1997, Robert H. Grubbs and his co-workers investigated the mechanism and activities of several ruthenium-based olefin metathesis catalysts of the formula $(PR_3)_2X_2Ru{=}CHCHCPh_2$ by monitoring the RCM of acyclic diene diethyl diallymalonate. They reported that the addition of CuCl to a ring closing reaction (see Scheme 2.4 as an example of RCM) catalysed by $(PR_3)_2X_2Ru{=}CHCHCPh_2$ tremendously increased the rate of olefin metathesis (see Figure 2.4). Since a dissociative pathway is responsible for 95% of metathesis in this system, the addition of CuCl drives the equilibrium for phosphine dissociation by reacting with the phosphine to form an insoluble, ill-defined complex [94].

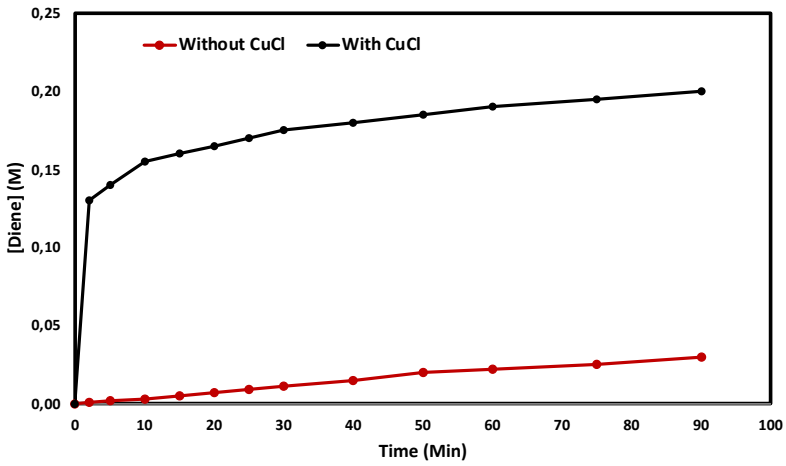

Figure 2.4: Graph of diene concentration against time. Red-without CuCl, Black-with CuCl

To determine whether a redox process or phosphine scavenging by Cu could be responsible for the enhanced catalytic activity, they employed another Cu salt, $CuCl_2$ that react with phosphine in a similar manner. The results revealed that both CuCl and $CuCl_2$ are phosphine scavengers and favours the dissociative mechanism pathway. Previously inactive catalysts could now carry out the ring-closing reaction because, in the presence of Cu-salts, the rate of metathesis by slower catalysts rivalled that of the faster catalysts examined. The exact nature of the generated specie upon addition of CuCl could not be determined but it was suggested that bimetallic copper ruthenium species $CuCl{\cdot}PR_3$ through chelation of the chloride ligands bridging with the metal centre might be the responsible [94,104].

In a study by Meyer and his groups, the addition of metal halides has positively improved the catalyst performance of **GI** in the SM of 1-octene to produce 7-tetradecene and ethene (Scheme **2.17:** Self metathesis of 1-octene to give 7-tetradecene and ethene (R = $(CH_2)_5CH_3$)

2.17).

In the SM of 1-octene, the selectivity of **GI** towards the desired product was compromised by the formation of octene isomers catalysed by the decomposed **GI** catalyst specie. This decomposition of **GI** was alleviated by the addition of tin(II) chloride hydrate as a stabilizing agent, which resulted in an isomerization free system and invariably increase the lifetime of **GI**. Since the hydrated salt was beneficial, the anhydrous salts were also explored to eliminate any effect of water and it was found that using the anhydrous salts conversion and selectivity were better. Other additives and

reaction conditions for **GII** catalysed SM of 1-octene were also investigated, see **Error! Reference source not found.** for the results [105].

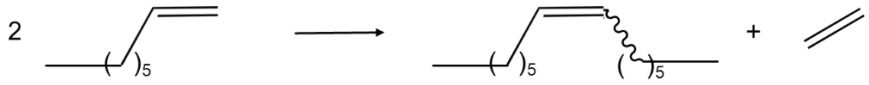

Scheme 2.17: Self metathesis of 1-octene to give 7-tetradecene and ethene (R = $(CH_2)_5CH_3$)

Table 2.1: Conversion and selectivity towards the formation 7-tetradecene after 6 h under different conditions

Entry	Catalyst	Additive[a]	Temperature (°C)	Conversion (%)	Selectivity (%)
1	**GI**	None	50	26	90
2	**GI**	$SnCl_2.2H_2O$	30	26	97
3	**GI**	$SnCl_2.2H_2O$	40	55	97
4	**GI**	$SnCl_2.2H_2O$	50	69	98
5	**GI**	$SnCl_2.2H_2O$	60	30	75
6	**GI**	$SnCl_2$	50	58	>99
7	**GI**	$SnBr_2$	50	72	>99
8	**GI**	SnI_2	50	4	>99
9	**GII**	None	40	76	98
10	**GII**	$SnCl_2$	40	78	98
11	**GII**	$SnBr_2$	40	80	99
12	**GII**	SnI_2	40	78	>99

[a] 20 equivalent.

The reported beneficial effect of metal halides as additives in metathesis reaction catalysed by ruthenium-based olefin metathesis catalyst has been corroborated by Lipshutz and his group. They explored the addition of different Cu(I) salts and found that CuI resulted in the highest conversion (Scheme **2.18:** Cross-metathesis between TBS-protected allylphenol and MVK for additives effect 2.18 and

Table 2.**2**). When employing CuI as the additive, non-chlorinated solvents and other reaction conditions were varied to obtain the best condition for optimal conversion and product yield (

Table 2.**2**). Under these newly developed conditions, cross-coupling of several different olefins were successful. High isolated yields were achieved even for difficult reactions like acrylic acid and methyl vinyl ketone (MVK).

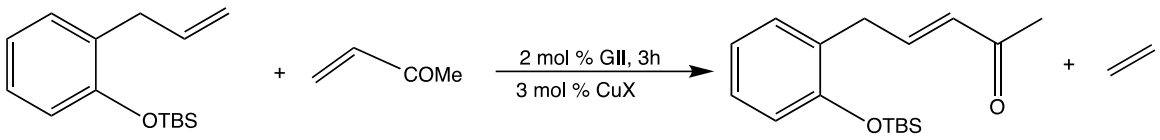

Scheme 2.18: Cross-metathesis between TBS-protected allylphenol and MVK for additives effect

Table 2.2: Optimizing reaction conditions

Entry	Additive	Solvent[a]	Conversion (%)[b]
1	No additive	Dichloromethane	45
2	Copper(I) cyanide	Dichloromethane	24
3	Copper(I) chloride	Dichloromethane	35
4	Copper(I) bromide	Dichloromethane	43
5[c]	Copper(I) Iodide	Dichloromethane	63
6[d]	Copper(I) Iodide	Dichloromethane	68
7	Copper(I) Iodide	Toluene	64
8	Copper(I) Iodide	Tetrahydrofuran	70
9	Copper(I) Iodide	Ethanol	71
10[e]	Copper(I) Iodide	Ethanol	76
11[f]	Copper(I) Iodide	Ethanol	85
12	No additive	Ethanol	43

[a]Reaction run in 0.5 M solution. [b]Based on 1H NMR. [c]Using 6 mol % CuI. [d]Using 3 mol % **GII** and 6 mol % CuI. [e]Reaction run in 0.2 M solution. [f]Reaction run 0.1 M solution; without CuI; isolated yield = 57%.

The NMR study data showed that both CuI and NaI had better conversion rates of *ca.* 57% isolated yield for the metathesis reaction between TBS-protected allylphenol and MVK catalysed by **GII** (Scheme **2.19:** Comparisons of NaI vs CuI as additive in **GII** catalysed olefin cross-metathesis 2.19) in diethyl ether compared to the 43% conversion in the absence of these additives. Studies conducted on other MVK olefin derivatives, e.g. methyl acrylate and acrylic acid, gave different results depending on the solvents employed for the reactions, but the influence of the additives were still imperative. The presence of copper iodide in ether appears to exhibit a dual role: it stabilizes the ruthenium through ligand effects and facilitates the phosphine dissociation from the ruthenium, effectively doubling the turnover of the **GII** catalyst (Table 2.3) [2,52].

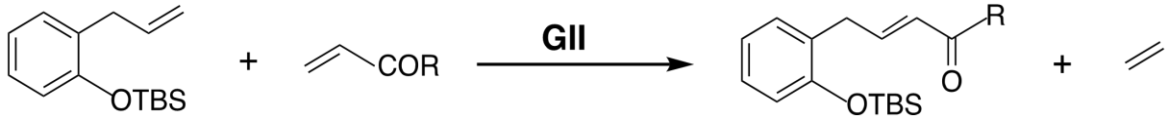

Scheme 2.19: Comparisons of NaI vs CuI as additive in **GII** catalysed olefin cross-metathesis

Table 2.3: Comparisons of NaI *vs* CuI as additive in **GII** catalysed olefin cross-metathesis.

Entry	R	Additive	Solvent	Conversion (%)
1	CH_3	NaI	Et_2O	100
2	CH_3	CuI	Et_2O	100
3	OCH_3	CuI	DME	48
4	OCH_3	NaI	DME	67
5	OCH_3	NaI	Et_2O	100
6	OCH_3	CuI	Et_2O	100
7	OH	NaI	Et_2O	64
8	OH	CuI	Et_2O	100

The beneficial effects of additives were extended to polyfunctionalized arenes, where two different tetrasubstituted benzenes were produced from the same starting material catalysed by **GII** with Cu salts. Understanding of the catalyst structure and tuning the catalytic active sites guaranteed the pathway to have the different products activated by different additives. Since the mechanism of **GII** revealed that the dissociation of a phosphine ligand creates a coordination site, which is required to propagate enyne metathesis while retaining both the Cl and carbene ligands to maintain the catalyst stability and reactivity. From previous reports, CuI is a good additive which will aid the dissociation of PCy_3 [2,94]. Both the enyne metathesis product **10** (22 %) and the non-metathesis product **11** (48 %) were observed in the treatment of diphenylacetylene **9** with **GII** without additives (Scheme **2.20:** Enyne metathesis of diphenyl acetylene mediated by **GII** (DMAD = dimethyl acetylenedicarboxylate)

2.20).

Several Cu salts were investigated but CuI used in the optimum mol % promoted the efficiency and selectivity to produce 1,2,4,5-tetrasubstituted benzene (Scheme **2.20:** Enyne metathesis of diphenyl acetylene mediated by **GII** (DMAD = dimethyl acetylenedicarboxylate)

2.20 and Table 2.4). CuI as additive also promoted enyne metathesis of both symmetrical and unsymmetrical alkynes with electron withdrawing groups or electron donating groups to produce the desired product with excellent isolated yields [106].

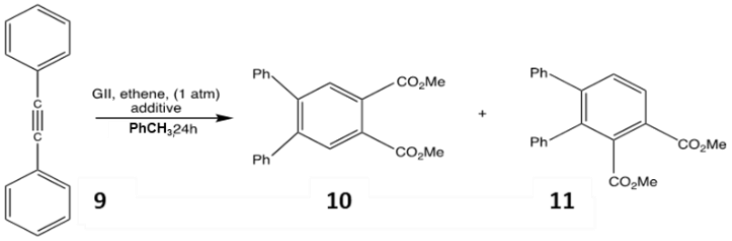

Scheme 2.20: Enyne metathesis of diphenyl acetylene mediated by **GII** (DMAD = dimethyl acetylenedicarboxylate)

Table 2.4: The effect of additives on product distribution from the same starting materials

Entry	**GII** (mol %)	Additives (mol %)	**10**[a] (%)	**11**[a] (%)
1	5.0	-	22	48
2[b]	5.0	CuCl (5.0)	18	8
3[b]	5.0	CuBr (5.0)	16	7
4	5.0	CuI (5.0)	59	6
5	5.0	CuI (5.0)	59	6
6	5.0	CuI (5.0)	69	<5
7	10.0	CuI (5.0)	85	5
8	10.0	CuCl (5.0)	85	5

The reactions were performed in a 0.125 mmol scale of **10** at 80 °C and 2.5 mL toluene was used. [a]Isolated yield. [b]0.25mmol **10** and 5 mL of toluene was used.

2.6.2.2 Phenols and alcohols

Forman and Tooze reported how the addition of *p*-cresol improved the performance of CM reaction between acrylate esters and olefins catalysed by **GII**. The invention of **GII** made the hitherto impossible CM between terminal olefin and an electron withdrawing functionalized such as α, β-unsaturated carbonyl compounds possible. High catalyst loading and low catalyst turnover are the setbacks of the reaction, but the addition of phenols allowed for lower catalyst loading and greatly improved the efficiency resulting in increased product yield and selectivity. They described from a mechanistic study, including NMR spectroscopy and DFT calculations, that phenol improves the active metathesis cycle and formed a hydrogen bond coordination of phenol to the chlorine in the active catalyst intermediate of **GII** (Scheme 2.21) [53,107]. Further investigation by Erasmus's group demonstrated that the addition of *p*-cresol to **GII** assists the cross-metathesis of acrylates with prop-1-en-1-ylbenzenes under conditions that would conventionally result in only the self-metathesis product of prop-1-en-1-ylbenzene. Spectroscopic analyses supported the formation of a ruthenium benzylidene-*p*-cresol adduct, influencing the electronic properties of the

catalyst and promoting cross-metathesis. Table 2.5 showed the comparative results of a series of CM reactions between acrylate esters and olefins using **GII** in the presence and absence of *p*-cresol [37].

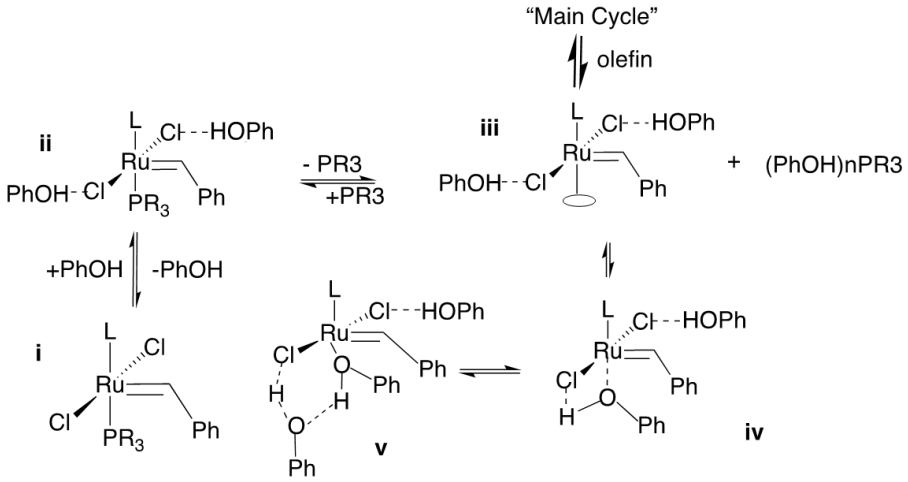

Scheme 2.21: Proposed mechanism for the formation of hydrogen bonds between phenols and the chloride ligands of the catalyst [37,107,108].

Table 2.5: Series of CM reactions catalysed by **GII** with and without an additive (*p*-cresol)

Entry	CM Partner Y	CM Partner Z	Ratio (Y:Z)	Cat. (Mol%)	% conv.	% conv. With additives
1	Methyl acrylate	1-decene	2:1	0.10	24	100
2	Methyl acrylate	1-decene	2:1	0.05	56	97
3	Methyl acrylate	1-decene	2:1	0.025	58	96
4	Methyl acrylate	1-decene	2:1	0.00625	47	71
5	Ethyl acrylate	1-decene	2:1	0.05	43	95
6	Methyl acrylate	Styrene	2:1	0.025	24	66
7	Methyl acrylate	Styrene	2:1	0.00625	16	57
8	Methyl acrylate	Styrene	2:1	0.025	8	40
9	Methyl acrylate	Methyl oleate	4:1	0.0125	45	82

The addition of *p*-cresol significantly increased the conversion rate for all the reported reactions. It is crucial to note that the phenol derivative addition only has a beneficial effect on CM reactions involving acrylate esters, and not CM reactions involving acrylonitrile, allyl acetate and 1,1-disubstituted olefins. Conclusively, the influence of phenols e.g., *p*-cresol was most pronounced

in the **GII** catalysed CM reaction involving acrylate esters by enhancing the activity, selectivity, and lifetime of the catalyst [53].

Ene-yne CM remains an indispensable synthetic method for producing conjugated 1,3-diene which is present in many bioactive natural products. Positional dienyl isomerization involves the conversion of 1,3-dienes to highly functionalized 1,3-dienes (Scheme 2.22). This method offers a novel approach that allows for an extensive range of diene substitution patterns, in contrast to the more limited substitution pattern attained through ene-yne metathesis. Ruthenium hydrides are known to promote dienyl isomerization, since Grubbs ruthenium carbenes are converted to ruthenium hydrides by primary alcohol, addition of alcohol increases the isomerization yield. Without the additives minimal conversion of the substrate with low product yield was observe, additionally aldehyde containing side products was formed. Through prior knowledge that ruthenium hydrides initiate dehydrogenation of alcohol, it is suggested that the oxidation of alcohol can be minimized by the addition of alcohol under the catalytic condition. When different alcohol additives were screened for the beneficial effect on dienyl isomerization, it was found to significantly improve conversion rate and product yield (see Table 2.6) [109].

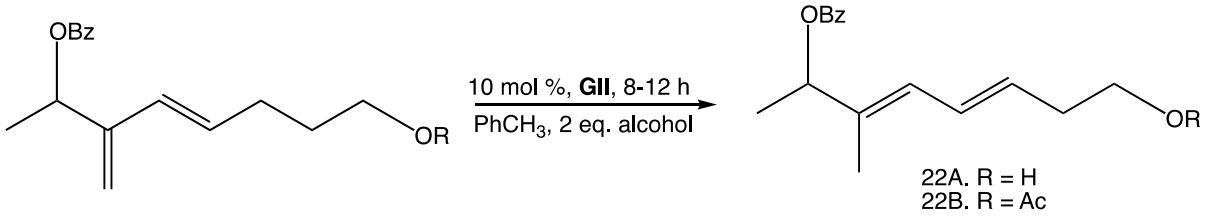

Scheme 2.22: An example of dienyl isomerization catalysed by **GII** with an alcohol as additive (R = H or CO(CH3))

Table 2.6: Screening of alcohol additives effect on dienyl isomerization catalysed by **GII** for the reaction displayed in Scheme 2.22**:** An example of dienyl isomerization catalysed by **GII** with an alcohol as additive (R = H or CO(CH3))

, using 0.05 M of the diene in toluene. % Conversion and ^{1}H NMR yield vs mesitylene as an internal standard is reported.

Entry	Reactant	Additive	Conversion %	22 %
1	**12a**	None	60	40
2	**12a**	1-butanol	100	75
3	**12b**	1-octanol	100	65
4	**12b**	2-propanol	80	70

5	**12b**	Cyclohexanol	100	80
6	**12b**	Tert-butanol	10	10
7	**12b**	Phenol	10	10
8	**12b**	1-butanol	97	80

Fogg adopted the use of poly(vinyl phenol) resins as additive to promote **GII** in the CM of anethole and 2-ethylhexyl acrylate to evaluate their impact on product yield and selectivity in comparison to *p*-cresol (scheme 2.23). Near quantitative conversion was achieved with >85% selectivity towards the desired CM product, cinnamate. Small amounts of the undesired CM product, anisole, and the SM product, stilbenoid, was also detected (Scheme 2.23 and Table 2.7). An important part of the methodology is the purging of the reacting system with argon to remove the volatile olefins such as ethene and propene. This minimizes the secondary/tertiary metathesis reactions which favours the formation of **23B** over **23A** and further inhibits catalyst decomposition [110,111].

Shown in **Table 2.6**Table 2.7 (entry 1) in the absence of phenol, the isolated yield of **23A** was 85%. As expected, the yield of **23A** increased to 96% upon the addition of 100 equivalents of *p*-cresol. It was envisaged that the different structural features in the poly(vinylphenol) resins might interfere with accessing the phenol sites, however the % conversion and selectivity were almost identical for the phenol resins as compared to *p*-cresol (entries 3-5). Since 100 equivalents of the phenol resins to catalyst gave the highest yield of 96% (entry 5), the effect of different equivalents was investigated. Increasing the ratio of the poly(vinyl phenol) resins to 500 eq or decreasing it to 50-fold resulted in a slightly lower yield of 92% (entries 6) and 91% (entries 7), respectively. For subsequent studies, the equivalents of the additive were maintained at 100. Quenching the reaction of entry 5 at 1 h (entry 8) revealed complete consumption of the limiting reagent (anethole) and fragments of anisole **23B** and stilbenoid **23C** were detected [108].

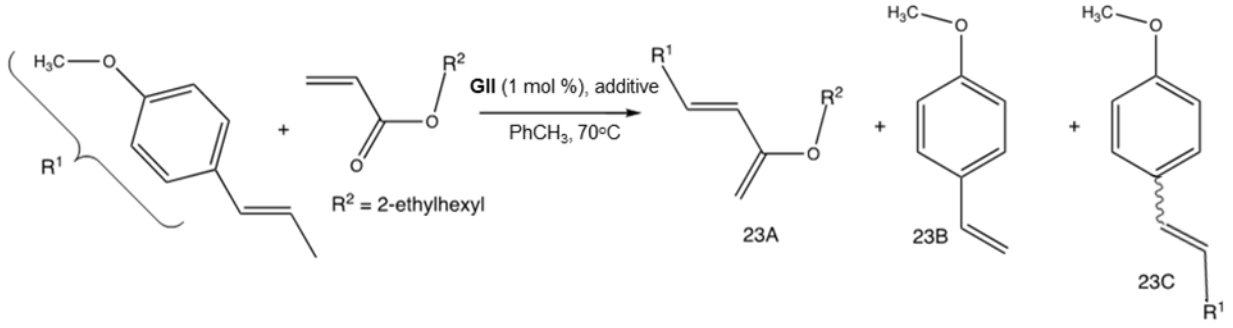

Scheme 2.23: Cross-metathesis of *trans*-1-methoxy-4-(1-propenyl)benzene and 2-ethylhexyl acrylate catalysed by **GII** in the presence of poly(vinyl phenol) resins as an additi

Table 2.7: Summarised data for phenol resins enhancement of the productivity of **GII** for CM of *trans*-1-methoxy-4-(1-propenyl)benzene (TA) and 2-ethylhexyl acrylate (EHA) as demonstrated in scheme 23[a]

				Yield %[b]		
Entry	Phenol	Phenol equiv.	Conversion %	**23A**	**23B**	**23C**
1	none	none	99	85	3	11
2	*p*-cresol	100	100	96	2	2
3	PVP- 11	100	99	94	4	2
4	PVP- 25	100	100	95	3	2
5	PVP-MMA	100	100	96	2	2
6	PVP-MMA	500	100	92	4	4
7	PVP-MMA	50	100	91	3	6
8	PVP-MMA	100	100	88	7	5

[a]Conditions: 4 equiv EHA vs TA, 1 mol % **GII**, 1,2-dichloroethane, 70°C, 4 h. [b]Yield assessed by GC, 4h.

Swart *et al.* established the beneficial effect of *p*-cresol on the CM of trans-β-methyl styrene and methyl acrylate when the desired CM product, methyl cinnamate, was formed in 38% yield together with the SM product, stilbene, in 36% yield; whereas only stilbene was formed in the absence of *p*-cresol (scheme 2.24). To optimise the influence of *p*-cresol, they modified the electronic properties of the olefin partner by functionalizing with electron withdrawing groups and electron donating groups, as well as adjusting the steric effect on the acrylate by increasing the chain length of the alkoxy group (24A and Table 2.8). With an electron donating group attached to the α,β-carbonyl compounds, the SM product prevailed again in the absence of *p*-cresol which substantiate the importance of the additive in this system.

The results revealed that both the decrease in the electrophilicity of the acrylate moiety and a decrease in the electron density on the α,β-carbonyl compounds catalysed by **GII** in the presence of *p*-cresol favours the CM product yield over the SM counterpart. The interaction of *p*-cresol with **GII** shielded the carbene carbon and hydrogen as revealed by ^{1}H and ^{13}C NMR spectroscopy. X-ray photoelectron spectroscopy (XPS) showed that the *p*-cresol decreased the electron density on the metal centre. This activated the **GII** for coordination and facilitated the ruthenacyclobutane formation with electron deficient alkenes [37]

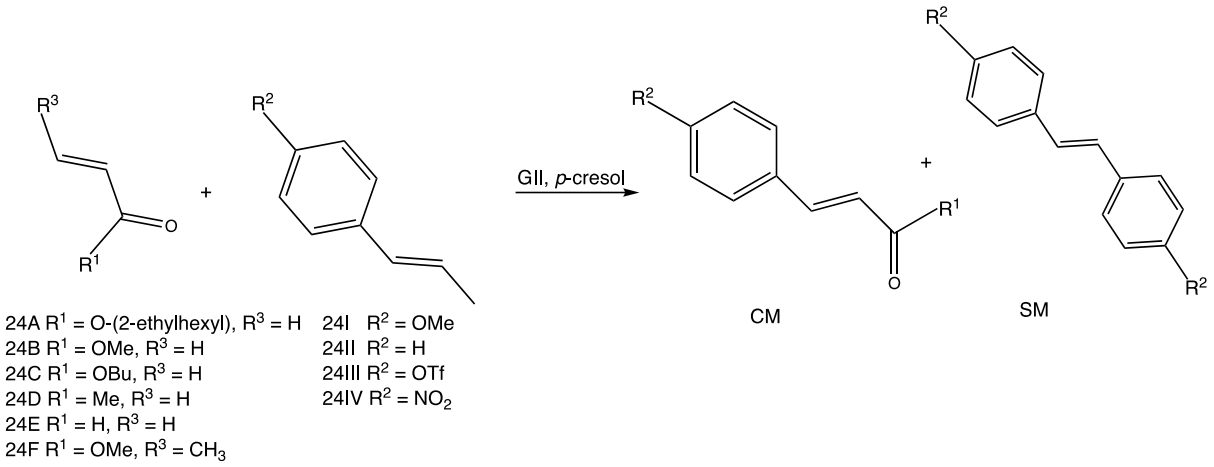

Scheme 2.24: Metathesis reaction of α,β-carbonyl compounds 24A-F and trans-β-methyl styrene **24I-IV** catalysed by **GII**

Table 2.8: Metathesis reaction of α,β-carbonyl compounds **19** and trans-β-methyl styrene **20** catalysed by **GII**[a]

Entry	Reactants		Substituents		CM yield %	SM yield %
			R^1	R^2		
1[b]	**24B**	**24II**	OMe	H	-	>99
2[b]	**24B**	**24I**	OMe	OMe	-	>99
3	**24B**	**24II**	OMe	H	38	36
4	**24B**	**24I**	OMe	OMe	36	61
5	**24B**	**24III**	OMe	OTf	43	7
6	**24C**	**24II**	OBu	H	55	18
7	**24C**	**24I**	OBu	OMe	41	57
8	**24D**	**24II**	Me	H	34	52
9	**24D**	**24I**	Me	OMe	32	47
10	**24E**	**24II**	H	H	Trace	76
11	**24E**	**24I**	H	OMe	Trace	94
12	**24A**	**24II**	O-(2-ethylhexyl)	H	64	12
13	**24A**	**24I**	O-(2-ethylhexyl)	OMe	47	53
14	**24F**	**24II**	OMe	H	3.8	54
15	**24B**	**24IV**	OMe	NO_2	56	-

[a]Reaction condition: 15A-F (1 eq.) and 24I-IV (2 eq.) were refluxed for 2 hours in dcm (10 mL) with **GII** (0.5 mol%) and *p*-cresol (0.25eq) in a set up with a dry ice condenser (-20 °C) while purging Ar to remove gaseous products. [b]No *p*-cresol added.

2.6.2.3 Phosphines

By utilising additives that have the tendency to restrict the formation of the undesirable isomerized by-product, Cossy and co-workers focused on developing a very effective CM between α-methylene-γ-butyrolactone and a wide range of olefinic partners [112]. Several groups have described the well-known method of olefin isomerization with ruthenium catalysts, unfortunately this unwanted side reaction diminishes the CM's effectiveness [113]. Cossy's group therefore prioritised the development of conditions that would inhibit, if not alleviate, the formation of the side reaction. They reported on the effects of several additives that would compete with ruthenium carbene for coordination.

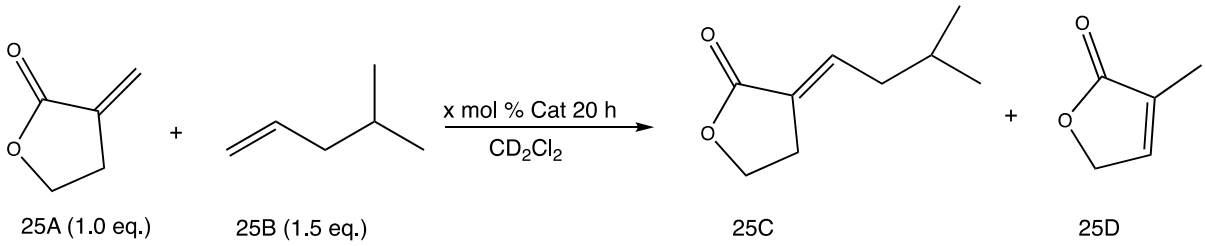

Scheme 2.25: Cross-metathesis between 25A and 25B for catalyst screening

Table 2.9: Screening of catalyst for reaction selectivity[a]

Entry	Catalyst	NMR ratio %		
		25A	**25C**	**25D**
1	**GI** (10 mol %)	100	0	0
2	**GII** (10 mol %)	10	42	48
3	**GII** (5 mol %)	9	55	36
4	**GII** (2.5 mol %)	31	50	19
5	**GII** (1.0 mol %)	46	44	10
6	**HGII** (10 mol%)	100	0	0

[a]Ratio are determined by ^{1}H NMR of the crude reaction mixture.

Preliminary experiments conducted to determine the most suitable catalyst and the optimum reaction using 1.5 eq. of 4-methylpentene **25A** (scheme 2.26), revealed that 2.5 mol% **GII** resulted in the highest yield of the desired product **25C** and lowest yield of the undesired isomerization by-product **25D** (see Table 2.9 entry 4).

The results in Table 2.10 revealed that complete conversion of the starting material was observed in entry 2-6, 8 and product distribution depend on the respective additives. Among all the additives,

chlorodiphenylphosphine, 2,6-dichloro-1,4-benzoquinone and B-chlorocatecholborane gave the desired product with isolated of yield of 71%, 77%, and 87% respectively (entries 6-8). On the account of 2,6-dichloro-1,4-benzoquinione as additive, there was no trace of the isomerization by-product detected by ^{1}H NMR. This suggests a complete inhibition of the isomerization process with 77% isolated yield, but the success of this additive was not consistent with all olefinic partners used and adjusting the reaction conditions did not improve result. Resultingly, chlorocatecholborane was adopted as the most suitable additive for **GII** catalysed olefin CM between α-methylene-γ-butyrolactone and terminal olefins. Employing an additive (such as chlorocatecholborane) in the CM reaction, has resulted in an effective and highly stereoselectivity route to prepare α-alkylidene-γ-butyrolactones, which are conventional building blocks of many organic compounds [112].

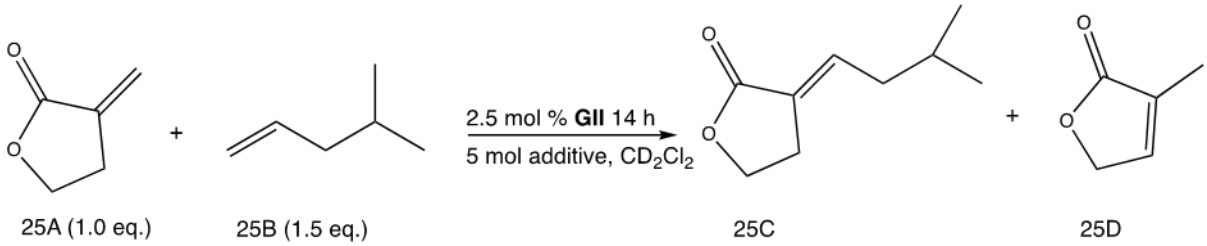

Scheme 2.26: Cross-metathesis between 25A and 25B for additives effect

Table 2.10: Influence of the additives on the reaction selectivity and isolated yield of the desired product **25C**

Entry	Additives	NMR ratio (%)			[a]Isolated yield (%)
		25A	**25C**	**25D**	**25C**
1	None	31	50	19	48
2	Cy_2PCl	0	16	84	14
3	Ph_3PO	0	60	40	56
4	Cy_3PO	0	67	33	64
5	Ph_3As	0	69	31	63
6	Ph_2PCl[b]	0	88	12	71
7	$C_6H_2Cl_2O_2$[c]	14	86	0	77
8	$C_6H_4BClO_2$	0	91	9	87

[a]Ratios are determined by ^{1}H NMR of the crude mixture. [b] 2,6-dichloro-1,4-benzoquinone. [c] B-chlorocatecholborane

Polymer chemists make use of additives when ruthenium-based catalysts are employed for ROMP. Norbornene and its functionalized derivatives are the preferred choice of monomers since they are

cheap, ease of synthesis and commercially available unlike cyclobutene and its derivatives. Cyclic trans-olefins are known for their high ring strain, making them attractive options for ROMP. However, cis- or trans- cyclooctene have not yet demonstrated the same potential in living ROMP reactions. This is due to the competing secondary metathesis reactions, which prevents their polymerization. Consequently, polymers with a polydispersity index (PDI) < 1.1, the benchmark for living ROMP, are not achieved. Several reports established that increasing the phosphine to catalyst ratio and using a more coordinating solvent like THF suppressed secondary metathesis. This produced polymers of PDI < 1.1 and inhibit the formation of high molecular weight species [18,114–116]. Grubbs's group investigated the ROMP of trans-cyclooctene (*t*CO) **26** with **GI** in the presence of various equivalent of triphenylphosphine (PPh_3) using THF and dichloromethane (Scheme 2.27) [117].

It was found that by increasing the phosphine to **GI** ratio to greater than 5 equivalent decreases the PDI and that no high molecular weight species were formed, suggesting that chain transfer reactions were suppressed. Time and concentration studies under the same condition revealed that quenching the reaction at 1 min or 10 mins had no significant changes as no higher molecular species was observed and the PDI remain the same in THF (Table 2.11, entry 12-13). The result from the concentration study was consistent showed that the critical monomer concentration is directly related to monomer ring strain. Therefore, decrease in concentration in THF also gave low PDIs, high isolated yield and molecular weight in agreement with the theoretical value (Table 2**.11** entry 8-9) [117].

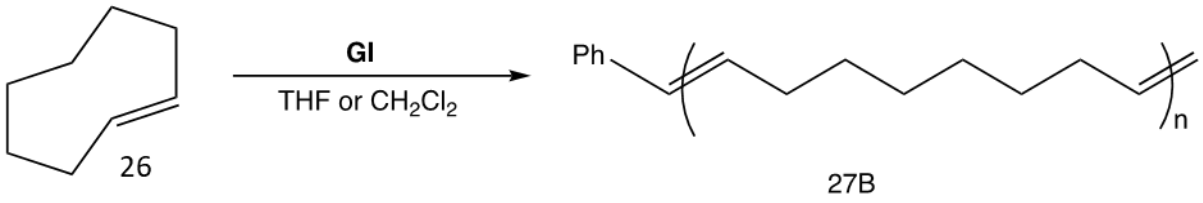

Scheme 2.27: ROMP of *trans*-Cyclooctene

Table 2.11: Polymerization of *t*CO with **GI** and increasing amounts of PPh_3

Entry	PPh_3/**GI**	$[M]_0$	M_n ($x10^3$) g/mol	**27B** (%)	PDI
1[a]	0	0.50	39	74	1.30
2[a]	10	0.50	32	72	1.31
3[a]	20	0.50	33	67	1.19
4[a]	60	0.50	55	97	1.06
5[b]	0	0.50	268	76	1.60
6[b]	20	0.50	57	96	1.18
7[b]	60	0.50	59	90	1.08
8[a]	60	0.25	54	95	1.08
9[b]	60	0.25	67	95	1.10
10[a, c]	60	0.50	39	66	1.10
11[a, d]	60	0.50	52	99	1.08
12[b, c]	60	0.50	55	90	1.08
13[b, d]	60	0.50	54	87	1.08

[a]CH_2Cl_2, [b]THF, [c]1 min, [d]10 mins

2.6.2.4 Others

Fukuyama and co-workers affirmed the better performance for the RCM of acyclic diene catalysed by the adduct of Schrodi-Grubbs catalyst (see Scheme 2.28 for chemical structure) and 1,6-heptadiene [118]. As a result, Sugiura *et al.* adopted this procedure (15 mol % of the catalyst) in the synthesis of cyclopentanones through the RCM of monostyrylated symmetrical dienone under the same condition and a similar activity with moderate yield was observed. Other commercially available ruthenium olefin metathesis catalysts were screened for the most effective catalyst type for the RCM olefin transformation. It was observed that **GI** was inactive toward this process but **HGII** in the presence of an additive (1,6-heptadiene or diallyl ether) significantly improved the yield (Table 2.12 and Scheme 2.28). It was also shown that gradual addition of the catalyst (5 mol% every 24 h for 72 h) had no influence on the yield when compared to adding 15% in one portion and stopping the reaction after 24 h (Table 2**.12**). But lowering catalyst load from 15 mol% to 10 mol% decrease the yield. Changing the solvent from benzene to toluene and simultaneously increasing temperature to 80°C improved the yield substantially. The amount of 1,6-heptadiene did not make a difference but its presence hinders the cyclization of monostyrylated symmetrical dienone. The success of the additive in this reaction system can also be attributed to the active ruthenium methylidene complexes which favours even the RCM of less reactive conjugated internal olefins [54].

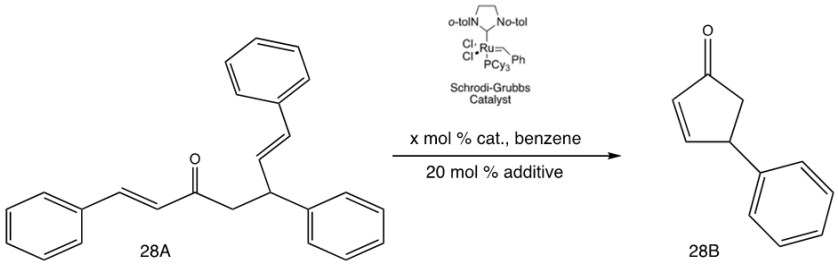

Scheme 2.28: RCM of monostyrylated products catalysed by **HGII** with 1,6-heptadiene as the additive

Table 2.12: Catalyst screening and additive effect on RCM of monostyrylated products.

Entry	Catalyst	X mol	Time	Yield %
1[a]	**GII**	15	72	56
2[a]	**GI**	15	72	0
3[a]	**HGII**	15	72	84
4[b]	**HGII**	15	24	84
5[b]	**HGII**	10	24	73
6[b, c]	**HGII**	10	24	98
7[b, c, d]	**HGII**	10	24	85
8[b, c, e]	**HGII**	10	24	0
9[b, c, f]	**HGII**	10	24	81

[a]The catalyst (5 mol %) was added every 24 h (total 15 mol %). [b]The catalyst was added in one portion. [c]Toluene at 80°C. [d]With 1,6-heptadiene (0.4 eq.). [e]Without 1,6-heptadiene. [f]With diallyl ether (0.2 eq.).

Despite the vast application of the less active but more economical **GI** to catalyse many olefins metathesis transformation such as CM, RCM, ADMET, and ROMP, the cyclopolymerization (CP) of terminal diynes remains unsuccessful [119], since it is more sensitive. Only the fast-initiating **GIII** analogue using weakly coordinating additives has been reported to conveniently mediate and produce a well-controlled living CP [120]. The handicap with the development of CP using ruthenium alkylidene catalyst are the that certain aromatic side products are generated during the reaction instead of the expected conjugated polymers. These side products such as the dimer and trimer of diynes are cyclization products which are promoted by a completely different [2+2+2] cycloaddition mechanism, and not through the conventional olefin metathesis mechanism [121]. The decomposition of the Grubbs catalyst generates an unknown Ru complex, with ruthenacyclopentatriene as an intermediate which are responsible for the formation of the side products. The answer to a successful CP employing Grubbs catalysts was not to increase their activity, but rather to stabilise the propagating carbenes to prevent their decomposition and the

competing [2 + 2 + 2] cycloaddition reaction [122–124]. To address the decomposition problem, it is imperative to employ additives as stabilizing agent to prevent catalyst decomposition.

Choi's group reported the first successful CP of 1,6-heptadiyne derivatives including a comprehensive mechanistic study of the reaction using **GI** and simple additives (Scheme 2.29). Additives such as CuCl, $AlCl_3$, pyridine, benzoic acid, sodium benzoate, and sodium acetate among others were screened to identify the most effective one for achieving optimal polymerization efficiency and obtain conjugated polymers in quantitative yield. Furthermore, **GI**, **HGII** and **GIII** were investigated for their reactivity towards CP of the monomer (**29A**) in dichloromethane without an additive as a control experiment (Table 2.13). It was noted that the competing [2+2+2] cycloaddition was predominant over the expected CP reaction. Although **GIII** largely suppressed the formation of the side products it was not advantageous to the expected product since its yield increased only slightly. The two most effective additives increased the CP efficiency by two distinct mechanisms, which were clearly shown by a thorough mechanistic investigation using kinetic studies and monitoring the changes in the carbene complexes by ^{1}H and ^{31}P NMR investigations. Sodium benzoate tends to coordinate competitively with the catalyst thereby hindering initiation, and equally produce a more active propagating carbene species by partial replacement of chloride ligand with the benzoate ligand leading to fast CP. Conversely, benzoic acid weakly coordinate to the catalyst promoting stabilization and partially traps phosphine thereby increasing both the rate of initiation and propagation [64,125–127].

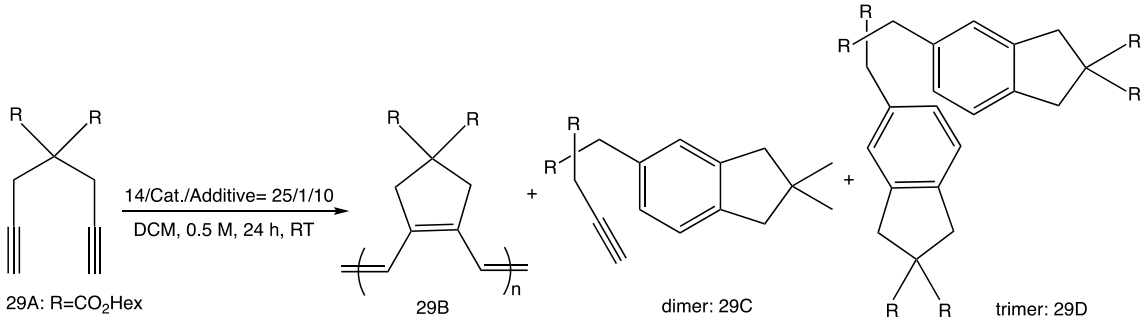

Scheme 2.29: Cyclopolymerization (CP) of 1,6-heptadiyne

Table 2.13: Screening of various catalyst and additives to obtain the maximum efficiency and selectivity.

Entry	Catalyst	Additive	Conversion %	29B[a]	29C[a]	29D[a]
1	**GI**	None	>99	8	52	38
2[b]	**GII**	None	80	17	49	11
3	**HGI**	None	82	18	44	17
4[c]	**HGII**	None	94	8	54	22
5	**GI**	$AlCl_3$	62	16	38	7
6	**GI**	PhCOOH	88	86	2	-
7	**GI**	CH_3COONa	>99	97	2	-
8	**GI**	CF_3COONa	67	48	13	-
9[b]	**GII**	PhCOOH	68	66	1	-
10	**GII**	PhCOONa	58	41	16	-
11	**HGI**	PhCOOH	44	8	15	-
12	**HGI**	PhCOONa	77	42	18	-
13[c]	**HGII**	PhCOOH	84	68	8	-
14[c]	**HGII**	PhCOONa	84	11	51	12

[a]Calculated from ^{1}H NMR spectroscopy. [b]20 h reaction. [c]1 h reaction.

Howell's group were prompted to explore the potential of CM as a feasible pathway for generating functionalized α-alkylidene-β-lactones, given that α-methylene-β-lactone, in contrast to α-alkylidene-β-lactones, could be readily derived from easily accessible Baylis-Hillman adducts [128]. To substantiate this claim, the CM between α-methylene-γ-butyrolactone, **30A**, and 1-acetoxy-9-decene, **30B**, catalysed by either **GII** or **HGII** was investigated (Scheme 2.30). Contrary to their expectation, only the isomerization to enone **30D** was favoured. Investigating this anomaly, they adopted the phosphine-free catalyst **HGII** since phosphine may facilitate the isomerization, however **30D** still formed. Although, olefin isomerization has been a great concern in olefin metathesis catalysed by ruthenium-based catalysts seeing as a ruthenium hydride complex could be aiding the isomerization of **30A**. Several measures to prevent isomerization which includes temperature increase, reaction of **30A** without **GII/HGII** etc. suggested that **30A** is a potential hydride donor owing to its π-allyl or π -alkyl/σ-allyl mechanism [129].

Benzoquinones functionalized with electron withdrawing groups has been identified as a good additive to circumvent olefin isomerization in olefin metathesis substrates such as amines and allylic alcohols [130]. The use of 2,6-dichloro-benzoquinone with **HGII** eliminated isomerization with an incomplete conversion of **30A** (Table 2.14). On the other hand, isomerization was partly prevented using the additive with **GII**, and increasing the catalyst **HGII** loading to 10 mol % in two rounds over 24 h led to the complete consumption of **30A** [131].

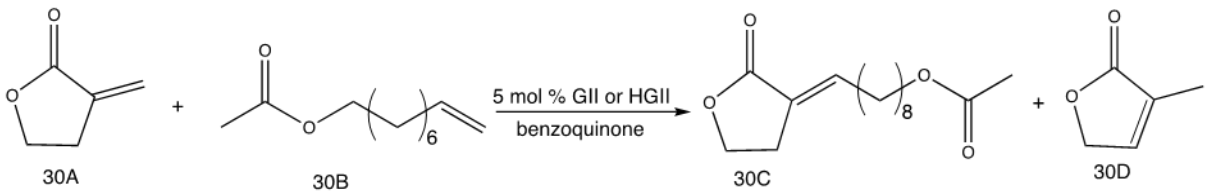

Scheme 2.30: Cross-metathesis of α-methylene-γ-butyrolactone, **30A**, and 1-acetoxy-9-decene, **30B**

Table 2.14: Investigation of cross-metathesis between α-methylene-γ-butyrolactone, **30A**, and 1-acetoxy-9-decene, **30B**, using 5 mol % of the catalyst.

			[a]Product distribution	
Entry	Catalyst	Additive (benzoquinone)	**30C**	**30D**
1	**GII**	-	0	92
2	**HGII**	-	0	87
3[b]	**GII**	-	-	98
4[b]	**HGII**	-	-	70
5	**GII**	0.10	23	25
6	**HGII**	0.10	67	0
7[c]	**HGII**	0.10	98	0

[a]Determined by ^{1}H NMR. [b]Absence of CM partner. [c]10 mol % of **HGII**.

Still addressing the problem of isomerization which is one of the non-metathetic reactions catalysed by ruthenium carbene complexes has inspired many researchers to search for an ideal additive that will either suppress or eliminate this unwanted side reaction because it hinders the formation of the desired metathesis product [132,133]. Unfortunately, the mechanism of this side reaction has not been deciphered. It has been suggested that a ruthenium hydride species formed in situ by impurities from the catalyst or catalyst decomposition are the cause of the isomerization process [134].

Phenyl phosphoric acid [P(=O)(OPh)$(OH)_2$] (PPA) has been identified as a potent isomerization inhibitor. Its inhibitory effect has been optimised by investigating the influence of temperature, stoichiometry, reaction time and nature of additive.

The result obtained from the competition between metathesis and isomerization reaction of substituted olefins are summarised in Table 2.15 and shown in scheme 2.31. Conventionally, the reaction of **31A** with 10 mol % of **GII** gave a mixture of 33 % of the metathesis product and 55% isomerization (entry 1). The addition of PPA to the same reaction quashed the side reaction

resulting to only the metathesis product **31C** (entries 2). Examining the influence of the amount of PPA and temperature will have on product distribution, both conditions were reduced to 5 mol % and 10 °C respectively. The reduction of both conditions was minimal on product distribution (entries 3), establishing the efficacy of PPA as an effective isomerization inhibitor. It has been proposed that chemical species capable of reacting with ruthenium hydride complexes will be good inhibitor for olefin isomerization. Consequently, it is reasonable to assume that the additive reacted with any available ruthenium hydride in the system thereby suppressing the isomerisation process of **31B** and other allylic substrates [135]. The mono-triethyl ammonium salt of PPA $[P(=O)(OPh)(OH)_2][NHEt_3]$ also inhibited both olefin isomerization and metathesis by deactivating **GII** (entries 4-5), assumably due to the amine/ammonium equilibrium which contributes to the catalyst deactivation [136]. In another experiment where mono-tetraethyl ammonium salt $[P(=O)(OPh)(OH)_2][NEt_3]$ was employed as additive, 80 % olefin isomerization was observed with no trace of metathesis product (entries 6). These outcomes identify PPA as an acidic additive and the **GII** is not tolerant to $[HNEt_3]^+$. The reaction was performed with benzoic acid present to see if the isomerization of **31A** would be prevented by a different acid. As expected, the metathesis product **31C** was formed in 43 % yield with no olefin isomerization product formed (entries 7) [137].

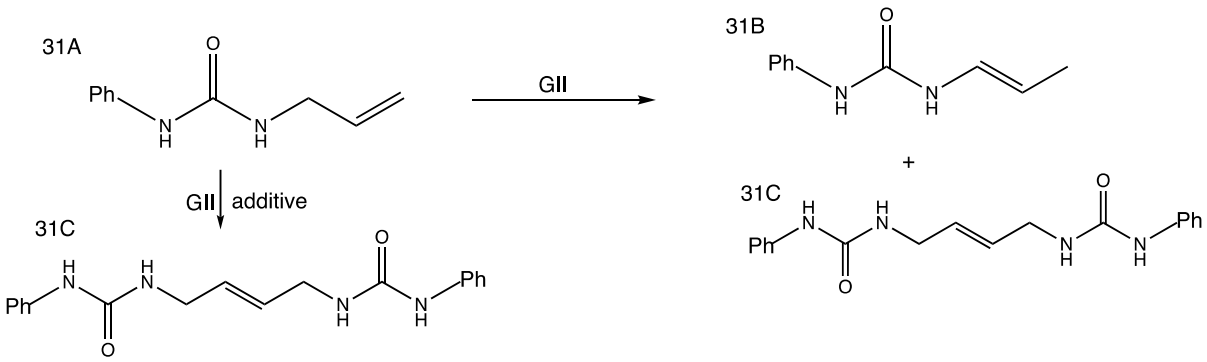

Scheme 2.31: Reactions showing isomerization against metathesis for 1-allyl-3-(phenyl)urea **31A**

Table 2.15: Results obtained for the different ruthenium-catalysed reactions of 1-allyl-3-(phenyl)urea **31A**

Entry	Additive	Amount of additive %	Temp. °C	% **31B**	% **31C**	% **31A**
1	-	-	40	55	33	10
2	PPA	50	40	-	56	30
3	PPA	5	10	-	50	50
4	PPA[$NHEt_3$]	50	40	-	-	100
5	PPA[$NHEt_3$]	50	10	-	-	100
6	PPA[NEt_3]	50	10	80	-	20
7	PhCOOH	5	10	-	43	57

[a]All reactions were carried out in CH_2Cl_2 using 10 mol % of **GII** and reaction time 16 h.

2.6.3 Additives to Schrock's catalysts

Even though the addition of additives as a co-catalyst in the olefin metathesis reactions is primarily being investigated on the ruthenium based Grubbs' catalysts, is worth mentioning that there are a few cases where additives are employed in metathesis reactions initiated by molybdenum alkylidene complexes.

Among the many works of Richard Schrock in developing a suitable catalyst with a wide range of application for olefin metathesis transformation, are the two well defined commercially available molybdenum catalyst with the formula $Mo(CHCMe_2Ph)(N\text{-}2,6\text{-}i\text{-}Pr_2C_6H_3)(OR)_2$ where OR = $OCMe_3$ or $OCMe(CF_3)_2$ (Figure 2.2) [138]. Prior to this discovery, the corresponding Mo complexes catalytic potential for polymerization of ethylene and norbornene were unknown. Hiya's group reported high catalytic activities of Mo complexes **32A-D** with the addition of additives towards the linear polymerization of ethylene and ROMP of norbornene in toluene at various temperature for 6 hours (Scheme 2.32**:** ROMP of norbornene with Molybdenum complexes 32A-D

). When $AlEt_3$ was used as an additive, it was observed that both yield, and molecular weights increases as temperature was increased from 0 °C to 25 °C and further to 60 °C. The optimal polymer yield was recorded at 60 °C for Mo complexes **32A-D** which suggests that increased temperatures favour the ROMP of norbornene. Complexes **32B** and **32C** both produced > 90% of the *cis* content of the polymer at 0 °C. When the time of reaction was drastically reduced to 5 mins under similar conditions, only complex **32A** catalysed polymerization gave a high yield, 99%, of poly(norbornene) while complexes **32B-D** gave extremely low yields (30%, 7%, and 18%

respectively). This suggest that the attached bulky group (*i*Pr) at positions 2 and 6 favour polymer ROMP.

The ROMP of norbornene was further investigated using modified methyl aluminoxane (MMAO, AlMeO:Al-isoBuO = 3:1) [139] instead of $AlEt_3$ and both the *cis*-selectivity and polymer yield were greatly enhanced especially when **32A**/MMAO system was employed for 12 h (Table 2.16). Change in time from 12 h to 1 h did not have a big impact on the *cis* content but the yields were lower when complexes **32B-D** were employed. In addition to the previous system where the bulky group 2,6-diisopropylphenylimino group improved the polymer yield, the ROMP of endo-dicyclopentadiene using the 2,6-bis-[1-(2,6-diisopropylphenylimino)ethyl]pyridine-$MoCl_3$ **32A**/MMAO system gave the desired polymer with 100 % cis selectivity (Table 2.16) [140].

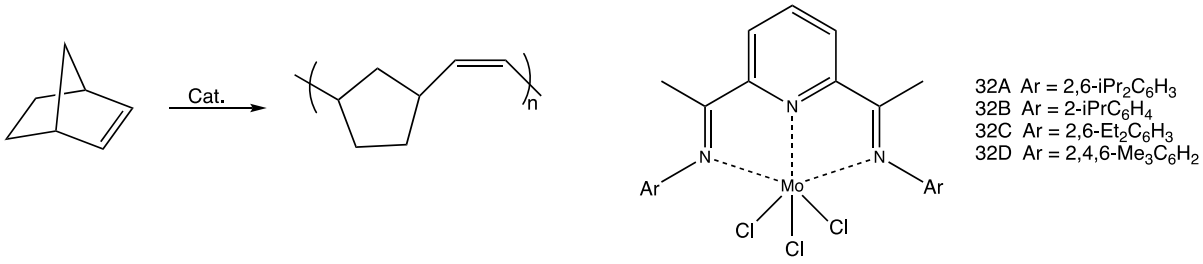

Scheme 2.32: ROMP of norbornene with Molybdenum complexes 32A-D

Table 2.16: Comparison of ROMP of norbornene catalysed by different catalyst/co-catalyst system[a].

Entry	Catalyst	Temp (°C)	Time (h)	Yield (%)	*cis* content (%)[b]
1	**32A**/$AlEt_3$	0	6	99	78
2	**32A**/$AlEt_3$	60	6	100	68
3	**32B**/$AlEt_3$	0	6	99	90
4	**32B**/$AlEt_3$	60	6	100	73
5	**32C** /$AlEt_3$	0	6	38	92
6	**32C**/$AlEt_3$	60	6	100	79
7	**32D** /$AlEt_3$	0	6	2	87
8	**32D**/$AlEt_3$	60	6	93	77
9	**32A**/MMAO	0	12	99	100
10	**32A**/MMAO	60	12	100	98
11	**32B**/MMAO	60	1	82	98
12	**32C**/MMAO	60	1	77	95
13	**32D**/MMAO	60	1	88	97

[a]Conditions: 0.5 mL of toluene, [b]Determined by ^1H NMR

Mortreux *et al*. conducted a thorough investigation on the effectiveness of phenols and silanol as additives in a $Mo(CO)_6$–based catalytic system for the metathesis of 4-decyne and 1-phenyl-1-propyne. Initially, this reaction was homogeneously catalysed by $Mo(CO)_6$ and resorcinol [141]. Thermal activation and a high phenol concentration have been reported to further enhance the Mo based systems [142]. Interestingly, zero oxidation state of Mo or high oxidation state Mo(VI) alkylidyne complexes have been developed by Furstner [143] and Tamm [144] as was found to be successful catalysts for alkyne metathesis in conjunction an additive. Phenol and its derivatives have historically been used as activators in most of the applications and conventional catalyst compositions. It is imperative to compare the activity of silanol and phenol derivatives as co-catalyst to $Mo(CO)_6$ in an in-situ catalytic system. The successful use of siloxy-molybdenum carbynes by the Furstner's group for 1-phenyl-1-propyne metathesis, has initiated screening of silanols as co-catalysts. Siloxy-molybdenum carbynes is formed in-situ through the reaction of a variety of potassium silanolates with a Mo tribromo alkylidyne complex, has dictated the choice of this silanols. Figure 2.5 shows some of the aryloxy- and siloxyl-based co-catalysts screened for 4-decyne metathesis using a molybdenum catalyst (Scheme 2.33) [143].

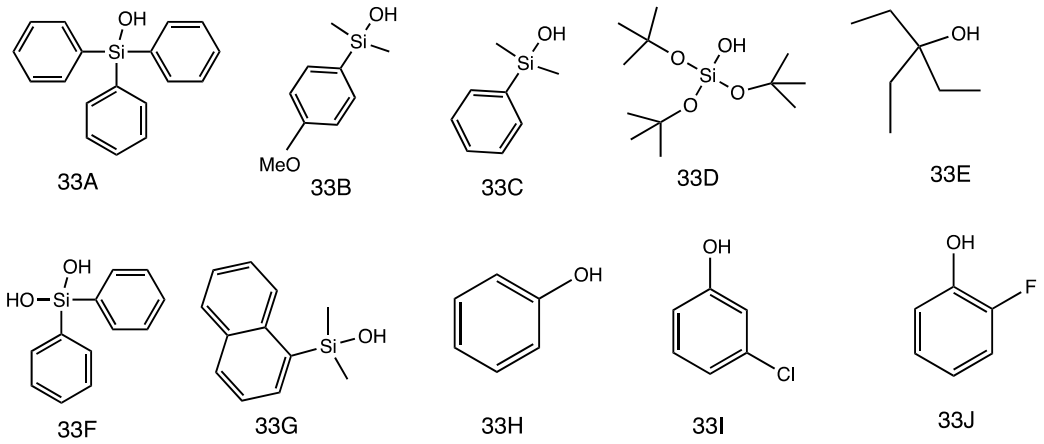

Figure 2.5: Some aryloxy- and siloxyl-based co-catalyst.

The screening of some of the aryloxy- and siloxyl-based co-catalysts screened for 4-decyne metathesis using different co-catalyst/molybdenum ratio.

Table 2.17 summarizes the results for 4-decyne metathesis using different aryloxy- and siloxyl-based co-catalyst/molybdenum ratio. As can be seen, all the aromatic silanols are effective additives for the self metathesis of 4-decyne. When phenol or its derivatives are used, it is evident

that it drives the reaction more rapidly to equilibrium. 3-Chlorophenol (**33I**) is found to be the most efficient co-catalyst for the reaction with a turnover rate of 41 h^{-1} at the lowest co-catalyst/Mo ratio of 2. The co-catalyst **33B** and **33G** also gave similar good conversions of 52 % after 120 min while **33C** gave 45 % conversion after 60 min. These reactions were conducted under inert gases and dry solvents condition to prevent unwanted reactions. Aryl-substituted silanols has proven to be an environmentally more friendly and more versatile replacements for phenol derivatives, to effectively co-catalyse alkyne metathesis utilizing molybdenum hexacarbonyl as the pre-catalyst. These results offer numerous avenues to produce derived systems that may exhibit improved performance, making them well suited for applications in organic and polymer chemistry. This is particularly notable since silylated phenols have been rarely used as a co-catalyst before, making a new development in this context [145–147].

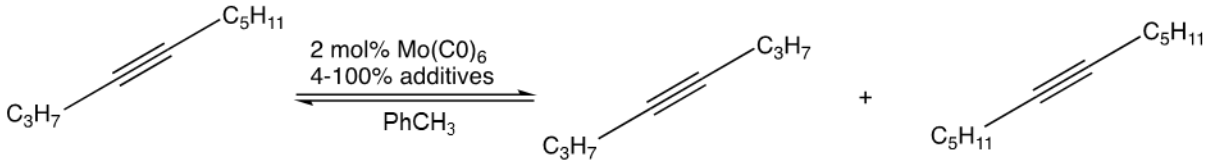

Scheme 2.33: Self metathesis of 4-decyne catalysed by Mo(CO)6 /additives

Table 2.17: Comparison of efficiency of different co-catalyst in the self metathesis of 4-decyne[a]

Entry	Additives RSiOH	RSiOH/Mo mol/mol	Conv. % 30 min[b]	Conv. % 60 min	Conv. % 120 min	TR (h^{-1})[c]
1	**33A**	50	1	7	22	8
		2	6	20	38	10
2	**33B**	50	44	50	52	44
		2	20	40	49	20
3	**33C**	2	22	45	-	22
4	**33D**	50	0.5	1.4	3	0.5
5	**33E**	50	5	14	24	7
6	**33F**	2	9	22	36	11
7	**33G**	2	18	47	52	29
8	**33H**	50	17	45	51	28
		2	16	26	31	16
9	**33I**	50	45	51	51	45
		10	51	51	51	51
10	**33J**	50	11	37	52	26
		10	34	43	54	34

[a]Conditions: dry toluene; inert atmosphere; reflux; 0.5 M in 4-decyne, 2 mol% $Mo(CO)_6$, [b]4-decyne conversion determined by GC using n-decane as internal standard, [c]moles 4-decyne

converted per mol per hour, calculated from the highest reaction rate using conversion vs time data.

2.7 Conclusion

In this review, we examined the history and development of the two general types of catalyst for olefin metathesis transformation known as Schrock's and Grubbs' catalyst. Further catalyst improvement to address the setbacks of their earlier invention through modification have orchestrated the different generations of Grubbs' catalyst with better activity, selectivity, and stability which has revolutionized the field of olefin and alkyne metathesis. Interestingly, some chemical substance e.g., alcohols, salts, phosphines, and organic dienes have been an excellent co-catalyst for many metathesis reactions including self-metathesis, cross-metathesis, ring closing metathesis, ring opening metathesis polymerization, and alkyne metathesis to mention but a few. The use of additives has gained the attention of many polymer and organic chemists to facilitate difficult reactions since it has been reported to improve the efficiency and selectivity of catalysts for specialized reactions, suppressing of non-metathetic reactions like olefin isomerization that competes with the desired metathesis system, and extending the life cycle of the catalyst. These additives do not alter the structural configurations of the catalyst but rather interacts with the catalyst through van der Waals interactions or facilitate ligand dissociation from the catalyst. Even though numerous questions are yet to be addressed through these findings, it does lay a great foundation for future research to build upon.

References

[1] R.H Grubbs, *Handbook of Metathesis*, Wiley, **2003**.

[2] K. Voigtritter, S. Ghorai, B. H. Lipshutz, *J. Org. Chem.* **2011**, *76*, 4697–4702.

[3] J. W. Morzycki, *Steroids* **2011**, *76*, 949–966.

[4] F. B. Hamad, T. Sun, S. Xiao, F. Verpoort, *Coord. Chem. Rev.* **2013**, *257*, 2274–2292.

[5] C. Bruneau, C. Fischmeister, X. Miao, R. Malacea, P. H. Dixneuf, *Eur. J. Lipid Sci. Technol.* **2010**, *112*, 3–9.

[6] M. R. Swart, C. Marais, E. Erasmus, Catalysts **2021**, 12, 1475-1483.

[7] Y. Chauvin, *Angew. Chem. Int. Ed.* **2006**, *45*, 3740–3747.

[8] J. H. Wengrovius, R. R. Schrock, M. R. Churchill, J. R. Missert, W. J. Youngs, *J. Am. Chem. Soc.* **1980**, *102*, 4515–4516.

[9] E. O. Fischer, A. Maasböl, *Angew. Chem. Int. Ed. Engl*. **1964**, *3*, 580–581.

[10] R. L. Banks, G. C. Bailey, *Ind. Eng. Chem. Res.* **1964**, *3*, 170–173.

[11] N. Calderon, H. Y. Chen, K. W. Scott, *Tetrahedron Lett.* **1967**, *8*, 3327–3329.

[12] H. S. Eleutrio, *U.S Patent 3074918*, **1963**.

[13] R. R. Schrock, *Angew. Chem. Int. Ed.* **2006**, *45*, 3748–3759.

[14] R. H. Grubbs, *Angew. Chem. Int. Ed.* **2006**, *45*, 3760–3765.

[15] D. Hughes, P. Wheeler, D. Ene, *Org. Process Res. Dev.* **2017**, *21*, 1938–1962.

[16] M. Yu, S. Lou, F. Gonzalez-Bobes, *Org. Process Res. Dev.* **2018**, *22*, 918–946.

[17] C. S. Higman, J. A. M. Lummiss, D. E. Fogg, *Angew. Chem. Int. Ed.* **2016**, *55*, 3552–3565.

[18] O. M. Ogba, N. C. Warner, D. J. O'Leary, R. H. Grubbs, *Chem. Soc. Rev.* **2018**, *47*, 4510–4544.

[19] Schrodi Yann, Pederson L. Richard, *Aldrichimica Acta* **2007**, *40*, 45–52.

[20] A. Briot, M. Bujard, V. Gouverneur, S. P. Nolan, C. Mioskowski, *Org. Lett.* **2000**, *2*, 1517–1519.

[21] M. Scholl, S. Ding, C. W. Lee, R. H. Grubbs, *Org. Lett.* **1999**, *1*, 953–956.

[22] M. Scholl, T. M. Trnka, J. P. Morgan, R. H. Grubbs, *Tetrahedron Lett.* **1999**, *40*, 2247–2250.

[23] M. S. Sanford, M. Ulman, R. H. Grubbs, *J. Am. Chem. Soc.* **2001**, *123*, 749–750.

[24] T. M. Trnka, R. H. Grubbs, *Acc Chem. Res.* **2001**, *34*, 18–29.

[25] A. H. Hoveyda, D. G. Gillingham, J. J. Van Veldhuizen, O. Kataoka, S. B. Garber, J. S. Kingsbury, J. P. A. Harrity, *Org. Biomol. Chem.* **2004**, *2*, 8.

[26] J. P. Martínez, B. Trzaskowski, *J. Phys. Chem. A* **2022**, *126*, 720–732.

[27] A. Fürstner, *J. Am. Chem. Soc.* **2021**, *143*, 15538–15555.

[28] G. A. Bailey, J. A. M. Lummiss, M. Foscato, G. Occhipinti, R. McDonald, V. R. Jensen, D. E. Fogg, *J. Am. Chem. Soc.* **2017**, *139*, 16446–16449.

[29] M. Al-Hashimi, C. Hongfa, B. George, H. S. Bazzi, D. E. Bergbreiter, *J. Polym. Sci. A Polym. Chem.* **2012**, *50*, 5211–5212.

[30] F. Bernardi, A. Bottoni, G. Pietro Miscione, *Organometallics* **2003**, *22*, 940–947.

[31] M. Vasiliu, A. J. Arduengo, D. A. Dixon, *J. Phys.. Chem. C* **2014**, *118*, 13563–13577.

[32] J. J. Lippstreu, B. F. Straub, *J. Am. Chem. Soc.* **2005**, *127*, 7444–7457.

[33] M. Jawiczuk, A. Marczyk, K. Młodzikowska-Pieńko, B. Trzaskowski, *J. Phys. Chem. A* **2020**, *124*, 6158–6167.

[34] W. J. van Rensburg, P. J. Steynberg, M. M. Kirk, W. H. Meyer, G. S. Forman, *J Organomet. Chem.* **2006**, *691*, 5312–5325.

[35] P. Śliwa, K. Kurleto, J. Handzlik, S. Rogalski, P. Żak, B. Wyrzykiewicz, C. Pietraszuk, *Organometallics* **2016**, *35*, 621–628.

[36] A. N. Roberts, A. C. Cochran, D. A. Rankin, A. B. Lowe, H.-J. Schanz, *Organometallics* **2007**, *26*, 6515–6518.

[37] D. R. Anderson, T. Ung, G. Mkrtumyan, G. Bertrand, R. H. Grubbs, Y. Schrodi, *Organometallics* **2008**, *27*, 563–566.

[38] A. Michrowska, R. Bujok, S. Harutyunyan, V. Sashuk, G. Dolgonos, K. Grela, *J. Am. Chem. Soc.* **2004**, *126*, 9318–9325.

[39] Y. Kim, C.-H. Chen, C. Hilty, *Chem. Comm.* **2018**, *54*, 4333–4336.

[40] M. V. Silva Elipe, A. Cherney, R. Krull, N. Donovan, J. Tedrow, D. Pooke, K. L. Colson, *Org. Process Res. Dev.* **2020**, *24*, 1428–1434.

[41] M. R. Swart, L. Twigge, E. Erasmus, C. Marais, B. C. B. Bezuidenhoudt, *Eur. J. Inorg. Chem.* **2021**, 1752–1762.

[42] M. S. Sandford, J. A. Love, R. H. Grubbs, *J. Am. Chem. Soc.* **2001**, *123*, 6543–6554.

[43] X. Zeng, X. Wei, V. Farina, E. Napolitano, Y. Xu, L. Zhang, N. Haddad, N. K. Yee, N. Grinberg, S. Shen, C. H. Senanayake, *J. Org. Chem.* **2006**, *71*, 8864–8875.

[44] E.-H. Kang, C. Kang, S. Yang, E. Oks, T.-L. Choi, *Macromolecules* **2016**, *49*, 6240–6250.

[45] S. H. Hong, A. G. Wenzel, T. T. Salguero, M. W. Day, R. H. Grubbs, *J. Am. Chem. Soc.* **2007**, *129*, 7961–7968.

[46] C. S. Higman, A. E. Lanterna, M. L. Marin, J. C. Scaiano, D. E. Fogg, *ChemCatChem* **2016**, *8*, 2446–2449.

[47] C. S. Higman, L. Plais, D. E. Fogg, *ChemCatChem* **2013**, *5*, 3548–3551.

[48] S. Kotha, M. K. Dipak, *Tetrahedron* **2012**, *68*, 397–421.

[49] F. C. Bargiggia, W. V. Murray, *J. Org. Chem.* **2005**, *70*, 9636–9639.

[50] P. K. Quach, J. H. Hsu, I. Keresztes, B. P. Fors, T. H. Lambert, *Angew. Chem. Int. Ed.* **2022**, *61*, e202203344.

[51] K. Jung, E.-H. Kang, J.-H. Sohn, T.-L. Choi, *J. Am. Chem. Soc.* **2016**, *138*, 11227–11233.

[52] D. M. Walba, H. Yang, P. Keller, C. Zhu, R. Shao, D. A. Coleman, C. D. Jones, N. A. Clark, *Macromol. Rapid Commun.* **2009**, *30*, 1894–1899.

[53] M. Renom Carrasco, C. Nikitine, M. Hamou, C. de Bellefon, C. Thieuleux, V. Meille, *Catalysts* **2020**, *10*, 435.

[54] C. Guo, X. Li, X. Zhu, W. Chu, S. Liu, Y. Wang, P. Zeng, S. Guo, L. Xu, *Chinese J. Catal.* **2018**, *39*, 37–46.

[55] F. Sinclair, M. Alkattan, J. Prunet, M. P. Shaver, *Polym. Chem.* **2017**, *8*, 3385–3398.

[56] A. Abera Tsedalu, *J. Chem.* **2021**, *2021*, 3590613.

[57] G. S. Forman, R. P. Tooze, *J. Organomet. Chem.* **2005**, *690*, 5863–5866.

[58] M. Sugiura, R. Kinoshita, M. Nakajima, *Org. Lett.* **2014**, *16*, 5172–5175.

[59] G. S. Sankaran, *J. Agric. Res.* **2018**, *3*, 16000203.

[60] H.-G. Schmalz, *Angew. Chem. Int. Ed.* **1995**, *34*, 1833–1836.

[61] C. O. Kangani, A. M. Brückner, D. P. Curran, *Org. Lett.* **2005**, *7*, 379–382.

[62] A. Rivkin, Y. S. Cho, A. E. Gabarda, F. Yoshimura, S. J. Danishefsky, *J. Nat. Prod.* **2004**, *67*, 139–143.

[63] F. Sinclair, M. Alkattan, J. Prunet, M. P. Shaver, *Polym. Chem.* **2017**, *8*, 3385–3398.

[64] L. Caire da Silva, G. Rojas, M. D. Schulz, K. B. Wagener, *Prog. Polym. Sci.* **2017**, *69*, 79–107.

[65] X. Wang, W. Zhao, K. Nomura, *ACS Omega* **2023**, *8*, 7222–7233.

[66] N. Momčilović, P. G. Clark, A. J. Boydston, R. H. Grubbs, *J. Am. Chem. Soc.* **2011**, *133*, 19087–19089.

[67] F. Stelzer, *J. Macromol. Sci., Part A* **1996**, *33*, 941–952.

[68] I. Mandal, A. F. M. Kilbinger, *J. Am. Chem. Soc. Au* **2022**, *2*, 2800–2808.

[69] Y. Liang, H. Sun, W. Cao, M. P. Thompson, N. C. Gianneschi, *ACS Macro Lett.* **2020**, *9*, 1417–1422.

[70] M. R. Yarolimek, H. R. Bookbinder, B. M. Coia, J. G. Kennemur, *ACS Macro Lett.* **2021**, *10*, 760–766.

[71] T. Steinbach, E. M. Alexandrino, F. R. Wurm, *Polym. Chem.* **2013**, *4*, 3800.

[72] P. Shieh, H. V.-T. Nguyen, J. A. Johnson, *Nat. Chem.* **2019**, *11*, 1124–1132.

[73] A. J. Myles, Z. Zhang, G. Liu, N. R. Branda, *Org. Lett.* **2000**, *2*, 2749–2751.

[74] J. D. Feist, Y. Xia, *J. Am. Chem. Soc.* **2020**, *142*, 1186–1189.

[75] S. T. Diver, A. J. Giessert, *Chem. Rev.* **2004**, *104*, 1317–1382.

[76] J. E. Marshall, J. B. Keister, S. T. Diver, *Organometallics* **2011**, *30*, 1319–1321.

[77] L. N. Rohde, S. T. Diver, *Tetrahedron Lett.* **2022**, *108*, 154121.

[78] J. R. Griffiths, J. B. Keister, S. T. Diver, *J. Am. Chem. Soc.* **2016**, *138*, 5380–5391.

[79] R. L. Banks, G. C. Bailey, *Ind. Eng. Chemistry Res.* **1964**, *3*, 170–173.

[80] Bradshaw C.P.C, Howman E.J, Turner L., *J. Catal.* **1967**, *7*, 269–276.

[81] G. S. Lewandos, R. Pettit, *Tetrahedron Lett.* **1971**, *12*, 789–793.

[82] R. H. Grubbs, T. K. Brunck, *J. Am. Chem. Soc.* **1972**, *94*, 2538–2540.

[83] C. Samojłowicz, M. Bieniek, K. Grela, *Chem. Rev.* **2009**, *109*, 3708–3742.

[84] Wilkinson G. Nobel Lecture, *Angew. Chem. Int. Ed.* **1974**, *86*, 664–667.

[85] Fischer E.O. Nobel Lecture, *Angew. Chem. Int. Ed.* **1974**, *86*, 651–663.

[86] Juvinall G.L, *J. Am. Chem. Soc.* **1964**, *86*, 4202–4203.

[87] R. R. Schrock, *J. Am. Chem. Soc.* **1974**, *96*, 6796–6797.

[88] L. J. Guggenberger, R. R. Schrock, *J. Am. Chem. Soc.* **1975**, *97*, 2935–2935.

[89] R. Schrock, S. Rocklage, J. Wengrovius, G. Rupprecht, J. Fellmann, *J. Mol. Catal. Chem.* **1980**, *8*, 73–83.

[90] J. H. Wengrovius, R. R. Schrock, M. R. Churchill, J. R. Missert, W. J. Youngs, *J. Am. Chem. Soc.* **1980**, *102*, 4515–4516.

[91] R. R. Schrock, J. S. Murdzek, G. C. Bazan, J. Robbins, M. DiMare, M. O'Regan, *J. Am. Chem. Soc.* **1990**, *112*, 3875–3886.

[92] J. Feldman, R. R. Schrock, Prog. Inorg. Chem., Wiley, **1991**, 39, pp. 1–74.

[93] F. W. Michelotti, W. P. Keaveney, *J. Polym. Sci. A* **1965**, *3*, 895–905.

[94] B. M. Novak, R. H. Grubbs, *J. Am. Chem. Soc.* **1988**, *110*, 7542–7543.

[95] Nguyen S.T, Grubbs R.H, *J. Am. Chem.l Soc.* **1993**, *115*, 9858–9859.

[96] P. Schwab, R. H. Grubbs, J. W. Ziller, *J. Am. Chem. Soc.* **1996**, *118*, 100–108.

[97] P. Schwab, M. B. France, J. W. Ziller, R. H. Grubbs, *Angew. Chem. Int. Ed.* **1995**, *34*, 2039–2041.

[98] S. T. Nguyen, R. H. Grubbs, *J. Organomet. Chem.* **1995**, *497*, 195–200.

[99] E. L. Dias, S. T. Nguyen, R. H. Grubbs, *J. Am. Chem. Soc.* **1997**, *119*, 3887–3897.

[100] M. S. Sanford, J. A. Love, R. H. Grubbs, *J. Am. Chem. Soc.* **2001**, *123*, 6543–6554.

[101] J. S. Kingsbury, J. P. A. Harrity, P. J. Bonitatebus, A. H. Hoveyda, *J. Am. Chem. Soc.* **1999**, *121*, 791–799.

[102] S. B. Garber, J. S. Kingsbury, B. L. Gray, A. H. Hoveyda, *J. Am. Chem. Soc.* **2000**, *122*, 8168–8179.

[103] J. A. Love, J. P. Morgan, T. M. Trnka, R. H. Grubbs, *Angew. Chem. Int. Ed.* **2002**, *41*, 4035–4037.

[104] R. M. Thomas, B. K. Keitz, T. M. Champagne, R. H. Grubbs, *J. Am. Chem. Soc.* **2011**, *133*, 7490–7496.

[105] J. M. Berlin, K. Campbell, T. Ritter, T. W. Funk, A. Chlenov, R. H. Grubbs, *Org. Lett.* **2007**, *9*, 1339–1342.

[106] T. Matsuo, *Catalysts* **2021**, *11*, 359.

[107] T. Matsuo, C. Imai, T. Yoshida, T. Saito, T. Hayashi, S. Hirota, *Chem. Comm.* **2012**, *48*, 1662.

[108] J. M. Berlin, K. Campbell, T. Ritter, T. W. Funk, A. Chlenov, R. H. Grubbs, *Org. Lett.* **2007**, *9*, 1339–1342.

[109] P. S. Engl, A. Fedorov, C. Copéret, A. Togni, *Organometallics* **2016**, *35*, 887–893.

[110] A. Hryniewicka, S. Suchodolski, A. Wojtkielewicz, J. W. Morzycki, S. Witkowski, *Beilstein J. Org. Chem.* **2015**, *11*, 2795–2804.

[111] M. Abbas, A. Leitgeb, C. Slugovc, *Synlett* **2013**, *24*, 1193–1196.

[112] W. H. Meyer, A. E. McConnell, G. S. Forman, C. L. Dwyer, M. M. Kirk, E. L. Ngidi, A. Blignaut, D. Saku, A. M. Z. Slawin, *Inorganica Chim Acta* **2006**, *359*, 2910–2917.

[113] C. Feng, X. Wang, B.-Q. Wang, K.-Q. Zhao, P. Hu, Z.-J. Shi, *Chem. Commun.* **2012**, *48*, 356–358.

[114] G. S. Forman, A. E. McConnell, R. P. Tooze, W. Janse Van Rensburg, W. H. Meyer, M. M. Kirk, C. L. Dwyer, D. W. Serfontein, *Organometallics* **2005**, *24*, 4528–4542.

[115] A. G. Santos, G. A. Bailey, E. N. dos Santos, D. E. Fogg, *ACS Catal.* **2017**, *7*, 3181–3189.

[116] J. R. Clark, J. R. Griffiths, S. T. Diver, *J. Am. Chem. Soc.* **2013**, *135*, 3327–3330.

[117] W. L. McClennan, S. A. Rufh, J. A. M. Lummiss, D. E. Fogg, *J. Am. Chem. Soc.* **2016**, *138*, 14668–14677.

[118] B. J. Ireland, B. T. Dobigny, D. E. Fogg, *ACS Catal.* **2015**, *5*, 4690–4698.

[119] J. Moïse, S. Arseniyadis, J. Cossy, *Org. Lett.* **2007**, *9*, 1695–1698.

[120] B. Schmidt, *J. Org. Chem.* **2004**, *69*, 7672–7687.

[121] J. B. Matson, R. H. Grubbs, *Macromolecules* **2008**, *41*, 5626–5631.

[122] C. W. Bielawski, R. H. Grubbs, *Macromolecules* **2001**, *34*, 8838–8840.

[123] S. T. Nguyen, L. K. Johnson, R. H. Grubbs, J. W. Ziller, *J. Am. Chem. Soc.* **1992**, *114*, 3974–3975.

[124] R. Walker, R. M. Conrad, R. H. Grubbs, *Macromolecules* **2009**, *42*, 599–605.

[125] J. A. Henderson, A. J. Phillips, *Angew Chem. Int. Ed.* **2008**, *120*, 8627–8629.

[126] J. P. A. Harrity, M. S. Visser, J. D. Gleason, Amir H. Hoveyda, *J. Am. Chem. Soc.* **1997**, *119*, 1488–1489.

[127] A. H. Hoveyda, Z. Liu, C. Qin, T. Koengeter, Y. Mu, *Angew. Chem. Int. Ed.* **2020**, *59*, 22324–22348.

[128] Y. Miura, N. Hayashi, S. Yokoshima, T. Fukuyama, *J. Am. Chem. Soc.* **2012**, *134*, 11995–11997.

[129] S. Alvarez, S. Medina, G. Domínguez, J. Pérez-Castells, *J. Org. Chem.* **2015**, *80*, 2436–2442.

[130] E.-H. Kang, S. Y. Yu, I. S. Lee, S. E. Park, T.-L. Choi, *J. Am. Chem. Soc.* **2014**, *136*, 10508–10514.

[131] P. S. Kumar, K. Wurst, M. R. Buchmeiser, *J. Am. Chem. Soc.* **2009**, *131*, 387–395.

[132] J.-U. Peters, *Chem. Comm.* **1997**, 1983.

[133] S. Alvarez, S. Medina, G. Domínguez, J. Pérez-Castells, *J. Org. Chem.* **2013**, *78*, 9995–10001.

[134] G. I. Peterson, S. Yang, T. L. Choi, *Acc Chem. Res.* **2019**, *52*, 994–1005.

[135] C. Kang, E. H. Kang, T. L. Choi, *Macromolecules* **2017**, *50*, 3153–3163.

[136] E. H. Kang, S. Y. Yu, I. S. Lee, S. E. Park, T. L. Choi, *J. Am. Chem. Soc.* **2014**, *136*, 10508–10514.

[137] K. Jung, K. Kim, J. C. Sung, T. S. Ahmed, S. H. Hong, R. H. Grubbs, T. L. Choi, *Macromolecules* **2018**, *51*, 4564–4571.

[138] R. Raju, A. R. Howell, *Org. Lett.* **2006**, *8*, 2139–2141.

[139] D. Finnegan, B. A. Seigal, M. L. Snapper, *Org. Lett.* **2006**, *8*, 2603–2606.

[140] S. H. Hong, D. P. Sanders, C. W. Lee, R. H. Grubbs, *J. Am. Chem. Soc.* **2005**, *127*, 17160–17161.

[141] R. Raju, J. A. Laura, C. D. Tri Le, D. T. Christopher, R. H. Amy, *Org. Lett.* **2007**, *9*, 1699–1701.

[142] D. Finnegan, B. A. Seigal, M. L. Snapper, *Org. Lett.* **2006**, *8*, 2603–2606.

[143] M. Arisawa, Y. Terada, M. Nakagawa, A. Nishida, *Angew. Chem. Ed.* **2002**, *41*, 4732–4734.

[144] D. Bourgeois, A. Pancrazi, S. P. Nolan, J. Prunet, *J. Organomet. Chem.*, **2002**, 643-644, 247-252

[145] P. Formentín, N. Gimeno, J. H. G. Steinke, R. Vilar, *J. Org. Chem.* **2005**, *70*, 8235–8238.

[146] G. C. Fu, S. T. Nguyen, R. H. Grubbs, *J. Am. Chem. Soc.* **1993**, *115*, 9856–9857.

[147] N. Gimeno, P. Formentín, J. H. G. Steinke, R. Vilar, *Eur. J. Org. Chem.* **2007**, *2007*, 918–924.

[148] R. R. Schrock, *Angew. Chem. Int. Ed.* **2006**, *45*, 3748–3759.

[149] B. L. Small, M. Brookhart, *J. Am. Chem. Soc.* **1998**, *120*, 7143–7144.

[150] K. Hiya, Y. Nakayama, H. Yasuda, *Macromolecules* **2003**, *36*, 7916–7922.

[151] A. Mortreux, M. Blanchard, *J. Chem. Soc. Chem. Commun.* **1974**, 786–787.

[152] A. Mortreux, O. Coutelier, *J. Mol. Catal. A Chem.* **2006**, *254*, 96–104.

[153] J. Heppekausen, R. Stade, A. Kondoh, G. Seidel, R. Goddard, A. Fürstner, *Chem. A Eur. J.* **2012**, *18*, 10281–10299.

[154] H. Ehrhorn, M. Tamm, *Chem. Eur. Journal* **2019**, *25*, 3190–3208.

[155] M. Zaranek, J. Robaszkiewicz, I. Janica, R. M. Gauvin, P. Pawluć, A. Mortreux, *Catal. Commun.* **2020**, *138*, 105944.

[156] J. Geng Lopez, M. Zaranek, P. Pawluc, R. M. Gauvin, A. Mortreux, *Oil Gas Sci. Technol.* **2016**, *71*, 20.

[157] D. Villemin, M. Héroux, V. Blot, *Tetrahedron Lett.* **2001**, *42*, 3701–3703.

CHAPTER 3

En route investigation of reaction conditions' influence on cross-metathesis yields employing Grubbs 2nd generation–*p*-cresol catalyst derivative

3.1 Abstract

A study investigated the ideal *p*-cresol to Grubbs second-generation catalyst (**GII**) ratio for maximizing selectivity in cross-metathesis reactions. Adding *p*-cresol to **GII** enhances selectivity for cross-metathesis over self-metathesis, with 100 equivalents of *p*-cresol ensuring optimal catalyst performance. The study focused on the cross-metathesis of 2-ethyl hexyl acrylate and *trans*-1-methoxy-4-(1-propenyl)benzene , varying *trans*-1-methoxy-4-(1-propenyl)benzene mole fractions from approximately 0.09 to 0.91. Using ^{1}H NMR spectroscopy, the reaction progress was monitored at 25°C and 35°C in CD_2Cl_2 solvent over 722 minutes, maintaining a constant *p*-cresol/**GII** ratio (100:1, X_1 = 0.33). The reaction setup followed previous protocols with slight adjustments for time-trace analysis. Results revealed an induction period at both temperatures, significantly shorter at 35 °C (4 minutes vs. 40 minutes at 25 °C). The elevated temperature notably increased the selectivity of the *p*-cresol/**GII** catalyst. Reaction kinetics showed the cross-metathesis rate with the modified catalyst was approximately 1.5 times faster than self-metathesis, with k'_{obs} values of 0.0575 min^{-1} (25 °C) and 0.68 min^{-1} (35 °C) for cross-metathesis compared to 0.033 min^{-1} and 0.41 min^{-1} for self-metathesis, respectively.

KEYWORDS: Grubbs 2nd generation catalyst; *p*-cresol; self-metathesis; cross-metathesis

3.2 Introduction

Olefin metathesis is a valuable technique for addressing various challenges in organic synthesis. It allows for the easy generation of carbon-carbon double bonds in a single step, while alternative methods often require multiple steps [2–5]. In 2001, Gladysz introduced the concept of an 'ideal catalyst' [6,7], challenging researchers globally to devise a catalyst capable of achieving synthesis with rapid reactions under atmospheric pressure, perfect atom economy, and 100% yields [7]. Over the past few decades, highly active olefin metathesis catalysts have been developed due to persistent research aimed at reducing synthetic steps and achieving desirable products in organic and polymer chemistry [8–11]. The development of these catalysts is a promising start towards attaining an 'ideal catalyst' [12–15]. They exhibit exceptional activity and stability, enabling them to tolerate a broad spectrum of organic functional groups.

Cross-metathesis is a practical synthetic method for forming desired olefinic products by adding a molecular fragment to a simple alkene, often one containing a functional group. This yields both the desired olefin and a smaller alkene which can also be recovered and utilized, addressing the issue of atom economy [16,17]. The commercially available imidazole-based Grubbs 2nd generation catalyst, **GII** (Figure 3.1a), is one of the most widely used homogeneous catalysts for olefin metathesis due its stability and functional group tolerance [3,18]. Prior to the invention of the Grubbs 2nd generation catalyst, functionalizing olefins through cross-metathesis with terminal alkenes containing electron-withdrawing functionalities such as α, β-unsaturated carbonyl compounds were a difficult task. The catalyst **GII** (Figure 3.1a), which contains a sterically hindering N-heterocyclic carbene was found to significantly reduce these restrictions [19,20]. As one of Gladysz's definitions for an ideal catalyst is a reasonable product yield [6,7], numerous researchers have made significant efforts to enhance selectivity towards CM product yield over undesired SM product in reactions between olefins and acrylate esters catalysed by Grubbs 2nd generation catalysts **GII** and phenol, such as *p*-cresol, as a co-catalyst [21–24].

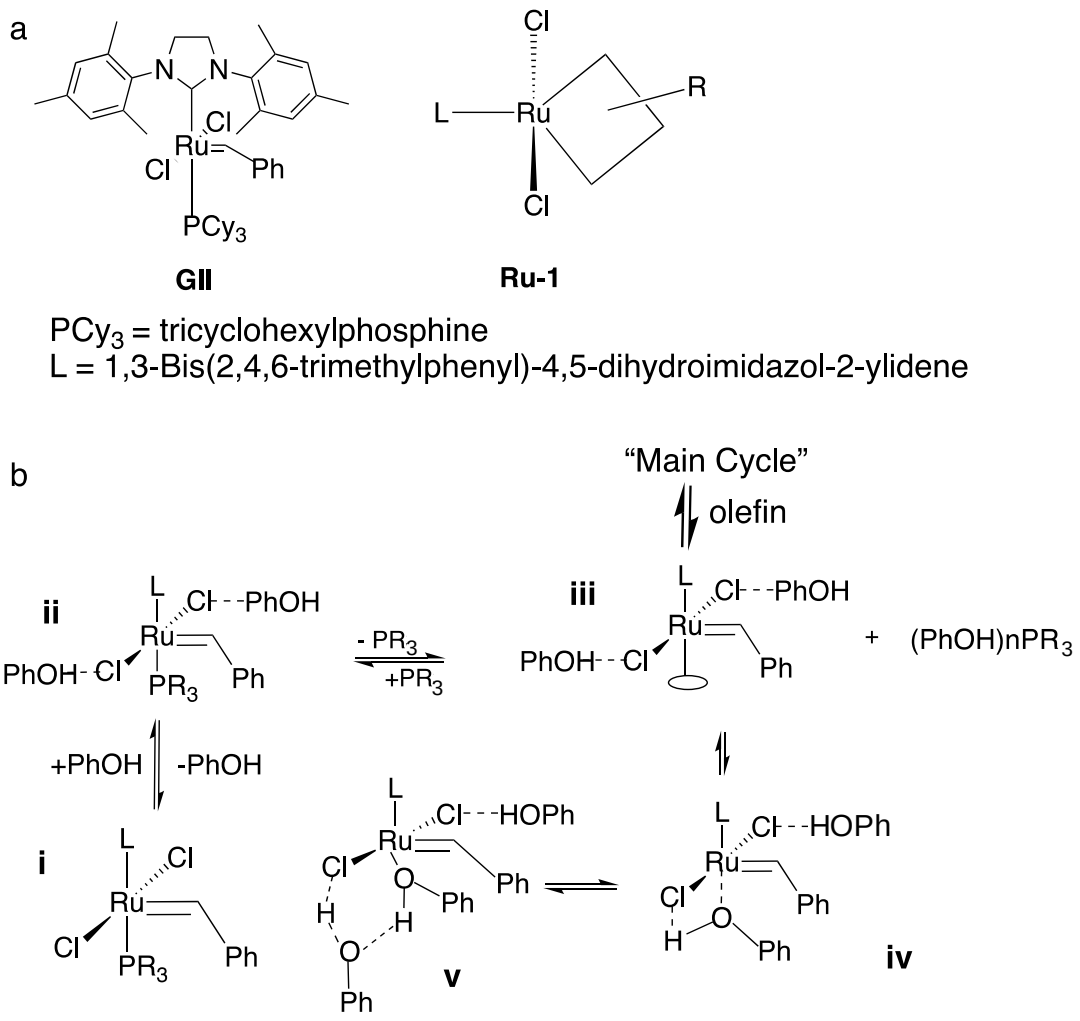

Figure 3.1: (a) Grubbs' 2nd generation catalysts (**GII**) and an intermediate ruthenacyclobutane (**Ru-1**), (b) the formation of hydrogen bonds between phenols and the chloride ligands of the catalyst [23–25].

Forman and Tooze (2005) discovered that the performance of the Grubbs 2nd generation catalyst (**GII**) for cross-metathesis reactions between acrylate esters and olefins could be enhanced by the addition of *p*-cresol [21]. Recently, Swart *et al*. (2021) demonstrated that the addition of *p*-cresol to **GII** assists the cross-metathesis of acrylates with prop-1-en-1-ylbenzenes under conditions that would conventionally result in only the self-metathesis product of prop-1-en-1-ylbenzene. Spectroscopic analyses supported the formation of a ruthenium benzylidene-*p*-cresol adduct, which influenced the electronic properties of the catalyst and promoted cross-metathesis [23].

Additionally, Forman *et al*. reported a mechanistic study, including NMR spectroscopy and DFT calculations, which showed that phenol improves the active metathesis cycle. This study also provided evidence for the hydrogen bond coordination of phenol to the chlorine in the active catalyst intermediate of **GII** (Figure 3.1 b) [23–25].

According to the report, the reflux of unsubstituted (*E*)-propen-1-ylbenzene and methyl acrylate in dichloromethane with **GII**, resulted in the quantitative yield of the undesired self-metathesis product of prop-1-en-1-ylbenzene, (*E*)-stilbene [23]. This confirms that the absence of *p*-cresol promotes self-metathesis products over cross-metathesis. The addition of *p*-cresol to **GII** resulted in the intended cross-metathesis product prevailing over self-metathesis [21,23,25].

Building on previous studies, this research aims to determine the extent to which *p*-cresol loading affects CM yield and to identify the optimal *p*-cresol/**GII** ratio for achieving the highest selectivity towards CM product formation. An investigation was conducted to evaluate the impact of reactant mole fraction on the production of CM products in the *p*-cresol/**GII** catalysed reaction between 2-ethyl hexyl acrylate and *trans*-1-methoxy-4-(1-propenyl)benzene , serving as a case study. These substrates were identified as model reagents since their cross-metathesis product, octyl methoxycinnamate (trade name: octinoxate or OMC), is an antioxidant and one of the active ingredients used in the formulation of sunscreen.

3.3 Results and Discussion

The chosen reactants for this study are *trans*-1-methoxy-4-(1-propenyl)benzene (**1**) and 2-ethylhexyl acrylate (**2**). They were selected due to the use of their cross-metathesis product in sunscreen formulation and the characteristic ^{1}H NMR resonances of both the reactants and possible CM and SM products in the ^{1}H NMR investigation of this study. Resonance overlap should be avoided, and characteristic resonances be easily distinguished from each other. Metathesis reaction investigation with these reagents make it both suitable for reaction comparison by product isolation and *in situ* investigating by means of ^{1}H NMR investigation.

The reaction between *trans*-1-methoxy-4-(1-propenyl)benzene (**1**) and 2-ethylhexyl acrylate (**2**) catalysed by *p*-cresol/**GII** can result in both cross-metathesis (CM) and self-metathesis (SM), as shown in Figure 3.2**:** The reaction scheme showing the cross-metathesis (CM) and self-metathesis

(SM) reactions pathways catalysed by *p*-cresol/**GII** between *trans*-1-methoxy-4-(1-propenyl)benzene (1) and 2- ethylhexyl acrylate (**2**) to form (E)-1,2-bis(4-methoxyphenyl)ethene (**3**), butene (**4**), (*E*)-2-ethylhexyl-3-(4-methoxyphenyl)acrylate (**5**), propene (**6**), bis(2-ethylhexyl) maleate (**7**), and ethene (**8**)

. The CM products are (*E*)-2-ethylhexyl-3-(4-methoxyphenyl)acrylate (**5**) and propene gas (**6**). Two different SM reaction pathways may occur for the reactants resulting in either (*E*)-1,2-bis(4-methoxyphenyl)ethene (**3**) and butene (**4**), the SM products of **1**, or bis(2-ethylhexyl) maleate (**7**) and ethene (**8**), the SM products of **2**. The metathesis gaseous products **4**, **6**, and **8** were removed from the reaction vessel by continuously purging with Ar gas throughout the reaction [26,27]. The reaction between *trans*-1-methoxy-4-(1-propenyl)benzene (1) and 2-ethylhexyl acrylate (2) catalysed by *p*-cresol/**GII** can result in both cross-metathesis (CM) and self-metathesis (SM), as shown in Figure 3.2. The CM products are (E)-2-ethylhexyl-3-(4-methoxyphenyl)acrylate (5) and propene gas (6). Two different SM reaction pathways may occur for the reactants, resulting in either (E)-1,2-bis(4-methoxyphenyl)ethene (3) and butene (4), the SM products of 1, or bis(2-ethylhexyl) maleate (7) and ethene (8), the SM products of 2. The metathesis gaseous products 4, 6, and 8 were removed from the reaction vessel by continuously purging with Ar gas throughout the reaction [26, 27]. Glittering particles form at the bottom of the reaction vessel due to the strong affinity of substrate **1** for itself, indicating the formation of the self-metathesis product **3**. However, the formation of SM product **3** was slower than expected due to the lower reactivity of internal olefins compared to terminal olefins, as reported in literature [1,28]. However, the SM product **7** was not detected by TLC under ultraviolet visible light (UV-Vis). As a result, it could not be isolated and monitored during separation of the products.

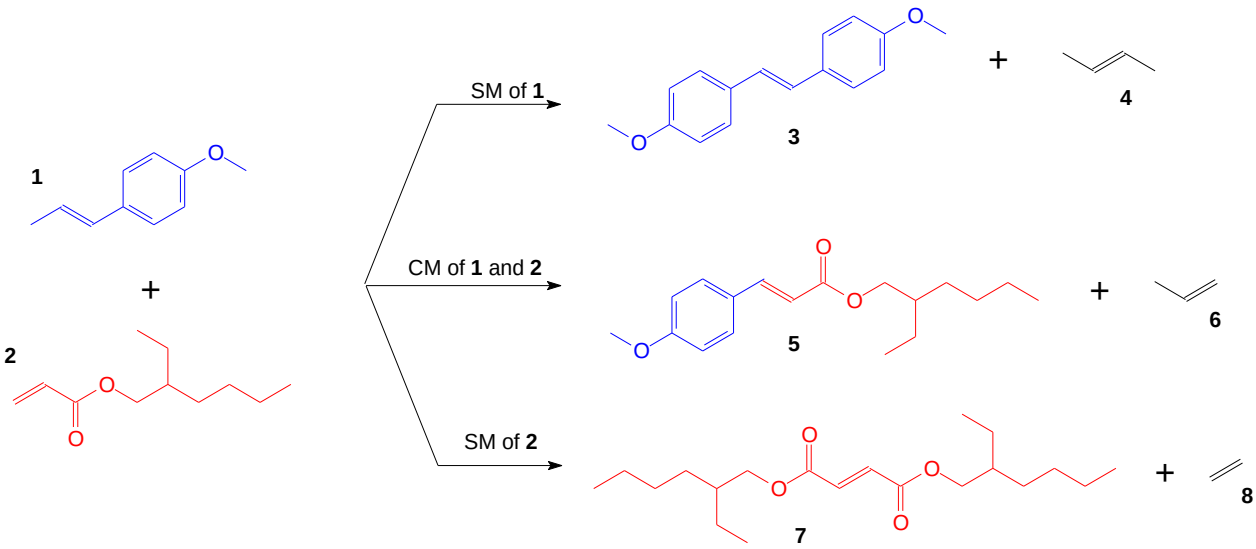

Figure 3.2: The reaction scheme showing the cross-metathesis (CM) and self-metathesis (SM) reactions pathways catalysed by *p*-cresol/**GII** between *trans*-1-methoxy-4-(1-propenyl)benzene (1) and 2- ethylhexyl acrylate (**2**) to form (E)-1,2-bis(4-methoxyphenyl)ethene (**3**), butene (**4**), (*E*)-2-ethylhexyl-3-(4-methoxyphenyl)acrylate (**5**), propene (**6**), bis(2-ethylhexyl) maleate (**7**), and ethene (**8**)

To determine whether the addition of *p*-cresol affected the outcome of the catalysis reaction, the reaction was first conducted in the absence of *p*-cresol under the same reaction conditions used as reported by Swart *et al.* The reaction involved refluxing one equivalent of **1** and two equivalents of **2** in dry dichloromethane under Ar purge for three hours, followed by isolation of the products.

In the absence of *p*-cresol, the percentage yield of the desired CM product, **5**, was only 15% (see table 3.1, entry 1) [21,23,25]. The addition of 0.5 equivalents of *p*-cresol (*vs* **GII** eq.) to the reaction conditions slightly increased the formation of the CM product (21% *vs* 15%). To determine if the selectivity of the reaction between **1** and **2** catalysed by *p*-cresol/**GII** can be further adjusted towards CM, the number of equivalents of *p*-cresol to that of **GII** was varied. The results are summarised in Table 3.1**:** Summarised data results of the *p*-cresol equivalent (vs **GII** eq.), resulting the isolated product yield of the cross-metathesis (for the reaction refluxed in CH_2Cl_2 under Ar and X1 = 0.33)

(the yield of the SM is presented in Table S3.1). As the equivalent amount of *p*-cresol increased from 0 to 100 equivalents (to **GII**), the isolated % yield of the CM product, **5**, increased from 15% to 46%, see Figure 3.3**:** The graphs showing the relationship between (A) the *p*-cresol:**GII** ratio and the isolated % yield of CM product, 5, (for the reaction refluxed in CH_2Cl_2 under Ar and X1 = 0.33) and (B) shows the CM product, 5, in terms of mole fraction of 1. [mole fracti A and Table

3**.1:** Summarised data results of the *p*-cresol equivalent (vs **GII** eq.), resulting the isolated product yield of the cross-metathesis (for the reaction refluxed in CH_2Cl_2 under Ar and X1 = 0.33)

(entries 2-9). However, increasing the equivalent amount of *p*-cresol to beyond 150 catalyst equivalents (Table 3.1**:** Summarised data results of the *p*-cresol equivalent (vs **GII** eq.), resulting the isolated product yield of the cross-metathesis (for the reaction refluxed in CH_2Cl_2 under Ar and X1 = 0.33)

entries 10-12) resulted in a decrease in the isolated % yield of the CM product, **5**.

In the context of **GII** molecules, it is important to note that each **GII** molecule can coordinate with two molecules of *p*-cresol through the -Cl ligands. At lower concentrations of *p*-cresol, incomplete coordination occurs due to limited availability of molecules, as diffusion in the solvent prevents all ligands from effectively binding. However, when the concentration of *p*-cresol increases, up to 100 times the equivalents of **GII**, there is a significant enhancement in coordination. This increase in equivalents allows for a higher degree of ligand coordination, ultimately contributing to improved CM yields.

When the concentration of *p*-cresol exceeds 100 equivalents of **GII**, the yield of CM decreases. This may be due to *p*-cresol acting as a solvent [29], which could affect the diffusion of reactants and the product distribution. Therefore, 100 equivalents of *p*-cresol ensure optimal catalyst performance as previously reported [23,30].

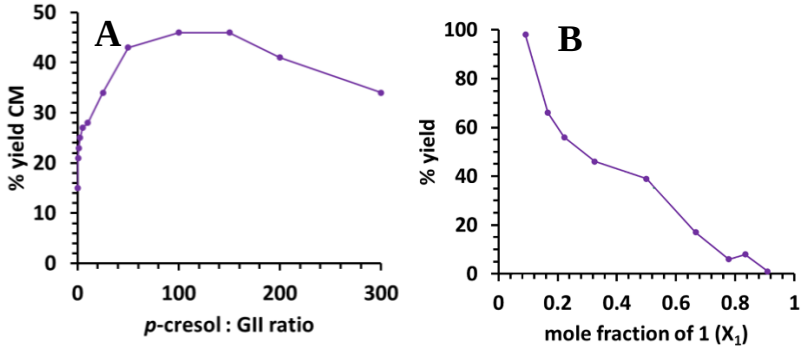

Figure 3.3: The graphs showing the relationship between (A) the *p*-cresol:**GII** ratio and the isolated % yield of CM product, 5, (for the reaction refluxed in CH_2Cl_2 under Ar and X1 = 0.33) and (B) shows the CM product, 5, in terms of mole fraction of 1. [mole fraction of 1. [mole fraction: $X_1 = (n_1)/(n_1 + n_2)$, where n is the mol of the reactants used]

In **GII** catalysed metathesis reactions, acrylate is often used in higher equivalents than the olefin due to its lower reactivity as an electron-poor α,β-unsaturated carbonyl compound. This is supported by Fogg *et al.* who use a five-fold excess of electron-poor reactants [22]. Our findings demonstrate that the mole fraction of reagent equivalents has a significant impact on product distribution. **Error! Reference source not found.** (and Table S3.2) summarise the data, while Figure 3**.3:** The graphs showing the relationship between (A) the *p*-cresol:**GII** ratio and the isolated % yield of CM product, 5, (for the reaction refluxed in CH_2Cl_2 under Ar and X1 = 0.33) and (B) shows the CM product, 5, in terms of mole fraction of 1. [mole fracti B presents the visual results.

Under the reaction conditions described in **Error! Reference source not found.**, the yield of CM product **5** decreases as the amount of olefin **1** increases when it is in excess ($X_A \geq 0.67$) (**Error! Reference source not found.** entries 1-4). Conversely, when the acrylate, **2**, is in excess ($X_A \leq 0.33$) the yield of CM product **5** increases significantly up to 98% (at $X_A = 0.09$) as the amount acrylate equivalents increases (**Error! Reference source not found.**, entries 6-9). Although olefin **1** has a higher affinity for itself, the results suggest that the CM pathway is kinetically more favourable. The ratio of substrate is a critical factor in determining the results of chemical reactions, as demonstrated in several studies [3,4]. However, our objective is to accurately measure the degree of this influence and evaluate the economic feasibility of pushing these ratios to the limit to increase CM yield. By investigating the effect of substrate ratios on reaction outcomes, we aim to offer valuable insights into optimizing CM yield while considering the practicality of such modifications.

Table 3.1: Summarised data results of the *p*-cresol equivalent (vs **GII** eq.), resulting the isolated product yield of the cross-metathesis (for the reaction refluxed in CH_2Cl_2 under Ar and X1 = 0.33)

Entry no	*p*-cresol eq.	CM yield %
1	0	15
2	0.5	21
3	1	23
4	2.5	25
5	5.0	27
6	10	28
7	25	34
8	50	43
9	100	46
10	150	46
11	200	41
12	300	34

Conditions: **GII** (0.5 mol%), *p*-cresol (varied amounts 0 to 300 equivalent *vs* 1eq. **GII**), refluxing in dry under a dry argon atmosphere.

Table 3.2: Table showing moles of reagent, mole fraction of 1, mole ratios, cross-metathesis yield, and self-metathesis yield

Entry no	Mole substrate		X_1	Substrate ratio		CM yield %
	1	2		1	2	5
	(mmol)	(mmol)				
1	13	1.3	0.91	10	1	1
2	6.5	1.3	0.83	5	1	8
3	4.55	1.3	0.78	3.5	1	6
4	2.6	1.3	0.67	2	1	17
5	1.3	1.3	0.50	1	1	39
6	1.3	2.7	0.33	1	2	46
7	1.3	4.55	0.22	1	3.5	56
8	1.3	6.5	0.17	1	5	66
9	1.3	13	0.09	1	10	98

Conditions: **GII** (0.5 mol%), *p*-cresol (0.25 eq. *vs* 1eq. **GII**), refluxing in dry under a dry argon atmosphere.

The formation and distribution of CM (**5**) products are significantly affected by reaction time. Therefore, we monitored the reaction using ^{1}H NMR spectroscopy in CD_2Cl_2 at different temperatures (25 °C and 35 °C) in the presence of *p*-cresol/**GII** (100:1 ratio) and X_1 = 0.33. The ^{1}H NMR spectral regions displayed in **Error! Reference source not found.** B and C were used to monitor the reaction and determine product concentrations for the metathesis reaction at 25 °C and 35 °C. Figure 3.5**:** The time trace of the metathesis reaction between 1 and 2 catalysed by *p*-cresol/**GII** A and B show the time traces for the formation of **3** and **5**, respectively, constructed

from the data obtained in **Error! Reference source not found.** B and C. The NMR spectra of **3** and **5** are shown in Figure S3.1 and S3.2, respectively.

Based on the time trace graphs in Figure 3.5**:** The time trace of the metathesis reaction between 1 and 2 catalysed by *p*-cresol/**GII** A and B, it is evident that an induction period occurs at both temperatures under investigation. The induction period, which is the initial slow kinetic stage, is more prominent at the lower temperature. This reaction's induction period may be associated with catalyst activation, dissociation of the phosphine ligand and/or catalyst modification through the formation of the *p*-cresol/**GII** adduct, as previously reported [31,32]. At 25 °C during this induction period, the SM reaction to form **3** is slow but present, since **GII** catalyses SM. An omissible amount of **5**, the CM product, is formed probably since the CM product formation is favoured by the modified the *p*-cresol/**GII** catalyst adduct, which has presumably not formed yet. After the induction period, when the *p*-cresol/**GII** adduct has started to form, the CM reaction proceeds slightly faster (k'_{obs} = 0.0575 min^{-1}, as shown in Figure S3.1 A) than the SM reaction (k'_{obs} = 0.033 min^{-1}, as shown in Figure S3.1 A), even though the concentration of the CM product formed is less (Figure 3**.5:** The time trace of the metathesis reaction between 1 and 2 catalysed by *p*-cresol/**GII** A). The reaction has not yet achieved full conversion or reached equilibrium after 700 min. At the higher temperature of 35 °C, the induction period is only 4 min compared to the *ca*. 40 min at 25 °C. The elevate temperature has a significant effect on the selectivity of the *p*-cresol/**GII** catalyst towards CM. The rate for the CM reaction (k'_{obs} = 0.68 min^{-1}, see Figure S3.1 B) is *ca.* 1.5 times that of the SM reaction k'_{obs} = 0.41 min^{-1}, see Figure S1 B). In addition, the selectivity towards the CM product (**5**) formation is by almost doubled at this higher temperature. After 150 min of reaction time, the concentration of the SM product, **3**, reached a steady-state value of 0.0278 M. However, the formation of the CM product, **5**, has not yet reached its equilibrium concentration.

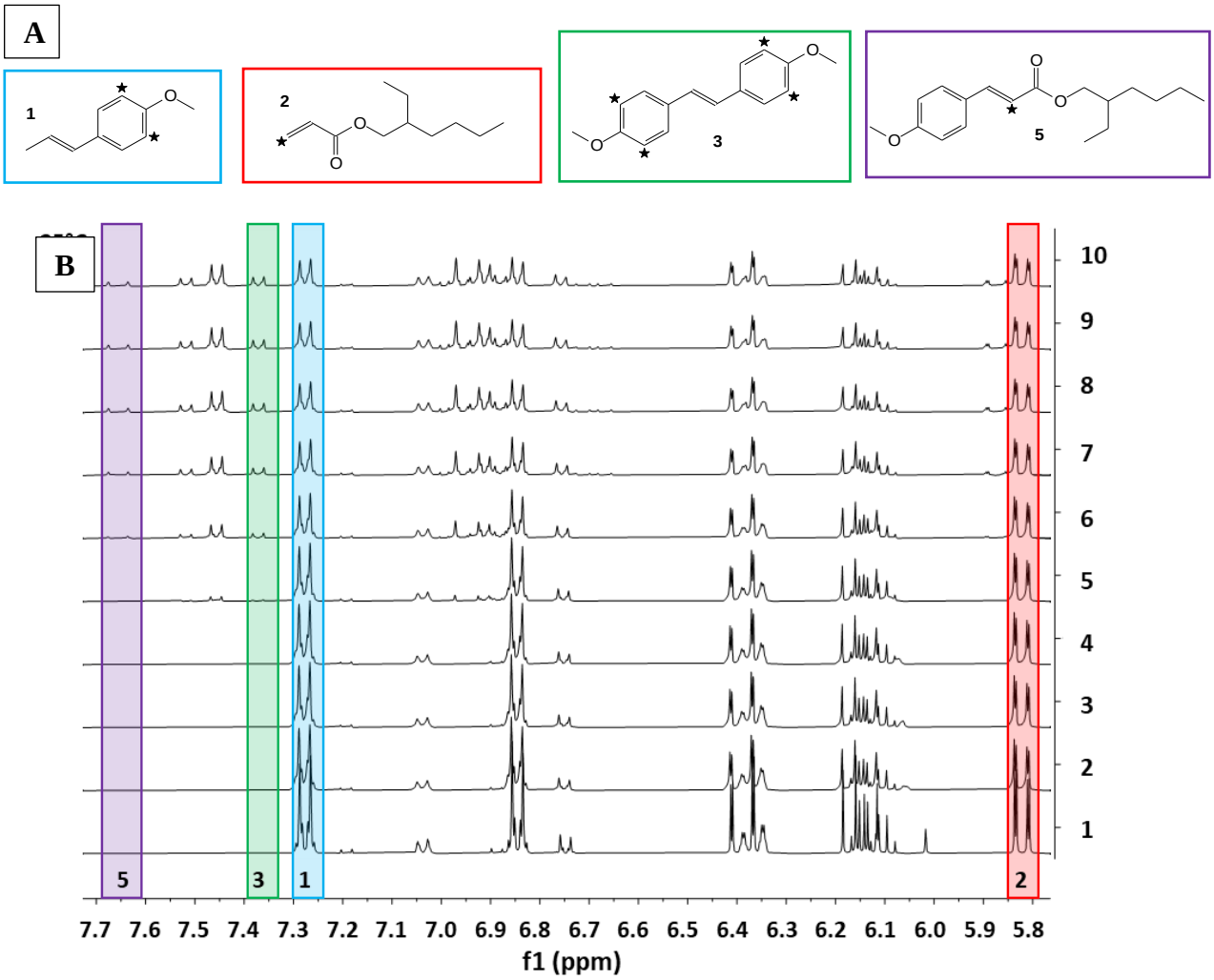
A
1
2
3
5
B
10
9
8
7
6
5
4
3
2
1
5
3
1
2
7.7 7.6 7.5 7.4 7.3 7.2 7.1 7.0 6.9 6.8 6.7 6.6 6.5 6.4 6.3 6.2 6.1 6.0 5.9 5.8
f1 (ppm)

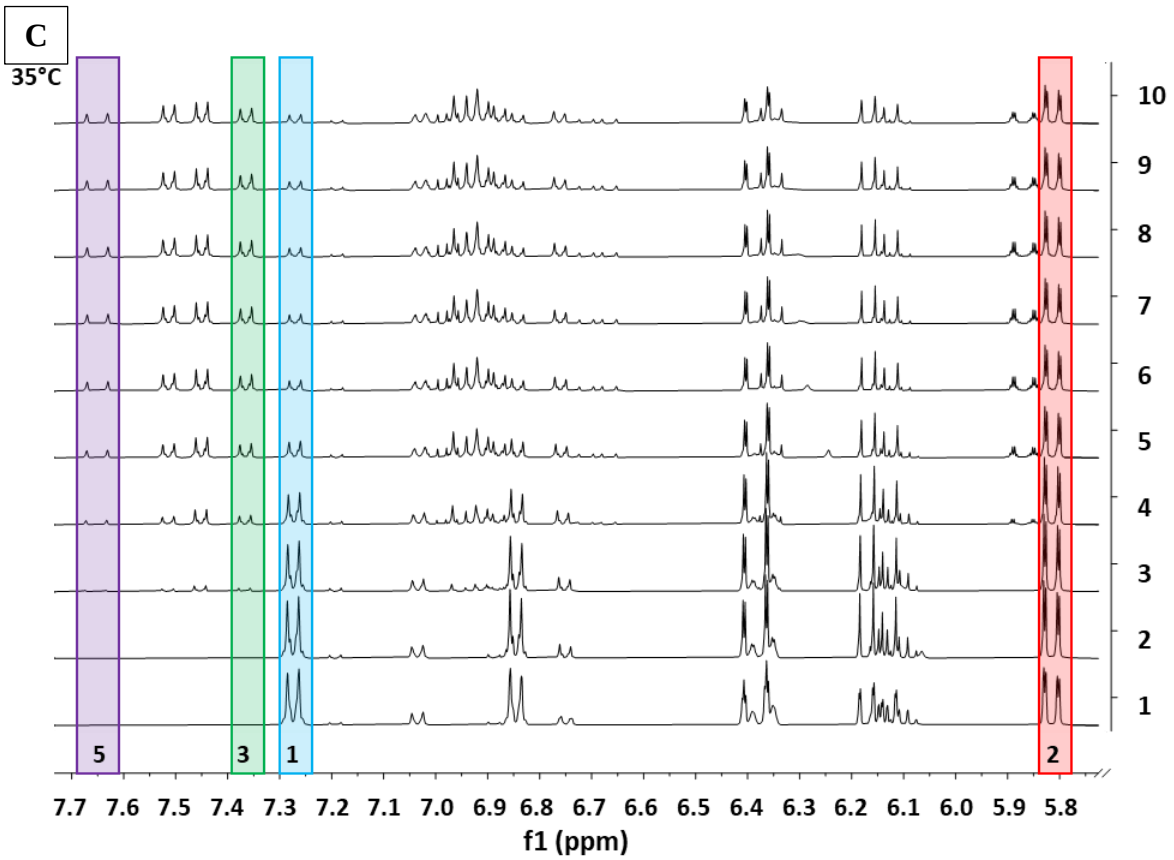

Figure 3.4: The assigned resonances used for the kinetic data belonging to 1, 2, 3, and 5 are indicated by blue, red, green, and purple respectively, ★ shows the assigned 1H NMR resonances used as characteristics compounds indicators. The time dependent ^{1}H NMR of the metathesis reaction mixture between trans-1-methoxy-4-(1-propenyl) benzene and 2-ethylhexyl acrylate in the presence of *p*-cresol/GII (100:1 ratio) at (B) 25 °C and (C) 35 °C in CD_2Cl_2. The spectra at times t = 0 min. (1), t = 3 mins. (2), t = 11 mins. (3), t = 30 mins. (4), t = 77 mins. (5), t = 162 mins. (6), t = 262 mins. (7), t = 392 mins. (8), t = 702 mins. (9) and t = 722 mins. (10) are shown

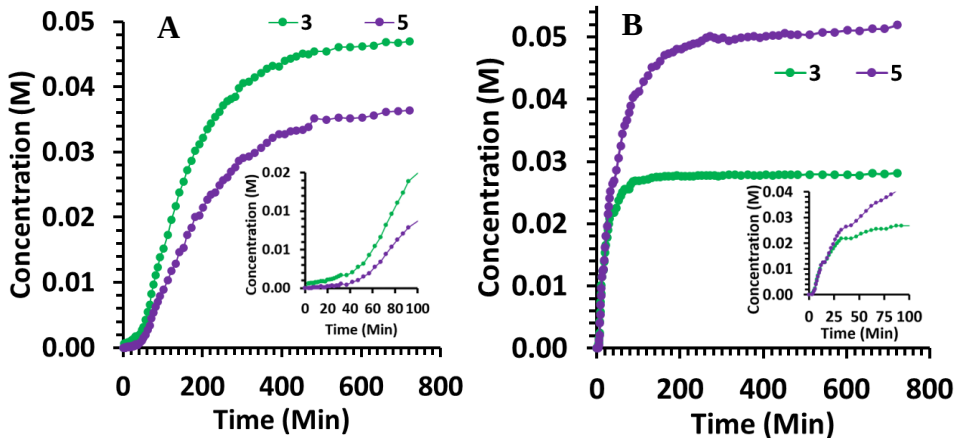

Figure 3.5: The time trace of the metathesis reaction between 1 and 2 catalysed by *p*-cresol/**GII** adduct at (A) 25 °C and (B) 35 °C in CD_2Cl_2 under Ar and $X_1 = 0.33$, following the appearance of the *in situ* metathesis product formation, SM (3, green), and CM (5, purple).

3.4 Materials and methods

3.4.1 General

p-Cresol (99%), *trans*-1-methoxy-4-(1-propenyl)benzene [(*E*)-anethole (99%)], **1**, 2-ethyl hexyl acrylate (98%), **2**, and the Grubbs 2nd generation catalyst [1,3-bis(2,4,6-trimethylphenyl)-2-imidazolidinylidene)dichloro(phenyl methylene)(tricyclohexylphosphino)ruthenium], **GII**, were all purchased from Sigma-Aldrich and used under inert conditions without further purification. Dry solvents were obtained by passing the solvent through a small column of activated neutral alumina (10% v/v) before use. Preparative Thin-Layer Chromatography (PTLC) using Silica Gel F254 (0.2 mm layer) on glass plates (20 cm × 20 cm) coated with a layer of Merck Kieselgel 60 PF254 that had been air-dried overnight at room temperature were used for isolation of the products.

3.4.2 ^{1}H NMR Spectroscopy

^{1}H NMR spectroscopy was recorded at different temperatures on a 400 MHz Bruker AVANCE III spectrometer in either $CDCl_3$ or CD_2Cl_2. Reported hydrogen shifts are relative to tetramethyl silane (TMS) in $CDCl_3$ or CD_2Cl_2 at δ0.00 ppm.

3.4.3 Influence of *p*-cresol equivalent to GII on metathesis reaction between 1 and 2

The following general procedure was used during the equivalent studies, which was adopted from the reported procedure described by Swart *et al.* [23]

GII (5.7 mg, 0.0067 mmol, 0.5 mol%), *p*-cresol (varied amounts 0 to 300 equivalent *vs* 1eq. **GII**), and dry DCM (10 mL) were heated to reflux while being stirred under a dry argon atmosphere. Trans-1-methoxy-4-((1-propenyl)benzene), **1**, (0.20 mL, 1.3 mmol, 1 eq.) and 2-ethylhexyl acrylate, **2**, (0.56 mL, 2.7 mmol, 2 eq.) were added to the existing mixture simultaneously and the reaction was allowed to proceed for 3 hours. The reaction mixture was concentrated in vacuo and the resulting mixture was applied on a preparative TLC plate for separation to obtain the purified SM and CM major products.

Characterization data of (*E*)-1,2-bis(4-methoxyphenyl)ethene (**3**):

^{1}H NMR (400MHz, CD_2Cl_2) [23]: δ = 7.53-7.42 (m, 4H), 6.98 (s, 2H), 6.93 (d, J = 8.9 Hz, 4H), 3.85 (s, 6H, -OCH_3)

Characterization data of (*E*)-2-ethylhexyl-3-(4-methoxyphenyl)acrylate (**5**):

^{1}H NMR (400MHz, CD_2Cl_2) [23]: δ = 7.65 (d, J=16.0, 1H), 7.54 (d, J = 8.9 Hz, 2H), 6.96 (d, J = 8.8Hz, 2H), 6.37 (d, J = 16.0 Hz, 1H), 4.18-4.08 (m, 2H), 3.86 (s, 3H, -OCH_3), 1.68 (dq, J = 12.2, 6.1 Hz, 1H), 1.51-1.32 (m, 8H), 0.95 (ddd, J = 8.8, 6.9, 5.3 Hz, 6H)

3.4.4 Influence of mole ratio of 1 on the metathesis reaction catalysed by *p*-cresol/GII

The following general procedure was used during the equivalent studies, which was adopted from the reported procedure described by Swart *et al.* [23]:

GII (5.7 mg, 0.0067 mmol, 0.5 mol%), *p*-cresol (0.072 g, 0.67 mmol, 0.25 eq.), and dry DCM (10 mL) was heated to reflux while being stirred under a dry argon atmosphere. Trans-1-methoxy-4-(1-propenyl)benzene, **1**, and 2-ethyl hexyl acrylate, **2**, (with mole fraction X_1 varying between 0.91 and 0.09) were added to the existing mixture simultaneously and the reaction was allowed to proceed for 3 hours. The reaction mixture was concentrated in vacuo and the resulting mixture was applied on a preparative TLC plate for separation to obtain the purified SM and CM products.[26]

3.4.5 Monitoring of the metathesis

The following general procedure was used during the equivalent studies, which was adopted from the reported procedure described by Swart *et al.* [1,23]

The metathesis reaction between trans-1-methoxy-4-(1-propenyl) benzene, **1**, and 2-ethylhexyl acrylate, **2**, catalysed by *p*-cresol/**GII** adduct in CD_2Cl_2 in an NMR tube was monitored in real time by ^{1}H NMR spectroscopy at different temperatures (25 °C and 35 °C).

Trans-1-methoxy-4-(1-propenyl) benzene, **1**, (0.0975 mmol) and 2-ethylhexyl acrylate, **2**, (0.042 mmol) were dissolved in CD_2Cl_2 (0.75 mL) with **GII** (0.503 μmol, 0.5 mol %) and *p*-cresol (0.050 mmol), in a standard NMR tubes under argon atmosphere and the tube closed with an NMR tube cap. ^{1}H NMR were recorded at differing time intervals for *ca*. 12 hours at 25 °C and 35 °C. The concentration of each reagent and products was determined in M by integration of characteristics resonances with TMS as an internal standard (∫ 1.0). Because we know the initial concentration of our reagents, and the concentration of TMS does not change over time, the concentration of the of the starting materials and products [C_χ] at differing times can be calculated using the ratio between the integral of the TMS and characteristic resonances of the starting materials and products with Equation 1[1]

$$[C_x]_t = \frac{(I_\chi)_t \times [C]_0}{(I)_{tot}}$$

$[C_\chi]_t$ = Concentration of compounds (χ) at t_t

$[C]_0$ = Concentration of reagents at t_0

$(I_\chi)_t$ = Sum of resonance integrals (∫) for compound (χ) at t_t

$(I)_{tot}$ = Total resonance integral of reaction mixture at time t_t

3.5 Conclusion

As the ideal metathesis catalyst might not exist yet, ideal reaction conditions for the metathesis catalyst can be optimised to favour cross-metathesis. The highest selectivity for the desired cross-metathesis product was achieved with a *p*-cresol/**GII** ratio of 100:1, which confirms the impact of *p*-cresol in promoting the CM product. In metathesis reactions involving olefins and acrylates, it

is conventional to use an excess of the acrylate since it is the less reactive starting material. Our findings demonstrates that the reagent equivalent has a significant impact on the product distribution. When the acrylate, **2**, was in excess ($X_A \leq 0.33$), the yield of the CM product, **5**, increased exceptionally up to 98% (at $X_A = 0.09$). The results indicate that under these conditions, the CM pathway is more favoured kinetically despite **1** having a strong affinity for itself. Temperature and time studies revealed that an increase in temperature aids the formation of the *p*-cresol/**GII** adduct, which catalyses the formation of the CM product, **5**, product as its formation proceed at ($k'_{obs} = 0.0575\ min^{-1}$) at 25 °C compared to its rate ($k'_{obs} = 0.68\ min^{-1}$) at 35 °C. Additionally, the selectivity towards the formation of the CM product, **5**, is approximately twice as high when the reaction is conducted at 35 °C compared to 25 °C. The concentration of the SM product, **3**, reached a steady-state value of 0.0278M after 700 min of reaction time. However, the concentration of the CM product, **5**, did not appear to have reached equilibrium at the same time.

References

[1] M. R. Swart, C. Marais, E. Erasmus, Catalyst **2021**, *11*, 1483

[2] F. B. Hamad, T. Sun, S. Xiao, F. Verpoort, *Coord. Chem. Rev.* **2013**, *257*, 2274–2292.

[3] J. W. Morzycki, *Steroids* **2011**, *76*, 949–966.

[4] F. C. Courchay, T. W. Baughman, K. B. Wagener, *J. Organomet. Chem.* **2006**, *691*, 585–594.

[5] X. Meng, K. J. Edgar, *Carbohydr Polym* **2015**, *132*, 565–573.

[6] A. Michrowska, K. Grela, *Pure Appl. Chem.* **2008**, *80*, 31–43.

[7] J. A. Gladysz, *Pure Appl Chem* **2001**, *73*, 1319–1324.

[8] P. Schwab, R. H. Grubbs, J. W. Ziller, *J. Am. Chem. Soc.* **1996**, *118*, 100–108.

[9] T. Matsuo, *Catalysts* **2021**, *11*, 359.

[10] M. Martinez-Amezaga, C. Delpiccolo, L. Méndez, I. Dragutan, V. Dragutan, E. Mata, *Catalysts* **2017**, *7*, 111.

[11] J. Engel, W. Smit, M. Foscato, G. Occhipinti, K. W. Törnroos, V. R. Jensen, *J. Am. Chem. Soc.* **2017**, *139*, 16609–16619.

[12] J. I. Yun, H. R. Kim, S. K. Kim, D. Kim, J. Lee, *Tetrahedron* **2012**, *68*, 1177–1184.

[13] T. Bano, A. F. Zahoor, N. Rasool, M. Irfan, A. Mansha, *J. Iran. Chem. Society*, **2022**, 19, 2131-2170

[14] M. Felischak, T. Wolff, L. Alvarado Perea, A. Seidel-Morgenstern, C. Hamel, *Catalysts* **2022**, *12*, 188.

[15] S. Monfette, D. E. Fogg, *Chem Rev* **2009**, *109*, 3783–3816.

[16] R. Palkovits, D. Arlt, H. Stepowska, F. Schüth, *Micropor Mesopor Mat.* **2010**, *132*, 319–327.

[17] P. H. Dixneuf, C. Bruneau, C. Fischmeister, *Oil Gas Sci. Technol.* **2016**, *71*, 19.

[18] O. M. Ogba, N. C. Warner, D. J. O'Leary, R. H. Grubbs, *Chem. Soc. Rev.* **2018**, *47*, 4510–4544.

[19] A. K. Chatterjee, J. P. Morgan, M. Scholl, R. H. Grubbs, *J. Am. Chem. Soc.* **2000**, *122*, 3783–3784.

[20] A. K. Chatterjee, T. L. Choi, D. P. Sanders, R. H. Grubbs, *J. Am. Chem. Soc.* **2003**, *125*, 11360–11370.

[21] G. S. Forman, R. P. Tooze, *J. Organomet. Chem.* **2005**, *690*, 5863–5866.

[22] G. A. Bailey, D. E. Fogg, *J. Am. Chem. Soc.* **2015**, *137*, 7318–7321.

[23] M. R. Swart, L. Twigge, E. Erasmus, C. Marais, B. C. B. Bezuidenhoudt, *Eur. J. Inorg. Chem.* **2021**, *18*, 1752–1762.

[24] A. G. Santos, G. A. Bailey, E. N. dos Santos, D. E. Fogg, *ACS Catal.* **2017**, *7*, 3181–3189.

[25] G. S. Forman, A. E. McConnell, R. P. Tooze, W. Janse Van Rensburg, W. H. Meyer, M. M. Kirk, C. L. Dwyer, D. W. Serfontein, *Organometallics* **2005**, *24*, 4528–4542.

[26] W. L. McClennan, S. A. Rufh, J. A. M. Lummiss, D. E. Fogg, *J. Am. Chem. Soc.* **2016**, *138*, 14668–14677.

[27] B. J. Ireland, B. T. Dobigny, D. E. Fogg, *ACS Catal.* **2015**, *5*, 4690–4698.

[28] A. Abera Tsedalu, *J Chem* **2021**, *2021*

[29] B. Al Samak, V. Amir-Ebrahimi, D. G. Corry, J. G. Hamilton, S. Rigby, J. J. Rooney, J. M. Thompson, *J. Mol. Catal. A. Chem.* **2000**, *160*, 13–21.

[30] A. G. Santos, G. A. Bailey, E. N. dos Santos, D. E. Fogg, *ACS Catal.* **2017**, *7*, 3181–3189.

[31] M. R. Swart, B. C. B. Bezuidenhoudt, C. Marais, E. Erasmus, *Inorganica Chim. Acta* **2021**, *514*, 120001.

[32] M. R. Swart, C. Marais, E. Erasmus, *ACS Omega* **2021**, *6*, 28642–28653.

CHAPTER 4

Spectroscopic Exploration of Catalyst Dynamics and Electrochemical Properties of Grubbs Second Generation in Different Solvent

4.1 Abstract

The phosphine (PCy_3) ligand dissociation equilibrium from Grubbs second generation catalyst (**GII**) in different solvents (dichloromethane, dichloroethane, chloroform, tetrahydrofuran, and toluene) were determined to be pseudo first order with k_{obs} = 4.8 - 15.6 x 10^{-3} min^{-1}. An electrochemically reversible behaviour was observed for **GII** dissolved in the chlorinated solvents (DCM, DCE, and CLF). The formal reduction potentials, E°', of **GII** in the different chlorinated solvents increased as the polarity index of the solvent became larger. In THF, however, only the oxidation of **GII** could be detected. Upon oxidation of **GII**, THF (with a lone pair electron on the oxygen) which is highly coordinative solvent, nucleophilically attach to the electrochemically produced $Ru^{\bullet+}$, resulting in a redox inactive THF associated compound. A correlation was established between the ease of **GII** oxidation in the different solvents and the rate of PCy_3 dissociation in that solvent. The % yield of the cross-metathesis product in the different solvents at 40 °C catalysed by **GII** exponentially increased as the Gutmann donor number of the solvent increased, with DCM showing highest yield. In THF, no metathesis could be detected, agreeing the electrochemical data, that THF coordinate to the positively charged or active **GII** rending it inactive.

Keywords: Grubbs 2nd generation catalyst, UV-Vis, electrochemistry, cross-metathesis, solvent influence

4.2 Introduction

Olefin metathesis has remained a fundamental and well-known technique for the formation of a variety of carbon-carbon double bonds. This metathesis transformation has provided organic chemists with an additional method for synthesizing value-added chemicals and modifying existing compounds in terms of their steric and electronic properties [1–4]. The value of this fundamental methodology is not only restricted to the academic community, but it has also been adopted for pharmaceutical manufacturing [5,6], polymer synthesis [7,8], material synthesis [9,10], and the chemical industry [11,12]. The emergence of Grubbs catalyst in 2005 [13] increased the versatility of olefin metathesis as researchers continued to explore the diverse applications of this transformation. The Grubbs second-generation catalyst, **GII**, (Figure 4.1) is notable for its profound functional group tolerance and stability, which have contributed to its success in acrylate metathesis. This has made it a catalyst of choice for the cross-metathesis of acrylates with alkenes, including as *trans*-1-methoxy-4-(1-propenyl)benzene which can be used to form value-added products with numerous health benefits. This includes the active ethylhexyl methoxycinnamate, which is used in a wide range of cosmetic products as a sunscreen against ultraviolet (UV) radiation. This subsequently prevents sunburn, skin cancer and premature ageing [14,15].

Although Grubbs second generation catalyst for acrylate metathesis has considerable merits, the dissociation of PCy_3 ligand from the catalyst is imperative for the initiation of the active catalytic cycle [15–19]. However, this dissociation also leads to the occurrence of unwanted side reactions, and the rebinding of the PCy_3 is detrimental to the active site of the catalyst [10,15–20]

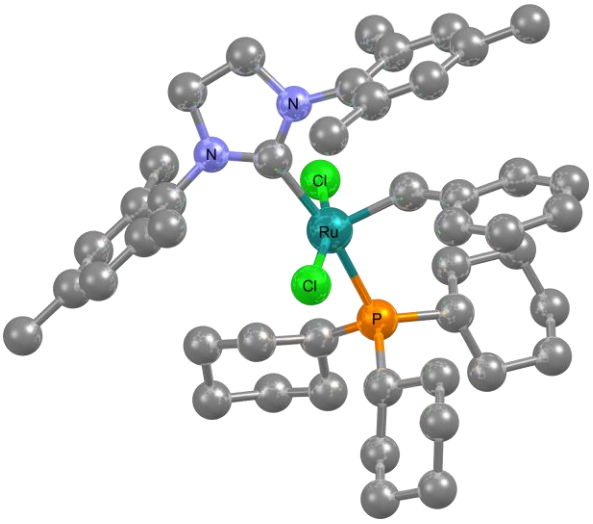

Figure 4.1: Optimised 3D structure of Grubbs' second-generation catalyst

During metathesis catalysed reactions, solvent effects are noted for being intricate, having varying effects on the rates of initiation activity, selectivity, and deactivation [16,20,21]. In 2007, Szadkowska *et al*. reported a significant increase in catalytic olefin metathesis activity when second-generation ruthenium pre-catalysts were added to solvents such as octa-fluorotoluene and hexafluorobenzene. Using common commercially available ruthenium pre-catalysts, challenging metathesis reactions including the production of tetrasubstituted C–C double bonds were made viable in these media [22]. Owing to the classification of DCE as a source of human carcinogen by U.S. Environmental Protection Agency and declared unsafe by CHEM21 consortium [23,24]. Fogg's group replaced DCE with toluene in anethole-2-ethylhexylacrylate cross-metathesis, and the CM yield obtained with **GII** were relatively lower than those in DCE. But the use of phenol resin with indenylidene analogue of **GII** markedly improved the performance increasing the yield to 96% [16]. In 2021, unsubstituted (E)-prop-1-en-1-ylbenzene and methyl acrylate catalysed by **GII** were refluxed in DCM, and the undesired self-metathesis, stilbene, prevailed in quantitative yield. An attempt to influence the selectivity of **GII** to favour CM yield using other solvents e.g. THF, and toluene had no effect on the outcome of the reaction [25].

Cross-metathesis reactions using **GII** as the catalyst commonly employ solvents that are effective in dissolving both the catalyst and the reactants while providing an appropriate environment for the reaction to proceed efficiently. Understanding the interaction between **GII** and the solvent is essential for optimizing the metathesis reaction conditions to yield the desired CM product. The five most commonly used solvents are dichloromethane (DCM, CH_2Cl_2), chloroform (CLF, $CHCl_3$), dichloroethane (DCE, $C_2H_4Cl_2$), tetrahydrofuran (THF, C_4H_4O), and toluene (TOL, $C_6H_5CH_3$). However, few studies are available on the characterization of **GII** in these solvents, their effects on the catalyst, and the outcome of the cross-metathesis catalysed reaction. The stability of **GII** in the aforementioned solvents was investigated using UV-Visible spectroscopy. An electrochemical study using cyclic voltammetry (CV), gave insight into how the different solvents influences the electrochemical properties of **GII**. This data will be discussed in terms of the effectiveness of cross-metathesis reaction catalysed by **GII** in the various solvents.

4.3 Results and Discussion

ATR-FTIR and UV-Visible spectroscopy. The characteristic absorption bands of a neat sample of **GII** in the FTIR spectra is the C-N stretching frequency of the SIMes ligand at 1262 cm^{-1} and the C-P stretching frequency at 740 cm^{-1} as previously reported [26]. The ν_{CN} and ν_{CP} of **GII** dissolved in the different solvents (dichloromethane (DCM), chloroform (CLF), dichloroethane (DCE), tetrahydrofuran (THF), and toluene (TOL)) has shifted significantly and these shifts are dependent on the solvent, see **Error! Reference source not found.** and Figure S4.1 in the supplementary information.

The UV–Vis absorption spectra of 0.10 mM solutions of **GII** in dry DCM, TOL, DCE, CLF, and THF at room temperature are shown in Figure 4.2**:** UV–Vis spectra of 0.10 mM solutions of **GII** in dry dichloromethane (grey), . The λ_{max} and ε_{max} for each solvent are summarised in **Error! Reference source not found.**. The λ_{max} of the bands ranging within 333-337 nm is assigned to the Ru-CHPh metal-ligand charge transfer (MLCT) in correlation to what was reported for homologue ruthenium benzylidene compounds [27,28]. The spectra of **GII** in the different solvents showed a second absorption band (λ_{2nd}) which was weaker in intensity at longer wavelengths ranging between 489-502 nm. This second band is ascribed to the forbidden Ru=C_{ene} visible metal ligand charge transfer. The ε_{2nd} values for the forbidden Ru=C_{ene} visible MLCT band ranges from 380 M^{-1} cm^{-1} (in DCM) to 590 M^{-1} cm^{-1} (in DCE). This is an indication that the degree of allowedness for transition in DCE is higher than in DCM [29].[i]

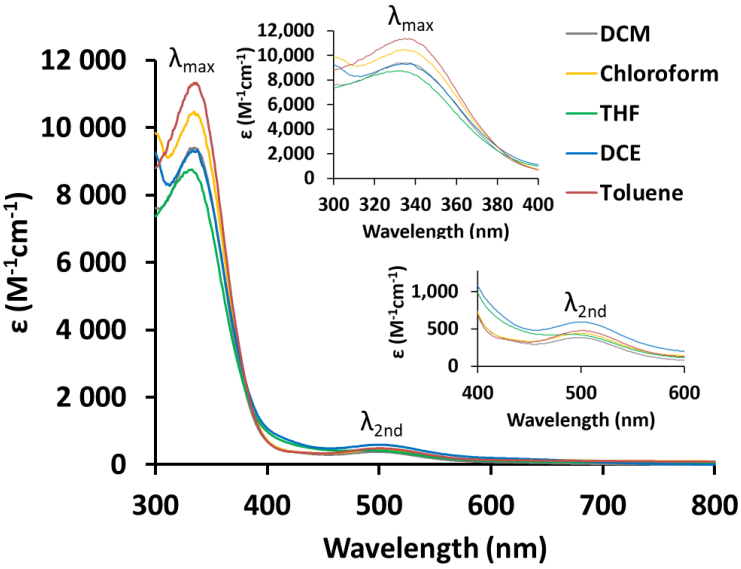

Figure 4.2: UV–Vis spectra of 0.10 mM solutions of **GII** in dry dichloromethane (grey), chloroform (yellow), dichloroethane (blue), tetrahydrofuran (green), and toluene (red). Insert: Expanded sections between 300-400 nm and 400-600nm. Color can be seen in the online version.

Table 4.1: Summary of the FTIR and UV-vis data of **GII** in different solvents

Solvents	FTIR		UV-vis data			
	$\nu_{C\text{-}P}$ (cm^{-1})	$\nu_{C\text{-}N}$ (cm^{-1})	λ_{max} (nm)	ε_{max} ($M^{-1}cm^{-1}$)	λ_{2nd} (nm)	ε_{2nd} ($M^{-1}cm^{-1}$)
Chloroform	747	1214	335	10480	500	440
Dichloromethane	735/703	1265	335	9400	499	380
Dichloroethane	707	1284/1232	333	9310	500	590
Tetrahydrofuran	754/659	1290/1241	334	8750	489	430
Toluene	726	1248/1210	337	11340	502	480
Neat **GII**	740	1262	-	-	-	-

Upon dissolving Grubbs' second-generation catalyst, the tricyclohexylphosphine dissociates slowly from the Ru metal centre. The free tricyclohexylphosphine in solution can again associate with the Ru metal centre, this kinetic process eventually attains a dynamic equilibrium [26,30], Scheme 4.1**:** An illustration of the phosphine dissociation/association equilibrium of **GII**, producing the active catalytic species, and other potential side reactions such as phosphine oxidation and decomposition of the active catalytic species depicts this process (as well as any additional modification that might occur), in correlation with NMR reports from literature [31]. This dissociation, association, and additional transformation of **GII** at 25 °C using 0.10 mM solutions in the different solvents (CLF, DCM, DCE, THF and TOL) was followed by UV-Vis spectroscopy under Ar. Figure 4.3**:** UV–Vis spectra measured over time for the dissociation of PCy_3 from a 0.10 mM illustrates the disappearance of the main absorption band over time as well as the time trace and kinetic plot of data for this equilibrium process that leads to the observed first order rate constant $k_{obs} = k_1 + k_{-1}$. The k_{obs} of the different solvents are summarised in Error! Reference source not found.. The dissociation of the phosphine ligand from **GII** results in the formation of the active catalytic species, (SIMes)$RuCl_2$(CHPh). The observed catalyst transformation rate constants, k_{obs}, in the different solvents ranged between 8 x 10^{-5} s^{-1} (for CLF) and 2.6 x 10^{-4} s^{-1} (for THF).

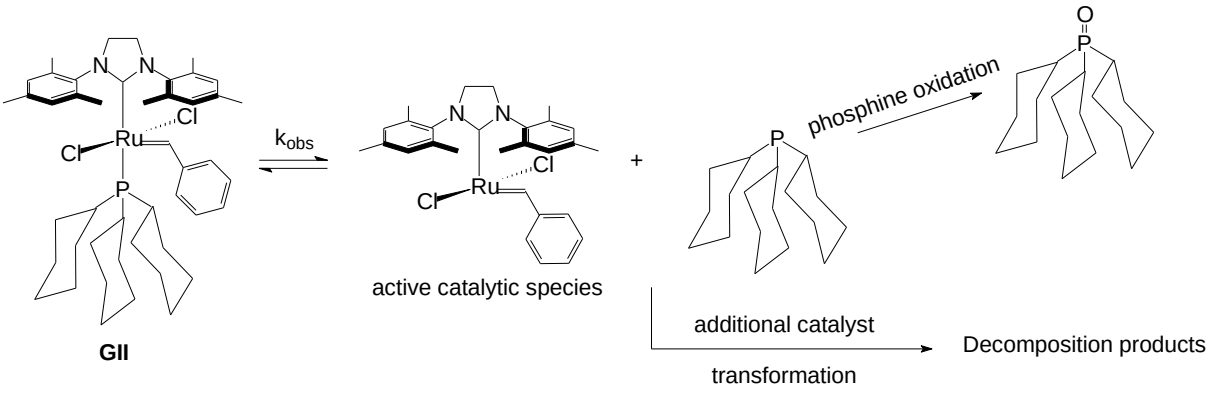

Scheme 4.1: An illustration of the phosphine dissociation/association equilibrium of **GII**, producing the active catalytic species, and other potential side reactions such as phosphine oxidation and decomposition of the active catalytic species

Table 4.2: The observed kinetic rate constant k_{obs}, for the transformation of 0.10 mM **GII** determined λ_{max} for the different solvents at 25 °C followed by UV-Vis spectroscopy under Ar. The C-P stretching frequency as measure by FTIR in the different solvent (from Table 4.1) is also shown

Solvents	Polarity index	Dipole moment	Kinetic data from UV-Vis		FTIR
			k_{obs} (min^{-1})	k_{obs} (s^{-1})	ν_{C-P} (cm^{-1})
Chloroform	4.1	1.15	4.8×10^{-3}	8×10^{-5}	747
Dichloromethane	3.1	1.14	9.6×10^{-3}	1.6×10^{-4}	735/703
Dichloroethane	3.5	1.83	9.8×10^{-3}	1.6×10^{-4}	707
Tetrahydrofuran	4.0	1.75	15.6×10^{-3}	2.6×10^{-4}	754/659
Toluene	2.4	0.31	6.8×10^{-3}	1.1×10^{-4}	726

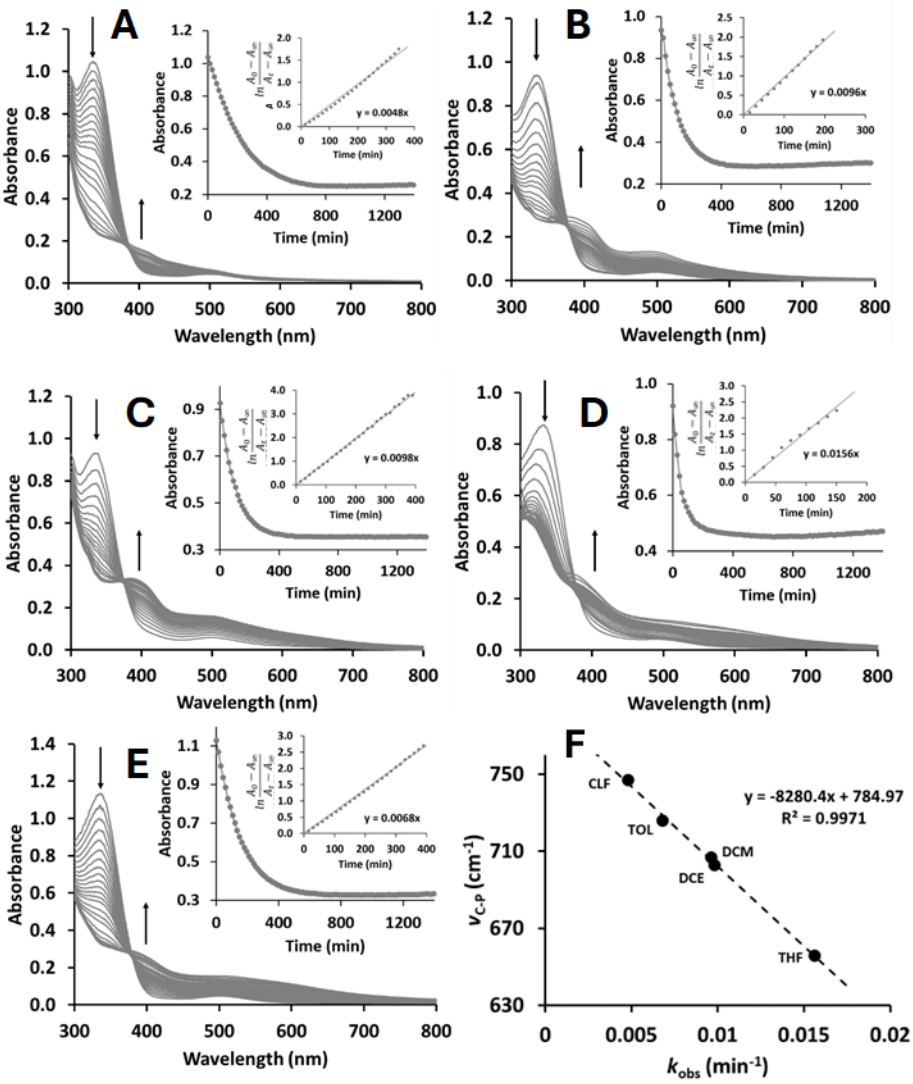

Figure 4.3: UV–Vis spectra measured over time for the dissociation of PCy_3 from a 0.10 mM **GII**, in dry (A) chloroform, (B) DCM, (C) DCE, (D) toluene, and (E) THF under Ar. 1st Insert: Absorbance *vs* time graph at λ_{max}. 2nd Insert: A first order kinetic plot of data for the process compiled from the data of the 1st insert; the slope gives the observed rate constant, k_{obs}. (F) The relationship between the k_{obs} and the C-P stretching frequency.

When the observe equilibrium rate constant, k_{obs}, is plotted against the C-P stretching frequency, a linear relationship was obtained (Figure 4.3**:** UV–Vis spectra measured over time for the dissociation of PCy_3 from a 0.10 mM F). A higher wavenumber for a stretching frequency of a bond (in this case the $\nu_{C\text{-}P}$) indicates a stronger bond C-P bond, this might imply a stronger interaction between the phosphine ligand and the Ru. This stronger interaction is indicative a more stable complex and hence a slower rate of phosphine dissociation.

Electrochemistry: The reduction and oxidation properties of a 0.8 mM **GII** solution in a variety of dry solvents (DCM, DCE, THF, and CLF) were investigated using cyclic voltammetry (CV) at 25 °C using 0.08 M tetrabutylammonium hexafluorophosphate, $[N(^nBu)_4][PF_6]$, as the electrolyte, on a glassy carbon working electrode under a blanket of argon. The electrolyte is insoluble in TOL hence it was excluded in this study. It has been reported that the reduction **GII** is a one-electron transfer process for the Ru^{II}/Ru^{III} couple in CH_2Cl_2 [26]. For this report, it can thus be assumed that **GII** will also be involved in a one-electron transfer process for the Ru^{II}/Ru^{III} redox couple in the different solvents.

The cyclic voltammetry results, which are reported *vs* the ferrocene couple (HFc/HFc^+) are summarised in Table 4.3. Figure 4.4**:** Comparative cyclic voltammograms of 0.8 mM **GII** in DCM, DCE, CLF, and THF at shows the comparative cyclic voltammograms of **GII** at 50 mV s^{-1} in DCM, DCE, CLF and THF. The CVs of **GII** in the chlorinated solvents (DCM, DCE, and CLF) consists of a reversible oxidation for the Ru^{II}/Ru^{III} couple, whereas in THF only the oxidation was detected. The peak anodic potential of **GII** in THF was measured at the lowest potential with E_{pa} = 20 mV. Indicating that the THF creates a more electron donating environment than the chlorinated solvents. The formal reduction potentials, E°', of **GII** increases from 11 to 14 to 29 mV in DCM, DCE and CLF, respectively. When the E°' of **GII** in the different chlorinated solvents was compared with the polarity index of the solvent, a directly proportional relationship was obtained (see Figure S4.2 in Supplementary Information). This could suggest that more polar solvents can create a more electron withdrawing environment, potentially attracting electron density away from **GII** resulting in increased oxidation potentials observed for the higher polarity index. More polar solvents could potentially also better solvate of the oxidized form of **GII**, increasing its stability. Additionally, it was found that as the k_{obs} (of the dissociation/association of the PCy_3) increases, the E°' of **GII** in the different chlorinated solvents decreases (Figure S4.3).

Thus, the easier it is to oxidize **GII** in a certain solvent, the faster the dissociation/association equilibrium of PCy_3 will be in a that particular solvent. Affirming the notion that more polar solvents better solvate both the reduced **GII** (**GII**$^{\bullet+}$) as well as the **GII** in its catalytically active form, (SIMes)$RuCl_2$(CHPh).

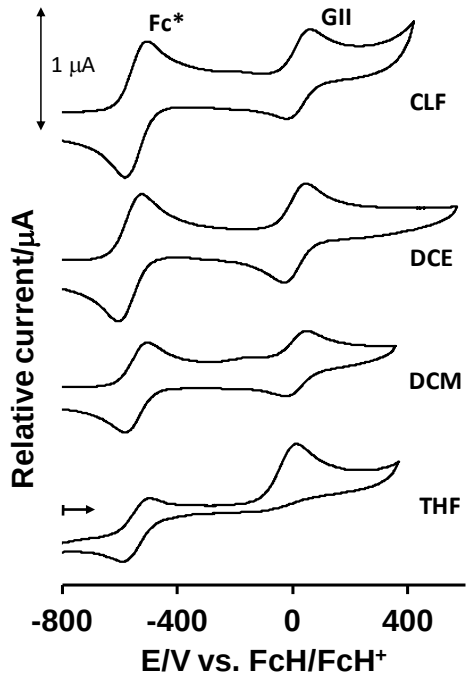

Figure 4.4: Comparative cyclic voltammograms of 0.8 mM **GII** in DCM, DCE, CLF, and THF at 25 °C using 0.08 M $[N(^nBu)_4[PF_6]$ as the electrolyte on a glassy carbon working electrode at a scan rate of 50 mV s^{-1}, under a blanket of argon.

The cyclic voltammogram of **GII** with scan rates ranging from 50 to 1000 mV s^{-1} in the different solvents are presented in Figure 4.5, with the CV data summarised in Table 4.3.

Electrochemical reversibility at 25 °C is theoretically defined by peak potential variations (ΔE_p) of 59 mV and chemical reversibility is defined at $i_{pc}/i_{pa} = 1$ [32,33]. The internal standard Fc* showed $72 < \Delta E < 90$ mV defining the range of electrochemical reversibility under our conditions.

In the chlorinated solvents DCM, DCE, and CLF the Ru^{II}/Ru^{III} redox couple at the different scan rates showed a single electrochemical reversible peak (labelled **GII**, Figure 4.5 A, B, and C) at *ca.* $E°' = 9$, 21, and 30 mV for $v \leq 400$ mV s^{-1}. As the scan rate was increased, the chemical reversibility (i_{pc}/i_{pa}) of the redox process decreased (Table 4.3, Figure S4.4). This suggests that the

electrochemically oxidized species of **GII** (**GII**$^{\bullet+}$), undergoes a chemical conversion (during an equilibrium reaction) to form an electrochemically inactive species (**X**), see

Scheme 4.**2:** Schematic representation of the . This is evidenced by the absence of additional oxidation or reduction peaks, or the peaks are outside the CV window. Consequently, it can be assumed that at slow scan rates, the electrochemically formed product (**GII**$^{\bullet+}$) is regenerated quickly enough from the chemically formed product (**X**) to maintain i_{pc}/i_{pa} ratios close to one. But, at fast scan rates, the chemical regenerative process is not rapid enough to convert **X** back to **GII**$^{\bullet+}$, causing the i_{pc}/i_{pa} ratio to deviate further from one. This type of action corresponds to an E_rC_r electrochemical mechanism (Er = reversible electrochemical step; Cr = reversible chemical step).

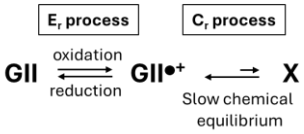

Scheme 4.2: Schematic representation of the E_rC_r electrochemical mechanism for **GII** in chlorinated solvents.

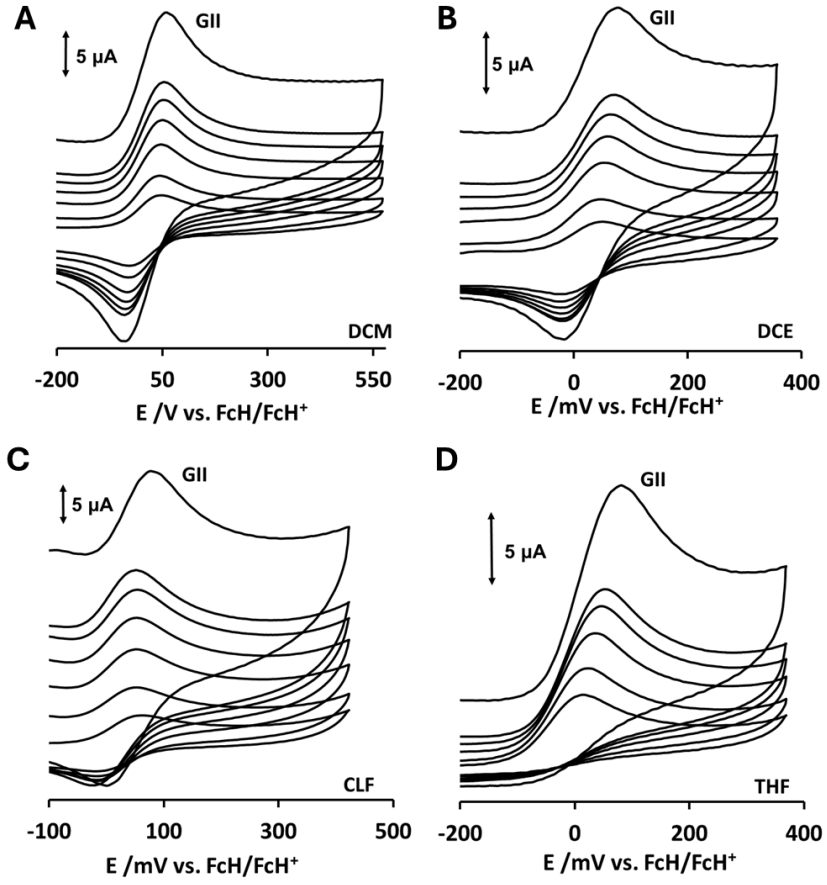

Figure 4.5: Cyclic voltammogram of a 0.8 mM solution of **GII** in the presence of 0.08 M $[N(^{n}Bu)_4[PF_6]$ as supporting electrolyte at 25 °C at scan rates ranging from 50-1000 mV s^{-1} in (A) DCM, (B) DCE, (C) CLF, and (D) THF.

Table 4.3. Peak anodic potentials, E_{pa}, peak potential difference ΔE_p, formal reduction potentials, E°, peak anodic current, i_{pa}, and current ratios i_{pc}/i_{pa} for 0.8mM solution of **GII** in DCM, DCE, CLF, and TOL containing 0.08M $[N(^nBu)_4][PF_6]$ as supporting electrolyte at 25°C for indicated scan rates of the Ru^{II}/Ru^{III} redox couples.

Grubbs' second-generation catalyst **GII** in DCM					
V (mV s^{-1})	E_{pa} (mV)	E°' (mV)	ΔE_p[a] (mV)	i_{pa} (μA)	i_{pc}/i_{pa}
50	48	11	75	3.50	0.97
100	47	10	72	5.00	0.96
200	47	10	74	6.84	0.94
300	51	9	85	7.60	0.93
400	53	8	90	9.50	0.92
500	55	8	95	10.26	0.91
1000	59	8	102	14.24	0.87
Grubbs' second-generation catalyst **GII** in DCE					
V (mV s^{-1})	E_{pa} (mV)	E°' (mV)	ΔE_p[a] (mV)	i_{pa} (μA)	i_{pc}/i_{pa}
50	49	14	70	2.16	0.81
100	49	14	70	3.09	0.79
200	54	17	74	4.32	0.77
300	61	21	82	5.13	0.76
400	67	24	87	5.81	0.73
500	71	27	88	6.45	0.72
1000	78	31	95	13.81	0.71
Grubbs' second-generation catalyst **GII** in CLF					
V (mV s^{-1})	E_{pa} (mV)	E°' (mV)	ΔE_{pa}[a] (mV)	i_{pa} (μA)	i_{pc}/i_{pa}
50	65	29	73	3.45	0.89
100	62	28	69	3.72	0.96
200	59	27	65	4.91	0.94
300	58	27	63	5.57	0.93
400	57	27	61	6.48	0.91
500	65	28	75	7.38	0.90
1000	83	44	78	10.68	0.80
Grubbs' second-generation catalyst **GII** in TOL					
V (mV s^{-1})		E_{pa} (mV)		i_{pa} (μA)	
50		20		5.13	
100		25		5.94	
200		37		7.83	
300		50		9.18	
400		56		9.99	
500		65		15.53	
1000		83		16.20	

[a] $\Delta E_p = E_{pa} - E_{pc}$.

Even at increased scan rates, only an oxidation peak was observed for **GII**. THF is known to be a highly coordinating, due to the lone pair electrons on the oxygen. Upon oxidation of **GII**, a positive

radical form on the ruthenium metal centre ((SIMes)$Ru^{\bullet+}Cl_2$(CHPh)(PCy_3)). Subsequently, the lone pair electrons (on the oxygen of the THF) nucleophilically attach to the Ru, creating a new THF associated compound. This new compound is either redox inactive or has oxidation and reduction potentials that lie outside the solvent window [27].

Cross-metathesis catalysed reaction: We previously reported [34], that the addition of 100 equivalents of *p*-cresol to **GII** for the metathesis reaction between *trans*-1-methoxy-4-(1-propenyl)benzene (**1**) and 2-ethylhexyl acrylate (**2**), increases the cross-metathesis (CM) product's % yield from 15 to 46%, thus in this study, *p*-cresol was also added to the metathesis reaction.

The metathesis reaction between *trans*-1-methoxy-4-(1-propenyl)benzene (**1**) and 2-ethylhexyl acrylate (**2**) catalysed by **GII**/*p*-cresol can result in the desired CM product, **3**, and the unwanted self-metathesis (SM) product, **4** (Scheme 4.3). The reaction was conducted in either DCM, DCE, CLF, THF or TOL at 40 °C under flowing Ar atmosphere (to remove the volatiles) for 24 h, see Table 4.4 for the % yield of CM. Under our conditions, in THF, no metathesis product could be isolated. This is in agreement with CV data, which revealed that **GII** did not produce a reduction peak, which we attributed to THF being highly coordinative. Upon comparing the % yield for the desired CM against the Gutmann donor number (DN) of the solvent (a quantitative measure of a solvent's electron-donating ability and also an indication of its coordinative ability) [35], as the electron donating ability of the solvent increased the CM % yield decreased, see

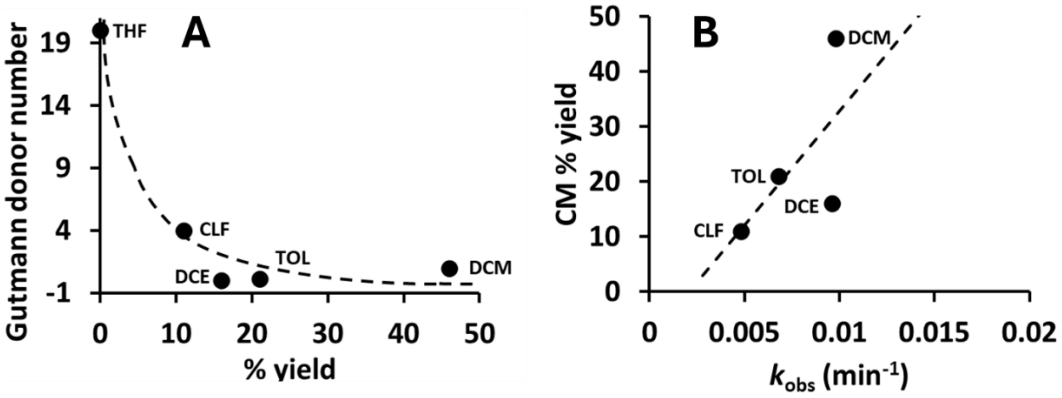

Figure 4**.6:** (A) The relationship between the % yield of the CM product for the A. As per literature, the PCy_3 needs to dissociate from **GII** (which is actually the pre-catalyst) to form the active catalyst ((SIMes)$RuCl_2$(CHPh)). When the active catalyst is formed, there exists a vacant site on the Ru, when the solvent has a high DN it will nucleophilically attach to the Ru, rendering

the catalyst inactive. The chlorinated solvents with the low DN value, showed the highest % yield for the CM product, with the solvent free system giving a 35% CM product yield. It can also be noted that the faster the rate of dissociation of the PCy_3 from **GII** in the different solvents, the higher the yield of the CM product (Figure 4.6**:** (A) The relationship between the % yield of the CM product for the B).

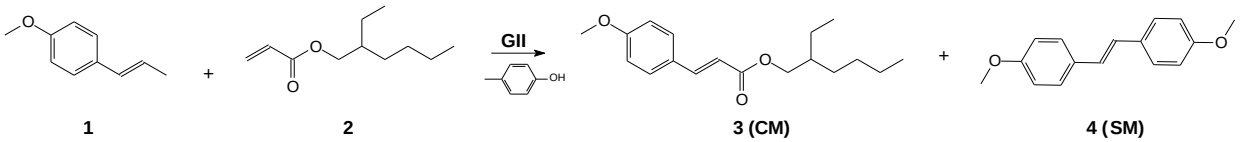

Scheme 4.3: The metathesis reaction between *trans*-1-methoxy-4-(1-propenyl)benzene (**1**) and 2-ethylhexyl acrylate (**2**) catalysed by **GII**.

Table 4.4: Solvent studies of the metathesis reaction between *trans*-1-methoxy-4-(1-propenyl) benzene (**1**) and 2-ethylhexyl acrylate (**2**) catalysed by *p*-cresol/**GII.**

Solvents	% CM	Gutmann donor number
Chloroform	11	4
Dichloromethane	46 15[a]	1
Dichloroethane	16	0
Tetrahydrofuran	0	20
Toluene	21	0.1
Solvent free	35	-

[a]No *p*-cresol, results from [34].

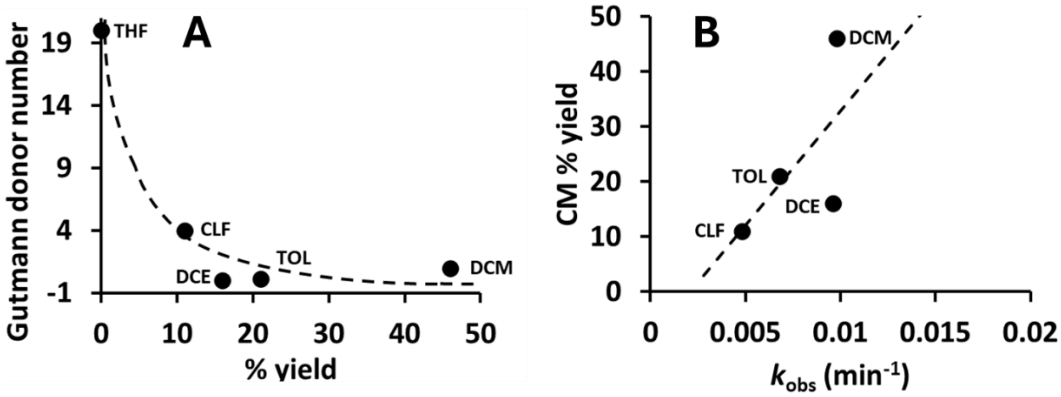

Figure 4.6: (A) The relationship between the % yield of the CM product for the **GII** catalysed metathesis reaction between **1** and **2**, and the Gutmann donor number of the different solvents. (B) The relationship between the k_{obs} (for the dissociation of $PCy_3$from **GII**) and the% yield of the CM product for the **GII** catalysed metathesis reaction between **1** and **2**.

4.4 Experimental section

General experimental methods. The Grubbs second generation catalyst [1,3-bis(2,4,6 trimethylphenyl)-2-imidazolidinylidene)dichloro(phenylmethylene)-(tricyclohexylphosphino)ruthenium] and other solid reagents and solvents used in the study were purchased from Sigma – Aldrich and were used without further purification. Solvents were dried using a small column of activated neutral alumina (10% v/v) prior to use. All reactions were carried out under Schlenk conditions in an argon atmosphere.

Procedure: The following general procedure was used during the solvent studies, which was adopted from the reported procedure described by Swart *et al.* [25]

GII (5.7 mg, 0.0067 mmol, 0.5 mol%) and *p*-cresol (100 equivalent *vs* 1eq. **GII**), was dissolved in 10 mL of the dry solvent (DCM, DCE, CLF, THF, or TOL) were heated to 40 °C while being stirred under a dry argon atmosphere. Trans-1-methoxy-4-((1-propenyl)benzene), **1**, (0.20 mL, 1.3 mmol, 1 eq.) and 2-ethylhexyl acrylate, **2**, (0.56 mL, 2.7 mmol, 2 eq.) were added to the existing mixture simultaneously and the reaction was allowed to proceed for 3 hours. The reaction mixture was concentrated in vacuo and the resulting mixture was applied on a preparative TLC plate for separation to obtain the purified SM and CM major products.

Characterization data of (*E*)-1,2-bis(4-methoxyphenyl)ethene (**3**):

^{1}H NMR (400MHz, CD_2Cl_2) [25]: δ = 7.53-7.42 (m, 4H), 6.98 (s, 2H), 6.93 (d, J = 8.9 Hz, 4H), 3.85 (s, 6H, -OCH_3)

Characterization data of (*E*)-2-ethylhexyl-3-(4-methoxyphenyl)acrylate (**5**):

^{1}H NMR (400MHz, CD_2Cl_2) [25]: δ = 7.65 (d, J=16.0, 1H), 7.54 (d, J = 8.9 Hz, 2H), 6.96 (d, J = 8.8Hz, 2H), 6.37 (d, J = 16.0 Hz, 1H), 4.18-4.08 (m, 2H), 3.86 (s, 3H, -OCH_3), 1.68 (dq, J = 12.2, 6.1 Hz, 1H), 1.51-1.32 (m, 8H), 0.95 (ddd, J = 8.8, 6.9, 5.3 Hz, 6H)

Spectroscopic characterization: Fourier Transform Infrared (FTIR) Spectroscopy. The FTIR spectra of **GII** in the different solvents were recorded using a Thermo Scientific IR spectrometer with a Nicolet iS50 ATR attachment. The Shimadzu UV – 1800 UV/Visible spectrophotometer was employed for recording 0.10 mM solution of **GII** in the different solvents under an argon atmosphere. A 2 mL quartz cuvette with a path length of 1cm was used. The UV-Vis stablity investigation over time (24 h) were carried out on 0.10 mM solution of **GII** in dry different solvents under argon atmosphere, and spectra were recorded every 15 min interval for 24 h.

Electrochemical Characterization. The electrochemical properties of 0.8 mM solution of Grubbs second generation catalyst were measured in different solvents in dry CH_2Cl_2 containing 0.08 M tetrabutylammonium hexafluorophosphate, [$N(^nBu)_4[PF_6]$, as supporting electrolyte (a large supporting electrolyte concentration is required to increase solution conductivity to guarantee charge balance and complete the electrical circuit)[36]. The experiments were conducted under a blanket of argon at 25°C, employing a BAS 100 B/W electrochemical workstation interfaced with a personal computer. A three-electrode set up was used, including a Pt auxiliary electrode, a glassy carbon working electrode with surface area of 3.14 mm^2, and a Pt reference electrode. Since it is

imperative that the surface of the working electrode must be extremely clean, it was polished repeatedly on a Buhler polishing mat, using a 1 μm and ¼ μm diamond paste. Experimental potentials measured against the Pt reference electrode, but the results presented are referenced against the ferrocene couple, FcH/FcH^+, as an internal standard as advised by IUPAC. However, the FcH/FcH^+ couple interfered with the oxidation and reduction peak of the Grubbs second generation catalyst, therefore, decamethylferrocene (FcH*) was subsequently used as an internal standard and referenced back to ferrocene. The formal reduction potential of Fc*, $E°_{Fc*}$ = -542 mV vs FcH/FcH^+.

4.5 Conclusion

The dissociation of the phosphine ligand from **GII** is a critical step during metathesis, since it results in the formation of the active catalytic species, $(SIMes)RuCl_2(CHPh)$. For the different solvents evaluated during this investigation (DCM, DCE, CLF, THF, and TOL), the observed dissociation/association equilibrium rate constants, k_{obs}, ranged between 8×10^{-5} s^{-1} (for CLF) and 2.6×10^{-4} s^{-1} (for THF). Even though THF resulted in the highest k_{obs}, it is not a good solvent for **GII** catalysed metathesis reactions. For our model reaction (*trans*-1-methoxy-4-(1-propenyl)benzene and 2-ethylhexyl acrylate), no metathesis product was observed, and this is attributed to the THF binding to **GII**, which is corroborated further by the electrochemical results, which revealed no reduction peak. For the other solvents (DCM, DCE, CLF, and TOL), however, a higher k_{obs}, resulted in a higher % yield for the CM product. Electrochemical results also affirmed this, since the easier it is to oxidize **GII** in a particular solvent, the faster k_{obs} was for the dissociation/association equilibrium in that solvent. This behaviour of **GII** in the different solvents is dependent on the intrinsic properties of the solvent, with polarity, donor ability, and the dipole moment being the most influential characteristics of the solvent. Thus, this must be taken into consideration when choosing the appropriate solvent for metathesis catalysed by **GII**.

References

[1] M. R. Swart, C. Marais, E. Erasmus, *Catalyst* **2021**, *11*, 1483.

[2] C. Theunissen, M. A. Ashley, T. Rovis, *J Am Chem Soc* **2019**, *141*, 6791–6796.

[3] Grela K, *Olefin Metathesis: Theory and Practice*, Wiley, Hoboken, NJ, **2014**.

[4] Grubbs R.H, Wenzel A.G, *Handbook of Metathesis*, Wiley-VHC, Weinheim, **2015**.

[5] C. S. Higman, J. A. M. Lummiss, D. E. Fogg, *Angew. Chem. Int. Ed.* **2016**, *55*, 3552–3565.

[6] D. Hughes, P. Wheeler, D. Ene, *Org Process Res Dev* **2017**, *21*, 1938–1962.

[7] F. Sinclair, M. Alkattan, J. Prunet, M. P. Shaver, *Polym Chem* **2017**, *8*, 3385–3398.

[8] F. Stelzer, *J. Macromol. Sci., Part A* **1996**, *33*, 941–952.

[9] D. P. Allen, M. M. Van Wingerden, R. H. Grubbs, *Org Lett* **2009**, *11*, 1261–1264.

[10] D. Sathe, S. Yoon, Z. Wang, H. Chen, J. Wang, *Chem Rev* **2024**, *124*, 7007–7044.

[11] J. Mol, *J Mol Catal A Chem* **2004**, *213*, 39–45.

[12] J. H. Phillips, in *Organometallic Chemistry in Industry*, Wiley, **2020**, pp. 259–282.

[13] R. H. Grubbs, *Angew. Chem. Int. Ed.* **2006**, *45*, 3760–3765.

[14] J. A. M. Lummiss, K. C. Oliveira, A. M. T. Pranckevicius, A. G. Santos, E. N. dos Santos, D. E. Fogg, *J Am Chem Soc* **2012**, *134*, 18889–18891.

[15] G. A. Bailey, D. E. Fogg, *J Am Chem Soc* **2015**, *137*, 7318–7321.

[16] A. G. Santos, G. A. Bailey, E. N. dos Santos, D. E. Fogg, *ACS Catal* **2017**, *7*, 3181–3189.

[17] W. L. McClennan, S. A. Rufh, J. A. M. Lummiss, D. E. Fogg, *J Am Chem Soc* **2016**, *138*, 14668–14677.

[18] Z. Zhao, H. Wang, Y. Guo, *Rapid Commun. Mass Spectrom.* **2011**, *25*, 3401–3410.

[19] B. R. Galan, M. Pitak, J. B. Keister, S. T. Diver, *Organometallics* **2008**, *27*, 3630–3632.

[20] S. K. Collins, in *Handbook of Metathesis*, Wiley, **2015**, pp. 343–377.

[21] G. S. Forman, A. E. McConnell, R. P. Tooze, W. Janse Van Rensburg, W. H. Meyer, M. M. Kirk, C. L. Dwyer, D. W. Serfontein, *Organometallics* **2005**, *24*, 4528–4542.

[22] A. Szadkowska, C. Samojłowicz, K. Grela, *Pure Appl. Chem.* **2011**, *83*, 553–563.

[23] D. Prat, A. Wells, J. Hayler, H. Sneddon, C. R. McElroy, S. Abou-Shehada, P. J. Dunn, *Green Chem.* **2016**, *18*, 288–296.

[24] U.S. Environmental Protection Agency, **1999**.

[25] M. R. Swart, L. Twigge, E. Erasmus, C. Marais, B. C. B. Bezuidenhoudt, *Eur J Inorg Chem* **2021**, 1752–1762.

[26] M. R. Swart, C. Marais, E. Erasmus, *ACS Omega* **2021**, *6*, 28642–28653.

[27] T. Matsuo, T. Yoshida, A. Fujii, K. Kawahara, S. Hirota, *Organometallics* **2013**, *32*, 5313–5319.

[28] V. Forcina, A. García-Domínguez, G. C. Lloyd-Jones, *Faraday Discuss.* **2019**, *220*, 179–195.

[29] Harris D, Bertolucci M, *Symmetry and Spectroscopy. An Introduction to Vibrational And Electronic Spectroscopy*, Dover Publications Inc., New York, **1989**.

[30] M. Ramesh, M. D. Kumar, M. Jaccob, B. Therrien, G. Venkatachalam, *Inorganica Chim Acta* **2018**, *477*, 40–50.

[31] J. R. Griffiths, J. B. Keister, S. T. Diver, *J Am Chem Soc* **2016**, *138*, 5380–5391.

[32] J. C. Swarts, E. H. G. Langner, N. Krokeide-Hove, M. J. Cook, *J Mater Chem* **2001**, *11*, 434–443.

[33] H. J. Gericke, N. I. Barnard, E. Erasmus, J. C. Swarts, M. J. Cook, M. A. S. Aquino, *Inorganica Chim Acta* **2010**, *363*, 2222–2232.

[34] Odewole O.A, Swart M.R, Erasmus E, *Eur J Inorg Chem* **2024**.

[35] V. Gutmann, *Coord Chem Rev* **1976**, *18*, 225–255.

[36] N. Elgrishi, K. J. Rountree, B. D. McCarthy, E. S. Rountree, T. T. Eisenhart, J. L. Dempsey, *J Chem Educ* **2018**, *95*, 197–206.

CHAPTER 5

Unveiling the power of additives: Enhancing Grubbs' catalyst performance with phenol derivatives

6.1 Abstract

Understanding the interaction between the Grubbs second-generation catalyst (**GII**) and phenol derivatives is key to enhancing metathesis reactions without structural modifications to commercially available catalysts. In this study, **GII** was employed for cross-metathesis reactions in the presence of various phenol derivatives, and the interactions were characterised using UV-Vis spectroscopy, ATR-FTIR, and cyclic voltammetry (CV). The ATR-FTIR spectra revealed distinct C-N and C-P stretching frequencies from the **GII**-phenol adducts, alongside phenol-associated O-H and C=C stretching bands. UV-Vis spectra displayed strong absorption bands at 335 nm and weaker bands between 503-509 nm, linked to metal-ligand charge transfer. Cyclic voltammetry showed electrochemical reversibility for most **GII**-phenol adducts, except those with electron-withdrawing groups. Metathesis reactions were performed between *trans*-1-methoxy-4-(1-propenyl)benzene and 2-ethylhexyl acrylate, revealing a correlation between electron-donating phenol groups and higher cross-metathesis (CM) yield. While phenol derivatives influenced catalyst activation rates, no direct correlation was found between activation rates and catalytic selectivity. The study highlights the significance of electron-donating phenol derivatives in enhancing catalytic efficiency by increasing Ru centre electrophilicity.

Keywords: Grubbs' second-generation catalyst, phenol derivatives, metathesis, catalyst-additive interaction, electrophilicity

6.2 Introduction

The introduction of the second generation Grubbs catalyst in 1999 marked a significant milestone, expanding the scope of olefin metathesis and inspiring further exploration of its potential [1]. The second-generation Grubbs catalyst (**GII**), see for the **Error! Reference source not found.** structure, has emerged as a preferred choice for α,β-unsaturated carbonyl compounds via cross-metathesis reactions involving acrylates and alkenes. This has led to the synthesis of value-added products with significant health benefits, for example ethylhexyl methoxycinnamate, a common sunscreen ingredient used in the cosmetic industry; pyrenophorol, a powerful antifungal against both Microbotryum violaceum and Saccharomyces cerevisiae; and neopeltolide, an anticancer agent that exhibit potential activity against adenocarcinoma, ovarian sarcoma and murine leukemia [2–4]. The olefin metathesis technique has proven to be a vital and versatile transformation in organic chemistry, enabling the efficient formation of carbon-carbon double bonds. This reaction has empowered chemists to synthesize high-value compounds and fine-tune the steric and electronic properties of existing molecules [5–8]. The impact of olefin metathesis extends beyond academia, with applications in polymer and materials synthesis [9–11], pharmaceutical manufacturing [12,13], and the chemical industry [14,15].

Although the Grubbs second-generation catalyst has shown success in acrylate metathesis, its limitations include the necessary dissociation of the PCy_3 ligand, which can lead to unwanted side reactions and catalyst deactivation. To address this, phosphine-free and Hoveyda-type catalysts have been explored as alternatives, with several reports demonstrating their efficiency in cross-metathesis reactions with acrylates [16–19]. However, the widespread use and cost-effectiveness of the Grubbs catalyst have motivated researchers to seek solutions to mitigate its limitations other than the alternative catalysts. In 2005, Forman and Tooze pioneered the use of phenol as a phosphine scavenger, proposing that it captures released PCy_3 to form an adduct, $(PhOH)nPCy_3$ [20]. Building on this work, Santos *et al*. and Swart *et al*. [8,21] investigated the scavenging potential of phenol derivatives, such as *p*-cresol, in acrylate metathesis, achieving significant improvements in catalyst performance. Notably, phenol and phenol-functionalized resin were found to enhance the selectivity of cross-metathesis products, favouring the formation of the desired product over self-metathesis in quantitative yields, compared to reactions without these additives [22].

Despite efforts to enhance catalyst efficiency, the current methodology remains unsatisfactory for economically viable processes, which require a turnover number of over 50,000 for homogeneous metathesis catalysts [23]. To improve the yield of the desired cross-metathesis product, researchers have explored various strategies, including modifying the electronic and steric properties of metathesis partners by introducing electron-donating and electron-withdrawing groups [8,24]. Other approaches include optimizing the ratio of **GII** catalyst to co-catalyst/additives [21,25], varying catalyst loading [16,26], and identifying the ideal catalyst composition [25,26]. It was found that reducing the electrophilicity of the acrylate moiety and decreasing the electron density on the α,β-carbonyl compound, catalysed by **GII** in the presence of excess phenol, led to increased cross-metathesis yields [8]. In contrast, Fogg's group observed that the beneficial effect of catalyst loading is offset by the rate of catalyst decomposition, as these parameters are interconnected. However, they achieved a breakthrough by using **GII** with poly(vinylphenol) resin as a PCy_3 stabilizer in acrylate cross-metathesis, resulting in catalyst efficiency comparable to the more expensive Hoveyda-Grubbs second-generation catalyst [21].

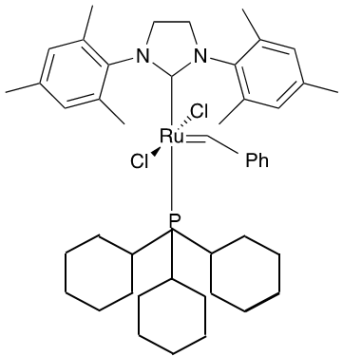

Figure 5.1: Grubbs' second-generation catalyst (GII)

Numerous studies have reported the use of non-structural modifications, involving the addition of chemical species such as salts, alcohols, and metal halides as co-catalysts or additives to Grubbs catalyst, to enhance its activity, selectivity, and stability through a simple and effortless method [20,21,27–32]. Thorough investigations using various spectroscopic techniques, including NMR, UV-Vis, and ATR-FTIR, were conducted to understand the catalytic behaviour, stability, and decomposition of Grubbs first- and second-generation catalysts [33]. Furthermore, research has been conducted on the electrochemical properties of ruthenium carbene complexes, which are structurally similar to Grubbs catalysts, revealing a one-electron oxidation process involving

Ru^{II}/Ru^{III}, with reversibility or irreversibility depending on the specific molecule [33–37]. To optimise Grubbs catalyst performance in metathesis reactions, it is essential to understand the interactions between additives and the catalyst. Investigating the effects of additives can provide valuable insights into the mechanisms of catalytic reactions, enabling the design and development of more effective catalysts or modifications to existing ones. However, there is a limited understanding of the characterization of the Grubbs catalyst-additive interaction, which is crucial to substantiate the beneficial effects of additives on **GII** and promote non-structural modification of commercially available metathesis catalysts. In this study, we report the metathesis reaction catalysed by **GII** in the presence of a selection of different phenol derivatives and employed UV-Vis, ATR-FTIR, and cyclic voltammetry to characterise **GII**-phenol derivative interaction, gaining insights into stability, electronic properties, catalyst behaviour.

6.3 Results and Discussion

There is a considerable amount of literature available on the catalytic behaviour, and comparative characterization studies of both first- and second-generation Grubbs' catalyst. However, there is a scarcity of literature on the characterization and catalytic behaviour of these catalyst in the presence of phenol derivatives. Here, the characterization of the interaction between second-generation Grubbs' catalyst (**GII**) and a selection of different phenols with varying amount of electron withdrawing- and electron-donating ability such as 4-nitrophenol (**NP**), 4-(trifluoromethyl)phenol (**TFP**), 4-bromophenol (**BP**), phenol (**P**), 4-methoxyphenol (**MOP**), 4-tertbutylphenol (**TBP**), 3-methylphenol (**3MP**, *m*-cresol), 4-methylphenol (**4MP**, *p*-cresol), 2-methylphenol (**2MP**, *o*-cresol) and 4-propylphenol (**PP**) are reported. The performance of the **GII**-phenol adducts for *trans*-1-methoxy-4-(1-propenyl)benzene -acrylate metathesis will also be discussed.

ATR-FTIR and UV-Visible spectroscopy. The ATR-FTIR spectra of the **GII**-phenol adducts (**GII-NP**, **GII-TFP**, **GII-BP**, **GII-P**, **GII-MOP**, **GII-TBP**, **GII-3MP**, **GII-4MP**, **GII-2MP**, and **GII-PP**, structures provided in the Supp Info) displayed the C-N stretching frequency (of the SIMes ligand) at 1262 cm^{-1}, and the C-P stretching frequency at 740 cm^{-1} which is characteristic of neat **GII** [33]. Additionally, these **GII**-phenol adducts exhibited O-H stretch frequency in the region 3300-3600 cm^{-1} and C=C stretching bands of cyclic alkenes in the region of 1500-1600 cm^{-}

[1] belonging to the phenol counterpart. See Error! Reference source not found. for the ATR-FTIR data (and Figure S5.1 in the Supp Info).

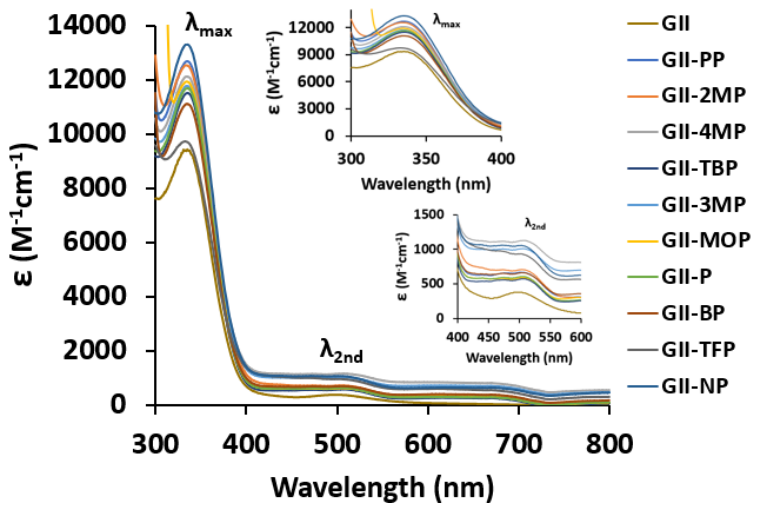

Figure 5.2: Comparative UV-Vis spectra of 0.10 mM solutions of **GII** and **GII**-phenol adducts in dry dichloromethane. Insert: Expanded sections between 300-400 nm and 400-600 nm.

Table 5.1: Summary of the ATR-FTIR and UV-vis data of GII and the GII-phenol adducts

GII-phenol adducts	FTIR			UV-vis data			
	ν_{C-P} (cm^{-1})	ν_{C-N} (cm^{-1})	ν_{O-H} (cm^{-1})	λ_{max} (nm)	ε_{max} (M^{-1} cm^{-1})	λ_{2nd} (nm)	ε_{2nd} (M^{-1} cm^{-1})
GII-PP	730	1264	3583	335	12663	505	670
GII-2MP	734	1265	3579	335	12530	504	709
GII-4MP	731	1264	3580	335	12100	509	1123
GII-TBP	731	1264	3566	335	11480	509	571
GII-3-MP	733	1265	3329	335	11750	506	1100
GII-MOP	731	1229	3365	335	11920	505	593
GII-P	733	1264	3580	335	11670	504	606
GII-BP	730	1264	3565	335	11100	508	661
GII-TFP	733	1264	3522	335	9720	503	930
GII-NP	753	1296	3358	335	13306	504	1058
Neat **GII**	740	1262	-	335	9400	504	380

The UV-Vis absorption spectra of 0.10 mM of the neat **GII** and the **GII**-phenol adducts in dry dichloromethane were measured at 289 K under an argon atmosphere. The UV-Vis spectra of both the neat **GII** and **GII**-phenol adducts display two characteristic peaks. A strong absorption band at a wavelength of 335 nm and a weak absorption band at a longer wavelength ranging between 503-509 nm was observed. The peak maxima (λ_{max}) and molar extinction coefficients (ε_{max}) of

both observed UV-Vis bands (see **Figure 5.2**) are summarised in Error! Reference source not found..

The absorption at λ_{max} = 335 nm, observed for all the samples, may be ascribed to the Ru-CHPh metal ligand charge transfer (MLCT). While the weak absorption wavelength 503-509 nm can be attributed to the forbidden Ru=C_{ene} visible metal ligand charge transfer when compared to similar ruthenium benzylidene [33,38,39]. The consistency in the wavelength proves that the phenol additive does not alter the chemical and structural configuration of the catalyst. On the other hand, the presence of the phenol additive caused a hyperchromic effect between the neat **GII** and **GII**-phenols adducts. The absorbance and consequently the molar extinction coefficients (ε_{max}) of the **GII**-phenol adducts were higher than that of the neat **GII** confirming the presence of the additives (Error! Reference source not found.).

In solution (DCM), the tricyclohexylphosphine (PCy_3) ligand will gradually dissociate from the **GII**-phenol adduct, leaving an empty coordination site. The free PCy_3 in solution can either oxidize to form $O=PCy_3$ or re-associate with the Ru centre, leading to a dynamic equilibrium [33,40]. This process, along with any additional transformation (or decomposition) that may occur, is depicted in **Scheme 5.1:** An illustration depicting the phosphine dissociation/association equilibrium of GII-phenol adducts, producing the active catalytic species (GII^A), . This proposed mechanism is consistent with NMR observations from the literature [41].

The dissociation, re-association, stabilization, and further transformation (or decomposition) of the **GII**-phenol adducts were monitored at 25 °C using 0.10 mM solutions in DCM via UV-Vis spectroscopy under Ar. The UV-Vis spectra of the **GII**-phenol adducts measured over time is shown in **Figure 5.3:** UV–Vis spectra measured over time for the dissociation of PCy3 from the 0.10 Mm . The spectra illustrate the gradual disappearance of the main absorption band over time, along with the time trace and kinetic plot for this equilibrium process, which yields the observed catalyst transformation rate constant $k_{obs}' = k_1 + k_{-1}$. The k_{obs}' values for the different **GII-**phenol adducts in DCM are summarised in **Table 5.**. The phosphine ligand dissociation from **GII**-phenol adducts results in the formation of the active catalytic species $\mathbf{GII^A}$ and $\mathbf{GII^{AS}}$ (**Scheme 5.1:** An illustration depicting the phosphine dissociation/association equilibrium of GII-phenol adducts, producing the active catalytic species (GII^A), **)**. The observed catalyst transformation rate

constants, k_{obs}', ranged between 5.1 x 10^{-3} min^{-1} (for **GII-TBP**) and 15.7 x 10^{-3} min^{-1} (for **GII-MOP**).

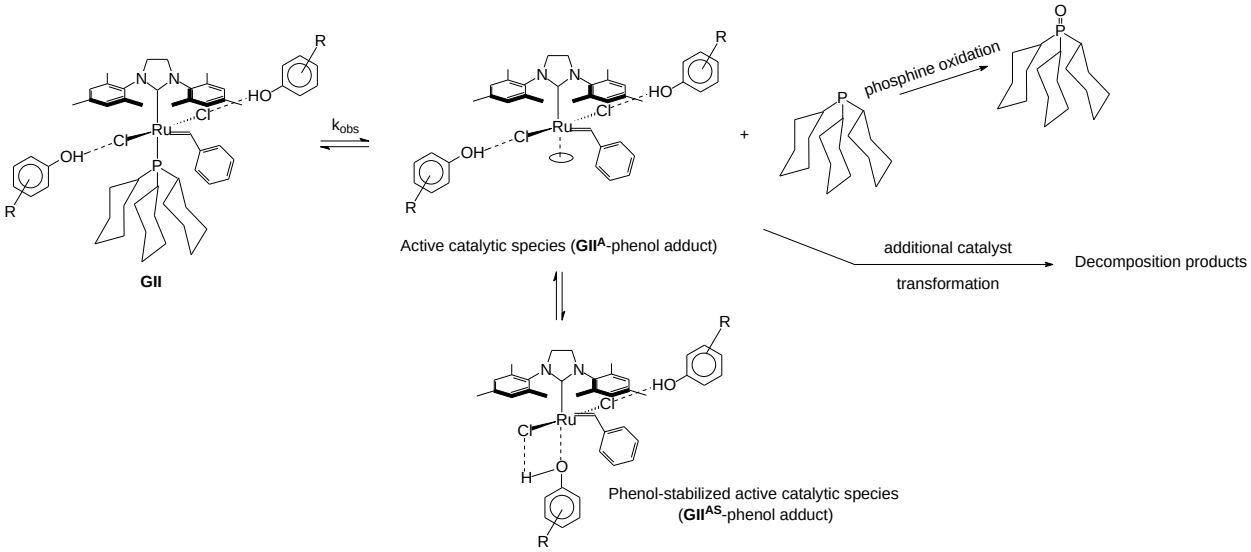

Scheme 5.1: An illustration depicting the phosphine dissociation/association equilibrium of GII-phenol adducts, producing the active catalytic species (GII^{A}), the phenol-stabilized active catalytic species (GII^{AS}), alongside other potential side reactions, including phosphine oxidation and decomposition of the active catalytic species.

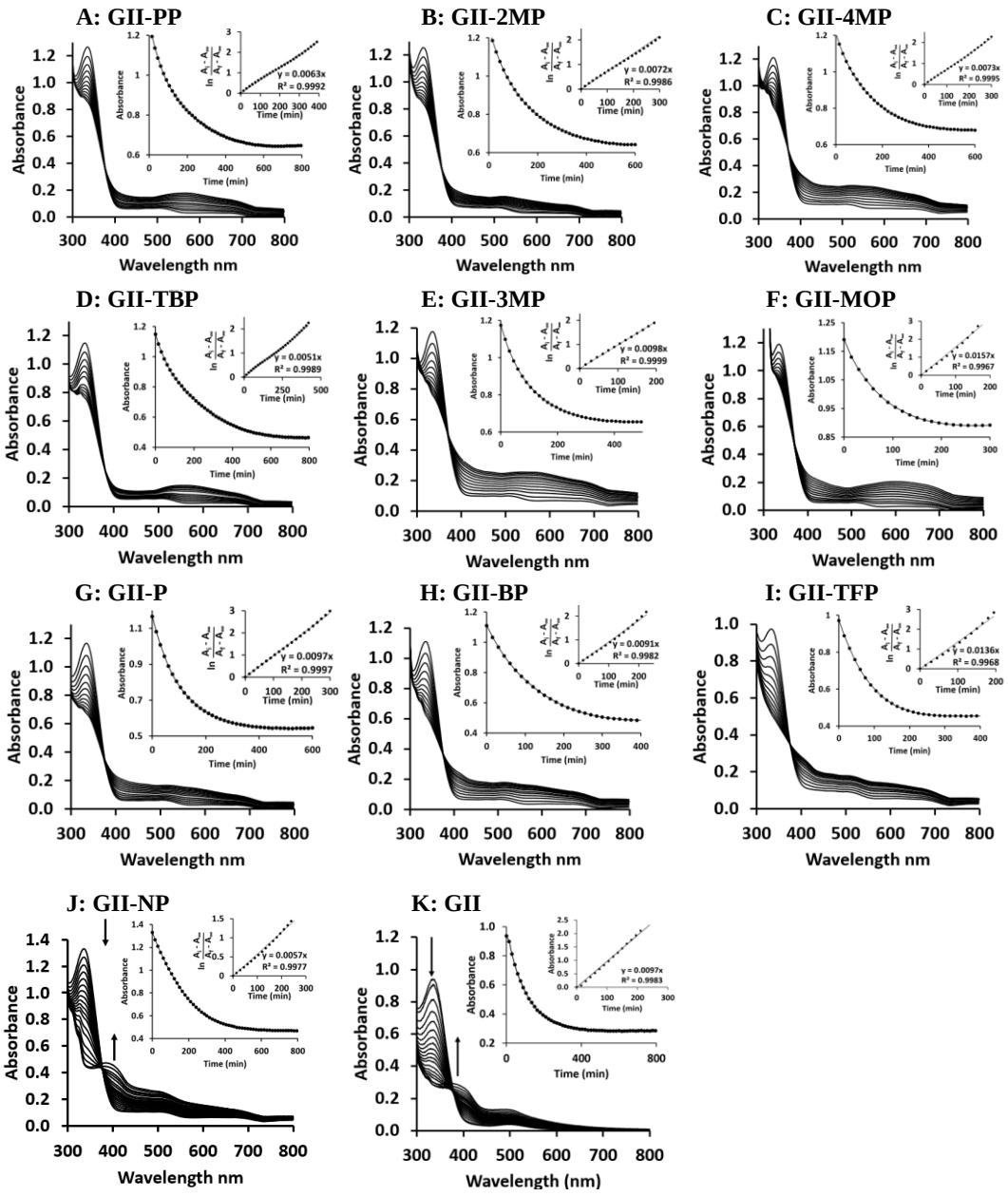

Figure 5.3: UV–Vis spectra measured over time for the dissociation of PCy3 from the 0.10 Mm GII-phenol adducts and GII in dry DCM under Ar. (A) GII-PP, (B) GII-2MP, (C) GII-4MP, (D) GII-TBP, (E) GII-3MP, (F) GII-MOP, (G) GII-P, (H) GII-BP, (I) GII-TFP, (J) GII-NP, and (K) GII. 1st Insert: Absorbance *vs* time graph at λ_{max}. 2nd Insert: A first order kinetic plot of data for the process compiled from the data of the 1st insert; the slope gives the observed catalyst transformation rate constant, k_{obs}.

Table 5.2: Summary of the observed catalyst transformation rate constant (k_{obs}') measured at 335 nm for the dissociation/decomposition of the PCy_3 from the **GII**-phenol adducts, the Hammett constants of the phenols (σ_R), the pk_a of the phenols, and isolated yield of the cross-metathesis product (CM %) between *trans*-1-methoxy-4-(1-propenyl)benzene 1, and 2-ethylhexyl acrylate 2 catalysed by **GII**-phenol adducts.

	k_{obs}' at 335 nm (min^{-1})	Hammett constant (σ_R)	pk_a	CM %
GII-PP	0.0063	-0.15	10.34	80
GII-2MP	0.0072	-0.13	10.28	59
GII-4MP	0.0073	-0.17	10.26	46
GII-TBP	0.0051	-0.268	10.16	47
GII-3-MP	0.0098	-0.07	10.09	92
GII-MOP	0.0157	-0.1	10.05	35
GII-P	0.0097	0	10	41
GII-BP	0.0091	0.232	9.17	29
GII-TFP	0.0136	0.54	8.68	33
GII-NP	0.0057	0.88	7.15	0
Neat **GII**	0.0097			15

A V-shape correlation was obtained between the Hammett constant (σ_R) and the observed catalyst transformation rate constant, k_{obs}' (**Table 5.** and **Figure 5.4 A**). The two linear lines represent the **GII**-phenol adducts where the phenol has either an electron-donating or an electron-withdrawing R-groups attached to it. The line of the electron-donating R-groups shows an inversely proportional relationship with k_{obs}'. This suggest that as the R-group becomes more electron-donating (lower σ_R), the observed catalyst transformation rate constant, k_{obs}' increases. The increased electron density destabilizes the δ^- on the -OH group of the phenol additive to counter the effect of the hydrogen bonding between the -OH group and the Cl-ligand of **GII** through a resonance/inductive effect, causing in increased PhO–H···Cl–Ru interaction. The stronger PhO–H···Cl–Ru interaction, results in a weaker Ru–PCy_3 bond and faster phosphine dissociation. Additionally, the increased electron density results in a better stabilization of **GII**^{A}-phenol adduct to form **GII**^{AS}-phenol adduct (**Scheme 5.1:** An illustration depicting the phosphine dissociation/association equilibrium of GII-phenol adducts, producing the active catalytic species (GII^A),).

For the electron-withdrawing R-groups, a directly proportional relationship is obtained, implying as the R-group becomes more electron-withdrawing (higher σ_R), the catalyst transformation rate constant, k_{obs}' also increases, contrary to what is expected. This implies that a different major driving force influences the k_{obs}' of the **GII**-phenol adducts containing electron-withdrawing R-groups. Considering that the Hammett constants quantify the electronic influence of substituents (R-groups at different position of an aromatic ring) on the acid dissociation equilibrium, see **Figure 5.4 B**, the acid dissociation constant of the phenol additives will also influence the k_{obs}'.

The relationship between the k_{obs}' and pk_a also showed a V-shaped correlation (**Table 5.** and **Figure 5.4 C**). Although the V-shaped curve again has two linear lines (one for electron-withdrawing R-groups and one for electron-donating R-groups), both lines show an inversely proportional correlation between k_{obs}' and pk_a, just with different slopes. The phenol derivatives that are more acidic (lower pk_a) for both electron-donating and electron-withdrawing R-groups, leads to a greater PhO–H·Cl–Ru interaction and consequently a weaker Ru–PR_3 bond in turn increasing phosphine dissociation [21,22]. **GII-NP** is not obeying any of these relationships, since the NP can form a zwitterion causing the H of the -OH group to dissociate and bind the Cl, which decomposes the **GII-NP** catalyst.

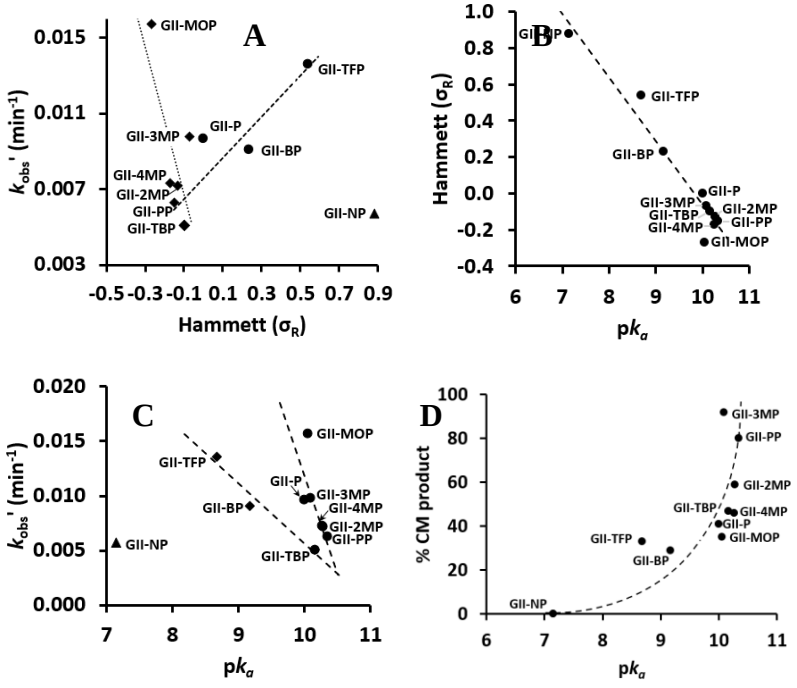

Figure 5.4: Relationship between the observed catalyst transformation rate constant (k_{obs}') for the for the dissociation/decomposition of the PCy_3 from the **GII**-phenol adducts vs (A) the Hammett

constant (σ_R), and (C) the pK_a of the phenols additives. The relationship between (B) the Hammett constant (σ_R) or (D) the isolated %CM product (of the reaction trans-1-methoxy-4-(1-propenyl) benzene and 2-ethylhexyl acrylate, catalysed by **GII**-phenol adducts) and the pK_a of the phenol additives.

^{31}P NMR of the **GII** catalyst recorded at 5 min and 60 min (after dissolution) showed the P-signal of the precatalyst PCy_3 ligand as a sharp singlet at δ 29.3 ppm with minor catalyst intermediates/decomposed products (δ 42.0, 34.1, 31.5, 31.3, 27.9 and 21.2 ppm) and tricyclohexylphosphine oxide at δ 49.1 ppm (**Figure 5.4**). The addition of **MP** had no effect on any of these observed resonances, except that the tricyclohexylphosphine oxide shifted downfield to δ 54.6 ppm, indicating deshielding of the phosphine oxide. This can be attributed to slight protonation of the phosphine oxide [8]. The addition of **NP** however had a different effect. From the onslaught of mixing, an unfavoured interaction was observed with the Ru-PCy_3 ligand shifting slightly upfield (17.6 Hz) to δ 29.3 ppm. A broadening of this resonance is also observed. There was also an increase of decomposed catalyst resonances observed at δ 42.0 and 21.2 ppm with another decomposed product resonance being observed at δ 32.2 ppm. The tricyclohexylphosphine oxide shifted even more downfield to δ 56.7 ppm indicating an even stronger protonation of the phosphine oxide by the phenol additive through stronger hydrogen bonding between the phenol and the tricyclohexylphosphine oxide.

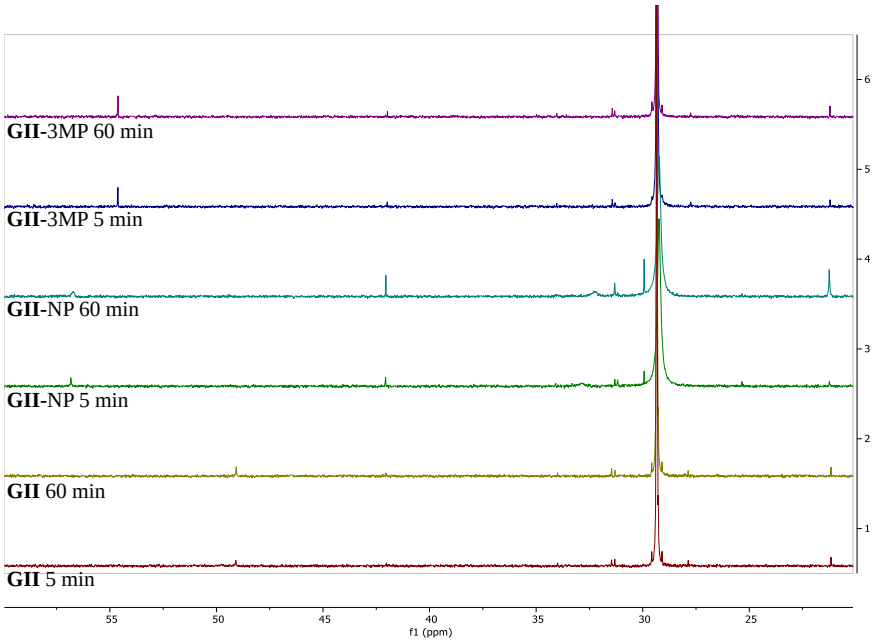

Figure 5.5: ^{31}P NMR of **GII** at time 5 min (1), **GII** at time 60 min (2), **GII-NP** at time 5 min (3), **GII-NP** at time 60 min (4), **GII-3MP** at **time 5 min (5), and GII**-3MP at time 60 min (6) in CD_2Cl_2 at 25 °C.

Electrochemistry: The electrochemical properties of **GII** and the **GII**-phenol adducts were investigated in dry dichloromethane using cyclic voltammetry (CV) at 25 °C with tetrabutylammonium hexafluorophosphate, $[N(^nBu)_4][PF_6]$, as the supporting electrolyte under a blanket of argon. The CVs are referenced vs ferrocene (HFc/HFc^+) but decamethylferrocene (Fc*) was used as the internal reference to avoid overlap of the ferrocene redox wave with the **GII** redox wave. It has been reported that the redox reaction of **GII** is a one-electron transfer process for the Ru^{II}/Ru^{III} couple in dichloromethane [33]. For this report, it can thus be assumed that the Ru metal centre in the **GII**-phenol adducts will also be involved in a one-electron transfer process (Ru^{II}/Ru^{III}).

The comparative CVs of **GII** and the **GII**-phenol adducts at 100 mV s^{-1} scan rate in dry DCM are presented in **Figure 5.6.5**, with the CV data summarised in **Table 5.2** (the CVs and data for the 50 to 1000 mV s^{-1} scan rates are provided in the Supp Info). Conventionally, electrochemical reversibility at 25 °C is theoretically defined by peak potential separation (ΔE_p) of 59 mV and chemical reversibility is defined at $i_{pc}/i_{pa} = 1$ [42,43]. The internal standard, decamethylferrocene (Fc*) showed $61 < \Delta E < 90$ mV defining the range of electrochemical reversibility under our conditions. At 100 mV s^{-1} all the **GII-**phenol adducts are electrochemically reversible, apart from **GII-BP** and **GII-TFP** (having electron-withdrawing R-groups on the phenol) which display quasi-electrochemical behaviour.

Only **GII**, **GII-MOP**, and **GII-NP** displayed $i_{pc}/i_{pa} = 1$, at 100 mV s^{-1}, implying chemical reversibility. The other **GII-**phenol adducts displayed varied degrees of chemical reversibility. It was also observed that upon varying the scan rate, the degree of chemical reversibility was not consistent for the adducts. For **GII** the benchmark compound, it was found that as the scan rate increases the chemical reversibility decreased (**Figure 5.7**). The behaviour has been reported previously and indicates that the redox process proceeds via an E_rC_r electrochemical mechanism (E_r = reversible electrochemical step; C_r = reversible chemical step) [33]. Similar behaviour has been observed for all the **GII**-phenol adducts (see Supp Info).

An E_rC_r electrochemical mechanism (see **Figure 5.7**) entails: At slow scan rates, the redox process is chemically reversible, with $i_{pc}/i_{pa} \approx 1$. However, as the scan rate increases, the chemical

reversibility decreases, leading to smaller i_{pc}/i_{pa} ratio. This indicates that the electrochemically oxidized species, **GII**$^{\bullet+}$, is chemically converted (via an equilibrium reaction) into electrochemically inactive species (no additional oxidation or reduction peaks were detected within the CV window, or these peaks are outside the solvent potential window) [44]. Consequently, it can be inferred that at slow scan rates, **GII**$^{\bullet+}$ is regenerated rapidly enough from the chemically formed product, allowing the i_{pc}/i_{pa} ratio to come closer to one. Conversely, at high scan rates, **GII**$^{\bullet+}$ cannot be regenerated quickly enough to maintain an i_{pc}/i_{pa} ratio of approximately one, causing the current ratio to deviate further from one. Given sufficient time, even at high scan rates, all chemically transformed products will eventually convert back to **GII**$^{\bullet+}$, but this would occur after the peak cathodic potential is reached during the reverse scan.

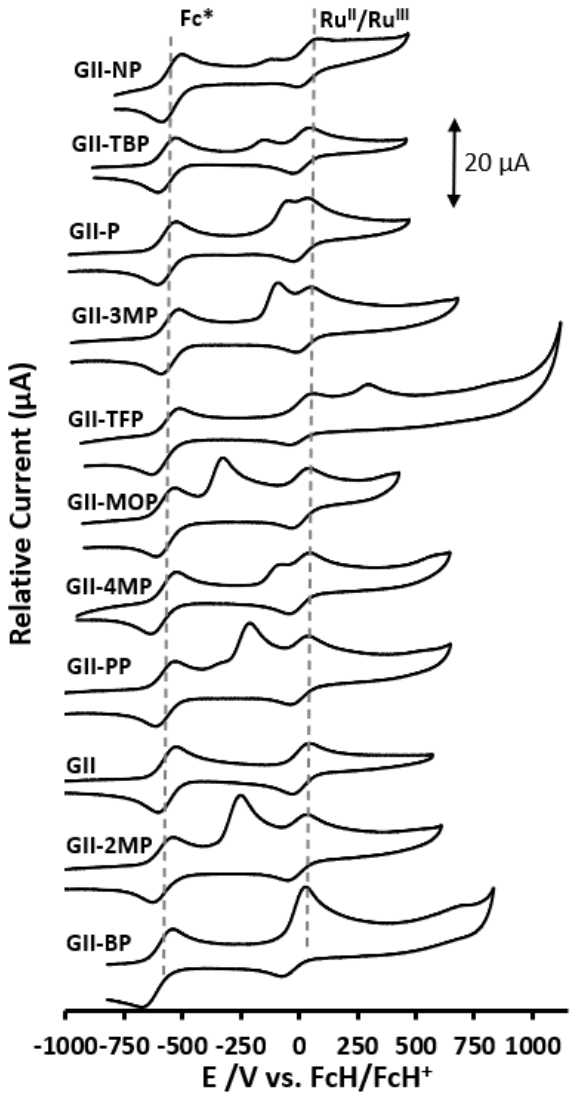

Figure 5.6: Comparative cyclic voltammogram of a 0.8 mM solution of **GII** and the **GII**-phenol adducts in the presence of 0.08 M $[N(^nBu)_4][PF_6]$ as supporting electrolyte at 25 °C at 100 mV s^{-1}, referenced vs ferrocene, but decamethylferrocene (Fc*) was used as internal reference.

Comparison of the reduction potentials (E°') of **GII** and **GII**-phenol adducts, revealed that the Ru^{II}/Ru^{III} process (E°') occurs between -20 and 42 mV (**Figure 5.6.5** and **Table 5.2**), indicating that the phenol additives have a large influence on the reduction potential of the Ru metal centre. An additional oxidation peak (which does not have a reduction peak) is also observed in the CV of **GII**-phenol adducts, which is ascribed to the oxidation of the phenol.

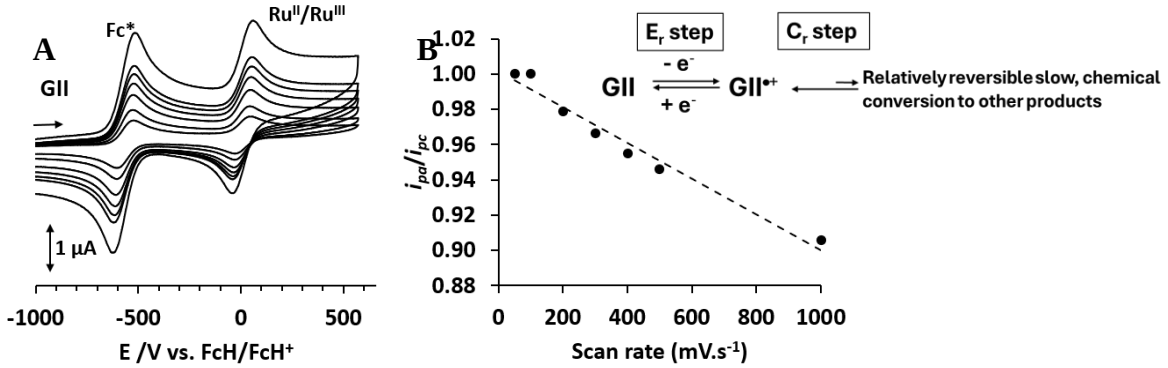

Figure 5.7: The cyclic voltammograms of a 0.8 mM solution of (A) **GII** in the presence of 0.08 M $[N(^nBu)_4][PF_6]$ as supporting electrolyte at 25 °C at scan rates ranging from 50-1000 mV s^{-1}. (B) The relationships between i_{pc}/i_{pa} and scan rates at 25 °C for the Ru^{II}/Ru^{III} process for **GII**. Insert: Schematic representation of the E_rC_r mechanism for **GII**.

Table 5.2: Peak anodic and cathodic potentials, E_{pa} and E_{pc}, peak potential difference ΔE_p, formal reduction potentials, E°, (vs ferrocene) peak currents, $i_{pa\ or\ pc}$, and current ratios i_{pc}/i_{pa} for 0.8mM solution of **GII** and the **GII**-phenol adducts containing 0.08M $[N(^nBu)_4][PF_6]$ as supporting electrolyte at 25°C for indicated scan rates of the Ru^{II}/Ru^{III} redox couples.

	Phenol oxidation		Ru^{II}/Ru^{III}							
	E_{pa}/mV	i_{pa}/µA	E_{pa}/mV	E_{pc}/mV	E^0 /mV	$\triangle E_p$/mV	i_{pc}/µA	i_{pa}/µA	i_{pc}/i_{pa}	i_{Ru}/i_{phenol}
GII-PP	-175	5.56	47	-31	8	78	4.00	3.33	0.83	0.15
GII-2MP	-218	8.89	39	-46	-4	85	5.08	3.81	0.75	0.08
GII-4MP	-27	4.02	48	-42	3	90	4.63	3.66	0.79	0.20
GII-TBP	-136	2.73	66	-15	26	81	4.55	3.86	0.85	0.31
GII-3MP	-107	7.89	54	-5	25	59	6.05	3.95	0.65	0.08
GII-MOP	-297	8.95	50	-26	12	76	4.21	4.21	1	0.11
GII-P	-40	6.58	57	-3	27	60	6.84	3.95	0.58	0.09
GII-BP			31	-70	-20	101	10.67	3.67	0.34	

GII-TFP	334	7.27	53	-49	2	102	5.45	3.18	0.58	0.08
GII-NP	-109	1.62	84	-1	42	85	3.24	3.24	1	0.62
GII			47	-27	10	74	4.34	4.34	1	

Cross-metathesis catalysed reaction: The beneficial effect of addition of phenol or *p*-cresol as an additive to **GII** catalysed cross-metathesis with respect to selectivity and improved product yield has been reported [8,20]. Though the results obtained are satisfactory, further optimization is possible to enhance cost efficiency. Hence, the **GII**-phenol adducts were tested for the metathesis reaction between *trans*-1-methoxy-4-(1-propenyl)benzene **1**, and 2-ethylhexyl acrylate **2** as a case study (see Scheme 5.2). The cross-metathesis product of this reaction is an active ingredient known as octinoxate used in cosmetics and beauty products as Ultraviolet (UV) rays filter from the sun. The metathesis reaction is catalysed by the **GII**-phenol adducts resulting in the cross-metathesis (CM) product **3**, and the undesired self-metathesis product (SM) **4**.

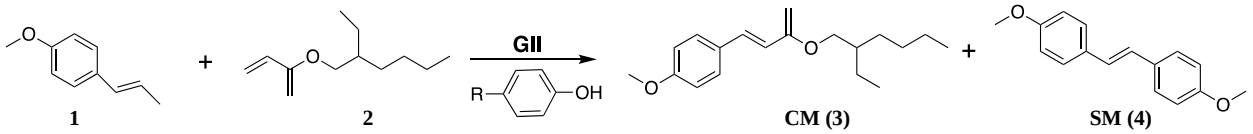

Scheme 5.2: The metathesis reaction between *trans*-1-methoxy-4-(1-propenyl) benzene, 1, and 2-ethylhexyl acrylate, 2, catalysed by **GII**-phenols.

The *trans*-1-methoxy-4-(1-propenyl)benzene, **1** (1 eq), and 2-ethylhexyl acrylate, **2** (2 eq), were refluxed in dichloromethane in the presence of **GII** (0.5 mol %) and 100 eq of the selected phenol derivatives for 3 hours under an argon atmosphere. The influence of the different phenol additives' effect on the isolated yield of the cross-metathesis product yield are summarised in **Table 5.**.

It is well-documented in literature that the hydroxyl group of the phenol forms a hydrogen bond with the chloride group of **GII**, which in turn facilitates the dissociation of PCy_3 (**Scheme 5.1:** An illustration depicting the phosphine dissociation/association equilibrium of GII-phenol adducts, producing the active catalytic species (GII^A),) which is a critical step for catalyst activation [4,8,20,21]. It can be assumed that the k_{obs}' for catalyst activation should be correlated with the catalytic ability of the catalyst. This may influence the rate of catalysis, but it does not influence the selectivity of the catalyst toward the CM product, since no meaningful correlation could be established between %CM and k_{obs}'.

As per literature the **GII-**phenol interaction, causes an increase in electrophilicity on the ruthenium centre and in turn a decrease in electrophilicity of the carbene carbon, which is postulated to be the cause of increased %CM when a phenol is added to **GII** [8]. For the **GII-**phenol additives, the phenol compounds with more electron donating groups are more basic (high pk_a), see **Figure 5.4 B**, causing an increase in electrophilicity on the Ru centre. This increase in electrophilicity on the Ru centre translates into higher %CM as see from the relationship between the pk_a and %CM (**Figure 5.4 D**).

6.3.1 Experimental section

General experimental methods. The Grubbs second generation catalyst [1,3-bis(2,4,6 trimethylphenyl)-2-imidazolidinylidene)dichloro(phenylmethylene)-(tricyclohexylphosphino) ruthenium], other solid reagents and solvents used in the study were purchased from Sigma – Aldrich and were used without further purification. Solvents were dried using a small column of activated neutral alumina (10% v/v) prior to use. All reactions were carried out under Schlenk conditions in an argon atmosphere.

Procedure: The following general procedure was used during the metathesis reaction (using **GII** and the different selected phenol derivatives) which was adopted from the reported procedure described by Swart *et al.* [8]

GII (5.7 mg, 0.0067 mmol, 0.5 mol%) and the selected phenol derivative (100 equivalents *vs* 1eq. **GII**), was dissolved in 10 mL of dry dichloromethane and heated to 40 °C while being stirred under a dry argon atmosphere. Trans-1-methoxy-4-((1-propenyl)benzene), **1**, (0.20 mL, 1.3 mmol, 1 eq.) and 2-ethylhexyl acrylate, **2**, (0.56 mL, 2.7 mmol, 2 eq.) were added to the existing mixture simultaneously and the reaction was allowed to proceed for 3 hours. The reaction mixture was concentrated in vacuo and the resulting mixture was applied on a preparative TLC plate for separation to obtain the purified SM and CM major products.

Characterization data of (*E*)-1,2-bis(4-methoxyphenyl)ethene (**4**, SM product):

^{1}H NMR (400MHz, CD_2Cl_2) [8]: δ = 7.53-7.42 (m, 4H), 6.98 (s, 2H), 6.93 (d, J = 8.9 Hz, 4H), 3.85 (s, 6H, -OCH_3)

Characterization data of (*E*)-2-ethylhexyl-3-(4-methoxyphenyl)acrylate (**3**, CM product):

^{1}H NMR (400MHz, CD_2Cl_2) [8]: δ = 7.65 (d, J=16.0, 1H), 7.54 (d, J = 8.9 Hz, 2H), 6.96 (d, J = 8.8Hz, 2H), 6.37 (d, J = 16.0 Hz, 1H), 4.18-4.08 (m, 2H), 3.86 (s, 3H, -OCH_3), 1.68 (dq, J = 12.2, 6.1 Hz, 1H), 1.51-1.32 (m, 8H), 0.95 (ddd, J = 8.8, 6.9, 5.3 Hz, 6H)

Spectroscopic characterization: Attenuated Total Reflection Fourier Transform Infrared (ATR-FTIR) Spectroscopy. The ATR-FTIR spectra of **GII** with 100 equivalents of the different phenol derivatives were recorded using a Thermo Scientific IR spectrometer with a Nicolet iS50 ATR attachment. The Shimadzu UV – 1800 UV/Visible spectrophotometer was employed for recording 0.10 mM solution of **GII** and the selected phenol derivatives in dichloromethane under an argon atmosphere. A 2 mL quartz cuvette with a path length of 1 cm was used. The UV-Vis stability investigation over time (24 h) were carried out on 0.10 mM solution of **GII** and the selected phenols under argon atmosphere, and spectra were recorded every 15 min interval for 24 h.

Electrochemical Characterization. The electrochemical properties of 0.8 mM solution of Grubbs second generation catalyst and the selected phenol derivatives were measured in dry dichloromethane containing 0.08 M tetrabutylammonium hexafluorophosphate, $[N(^{n}Bu)_4[PF_6]$, as supporting electrolyte (a large supporting electrolyte concentration is required to increase solution conductivity to guarantee charge balance and complete the electrical circuit)[45]. The experiments were conducted under a blanket of argon at 25°C, employing a BAS 100 B/W electrochemical workstation interfaced with a personal computer. A three-electrode set up was used, including a Pt auxiliary electrode, a glassy carbon working electrode with surface area of 3.14 mm^2, and a Pt reference electrode. Since it is imperative that the surface of the working electrode must be extremely clean, it was polished repeatedly on a Buhler polishing mat, using a 1 μm and ¼ μm diamond paste. Experimental potentials measured against the Pt reference electrode, but the results presented are referenced against the ferrocene couple, FcH/FcH^+, as an internal standard as advised by IUPAC. However, the FcH/FcH^+ couple interfered with the oxidation and reduction peak of the Grubbs second generation catalyst, therefore, decamethylferrocene (FcH*) was subsequently used as an internal standard and referenced back to ferrocene. The formal reduction potential of Fc*, $E°_{Fc*}$ = -542 mV vs FcH/FcH^+.

6.4 Conclusion

This study sheds light on the pivotal role of phenol derivatives in modulating the behaviour of the Grubbs' second-generation catalyst (**GII**) during metathesis. Using various spectroscopic and electrochemical methods, we have demonstrated that the nature of phenol additives significantly impacts the stability and electronic properties of the **GII**-phenol adducts. The distinct ATR-FTIR and UV-Vis spectral features, especially the absorption peaks characteristic of metal-ligand charge transfer, provides valuable insight into the complex interaction mechanisms. Phosphine ligand dissociation and the subsequent formation of the catalytically active species (**GII^{A}** and **GII^{AS}**) were shown to depend on the pK_a of the phenol substituents.

Electrochemical analysis via cyclic voltammetry revealed that most **GII-**phenol adducts exhibit electrochemical reversibility, with the notable exceptions of **GII-BP** and **GII-TFP**, which displayed quasi-electrochemical behaviour. The redox potential of the Ru^{II}/Ru^{III} process was significantly influenced by the phenol additives, further underscoring the role of the electronic effects.

Catalytic testing confirmed that the nature of the phenol additives affects the efficiency of the metathesis reaction, particularly in terms of cross-metathesis (CM) product yield. Additives with more electron-donating groups (higher pK_a) enhanced the electrophilicity of the Ru centre, resulting in improved catalytic performance, though no clear correlation was established between catalyst activation rate and product selectivity. This study provides insight into non-structural modifications of **GII** and avenues for optimizing performance in industrial metathesis applications.

References

[1] R. H. Grubbs, *Angew. Chem. Int. Ed.* **2006**, *45*, 3760–3765.

[2] B. Anusha, R. B. Kothapalli, M. Victor Prem Sagar, B. Surendra, U. V. Subba Reddy, *Synth Commun* **2024**, *54*, 323–347.

[3] A. E. Wright, J. C. Botelho, E. Guzmán, D. Harmody, P. Linley, P. J. McCarthy, T. P. Pitts, S. A. Pomponi, J. K. Reed, *J Nat Prod* **2007**, *70*, 412–416.

[4] G. A. Bailey, D. E. Fogg, *J Am Chem Soc* **2015**, *137*, 7318–7321.

[5] C. Theunissen, M. A. Ashley, T. Rovis, *J Am Chem Soc* **2019**, *141*, 6791–6796.

[6] Grela K, *Olefin Metathesis: Theory and Practice*, Wiley, Hoboken, NJ, **2014**.

[7] Grubbs R.H, Wenzel A.G, *Handbook of Metathesis*, Wiley-VHC, Weinheim, **2015**.

[8] M. R. Swart, L. Twigge, E. Erasmus, C. Marais, B. C. B. Bezuidenhoudt, *Eur J Inorg Chem* **2021**, 1752–1762.

[9] F. Sinclair, M. Alkattan, J. Prunet, M. P. Shaver, *Polym Chem* **2017**, *8*, 3385–3398.

[10] F. Stelzer, *J. Macromol. Sci., Part A* **1996**, *33*, 941–952.

[11] J. C. Foster, A. W. Cook, N. T. Monk, B. H. Jones, L. N. Appelhans, E. M. Redline, S. C. Leguizamon, *Adv. Sci.* **2022**, *9*,1-8.

[12] C. S. Higman, J. A. M. Lummiss, D. E. Fogg, *Angew. Chem. Int. Ed.* **2016**, *55*, 3552–3565.

[13] D. Hughes, P. Wheeler, D. Ene, *Org Process Res Dev* **2017**, *21*, 1938–1962.

[14] J. C. Mol, *J Mol Catal A Chem* **2004**, *213*, 39–45.

[15] J. H. Phillips, in *Organometallic Chemistry in Industry*, Wiley, **2020**, pp. 259–282.

[16] K. Kaczanowska, B. Trzaskowski, A. Peszczyńska, A. Tracz, R. Gawin, T. K. Olszewski, K. Skowerski, *ChemCatChem* **2020**, *12*, 6366–6374.

[17] K. Lafaye, L. Nicolas, A. Guérinot, S. Reymond, J. Cossy, *Org Lett* **2014**, *16*, 4972–4975.

[18] D. Schweitzer, K. D. Snell, *Org Process Res Dev* **2015**, *19*, 715–720.

[19] X. Meng, K. J. Edgar, *Carbohydr Polym* **2015**, *132*, 565–573.

[20] G. S. Forman, R. P. Tooze, *J Organomet Chem* **2005**, *690*, 5863–5866.

[21] A. G. Santos, G. A. Bailey, E. N. dos Santos, D. E. Fogg, *ACS Catal* **2017**, *7*, 3181–3189.

[22] G. S. Forman, A. E. McConnell, R. P. Tooze, W. Janse Van Rensburg, W. H. Meyer, M. M. Kirk, C. L. Dwyer, D. W. Serfontein, *Organometallics* **2005**, *24*, 4528–4542.

[23] K. A. Burdett, L. D. Harris, P. Margl, B. R. Maughon, T. Mokhtar-Zadeh, P. C. Saucier, E. P. Wasserman, *Organometallics* **2004**, *23*, 2027–2047.

[24] M. R. Swart, B. C. B. Bezuidenhoudt, C. Marais, E. Erasmus, *Inorganica Chim Acta* **2021**, *514*, 120001.

[25] Odewole O.A, Swart M.R, Erasmus E, *Eur J Inorg Chem* **2024**.

[26] J. I. Yun, D. Kim, J. Lee, *Tetrahedron Lett* **2011**, *52*, 1928–1930.

[27] E. L. Dias, S. T. Nguyen, R. H. Grubbs, *J Am Chem Soc* **1997**, *119*, 3887–3897.

[28] W. H. Meyer, A. E. McConnell, G. S. Forman, C. L. Dwyer, M. M. Kirk, E. L. Ngidi, A. Blignaut, D. Saku, A. M. Z. Slawin, *Inorganica Chim Acta* **2006**, *359*, 2910–2917.

[29] M. Abbas, A. Leitgeb, C. Slugovc, *Synlett* **2013**, *24*, 1193–1196.

[30] C. Feng, X. Wang, B.-Q. Wang, K.-Q. Zhao, P. Hu, Z.-J. Shi, *Chem. Commun.* **2012**, *48*, 356–358.

[31] B. J. Ireland, B. T. Dobigny, D. E. Fogg, *ACS Catal* **2015**, *5*, 4690–4698.

[32] O. A. Odewole, M. R. Swart, E. Erasmus, *Tetrahedron* **2024**, *162*, 134105.

[33] M. R. Swart, C. Marais, E. Erasmus, *ACS Omega* **2021**, *6*, 28642–28653.

[34] L. Maity, S. Das Adhikary, A. Mondal, H. K. Kisan, A. A. Isab, S. Goswami, J. Dinda, *Inorganica Chim Acta* **2018**, *479*, 141–147.

[35] A. Labande, J.-C. Daran, N. J. Long, A. J. P. White, R. Poli, *New J. Chem.* **2011**, *35*, 2162-2168.

[36] T. K. Maishal, B. Mondal, V. G. Puranik, P. P. Wadgaonkar, G. K. Lahiri, A. Sarkar, *J Organomet Chem* **2005**, *690*, 1018–1027.

[37] S. Leuthäußer, V. Schmidts, C. M. Thiele, H. Plenio, *Chem. Eur. J.* **2008**, *14*, 5465–5481.

[38] T. Matsuo, T. Yoshida, A. Fujii, K. Kawahara, S. Hirota, *Organometallics* **2013**, *32*, 5313–5319.

[39] V. Forcina, A. García-Domínguez, G. C. Lloyd-Jones, *Faraday Discuss* **2019**, *220*, 179–195.

[40] M. Ramesh, M. D. Kumar, M. Jaccob, B. Therrien, G. Venkatachalam, *Inorganica Chim Acta* **2018**, *477*, 40–50.

[41] J. R. Griffiths, J. B. Keister, S. T. Diver, *J Am Chem Soc* **2016**, *138*, 5380–5391.

[42] J. C. Swarts, E. H. G. Langner, N. Krokeide-Hove, M. J. Cook, *J Mater Chem* **2001**, *11*, 434–443.

[43] H. J. Gericke, N. I. Barnard, E. Erasmus, J. C. Swarts, M. J. Cook, M. A. S. Aquino, *Inorganica Chim Acta* **2010**, *363*, 2222–2232.

[44] S. Trupia, A. Nafady, W. E. Geiger, *Inorg. Chem Commun.* **2003**, *42*, 5480–5482.

[45] N. Elgrishi, K. J. Rountree, B. D. McCarthy, E. S. Rountree, T. T. Eisenhart, J. L. Dempsey, *J Chem Educ* **2018**, *95*, 197–206.

CHAPTER 6
CRITICAL EVALUATION OF THIS STUDY AND FUTURE WORK

The purpose of this chapter is to evaluate the research outcomes in this study in relation to the initial objectives established in Chapter 1. Potential avenues for further investigation are enumerated to enhance contribution to this field of study.

6.1 Critical Evaluation of this study

The pursuit of an ideal metathesis catalyst remains an ongoing challenge, necessitating the optimization of reaction conditions to favour cross-metathesis (CM). This study aimed to determine the optimal *p*-cresol/Grubbs second-generation (GII) catalyst ratio for improved product yield. The findings indicate that the highest selectivity for the CM product was obtained at a *p*-cresol/**GII** ratio of 100:1, highlighting the role of *p*-cresol in promoting the desired reaction pathway. The established convention of using an excess of acrylate, due to its lower reactivity, was supported by experimental data demonstrating that reagent equivalence significantly impacts product distribution. When the acrylate was in excess ($X_A \leq 0.33$), CM product yield increased up to 98% at $X_A = 0.09$, suggesting that the CM pathway is kinetically favoured despite the inherent self-affinity of the olefinic substrate.

Temperature and time studies further elucidated the mechanistic aspects of the reaction. An increase in temperature facilitated the formation of the p-cresol/**GII** adduct, which in turn enhanced CM product formation. Notably, the observed reaction rate constant (k'_{obs}) increased from 0.0575 min^{-1} at 25 °C to 0.68 min^{-1} at 35 °C. Moreover, selectivity toward CM product formation was approximately twice as high at 35 °C compared to 25 °C. The data further revealed that the CM product had not reached equilibrium after 700 minutes, in contrast to the steady-state concentration observed for the self-metathesis (SM) product. These findings suggest that under the

investigated conditions, CM remains a kinetically driven process rather than a thermodynamically controlled one.

The dissociation of the phosphine ligand from GII is a crucial step in catalyst activation, forming the active species (SIMes)$RuCl_2$(CHPh). The study examined solvent effects on this dissociation/association equilibrium across dichloromethane (DCM), 1,2-dichloroethane (DCE), chloroform (CLF), tetrahydrofuran (THF), and toluene (TOL). Rate constants (k'_{obs}) varied from 8×10^{-5} s^{-1} (CLF) to 2.6×10^{-4} s^{-1} (THF). Although THF exhibited the highest k'_{obs}, it proved unsuitable for **GII**-catalyzed metathesis due to its strong binding affinity, which hindered product formation. This was further corroborated by electrochemical data indicating the absence of a reduction peak for **GII** in THF. For the other solvents, a direct correlation between higher k'_{obs} and increased CM product yield was observed, emphasizing the importance of solvent choice. The electronic properties of **GII** were influenced by solvent polarity, donor ability, and dipole moment, necessitating careful solvent selection for optimized catalysis.

Spectroscopic and electrochemical analyses provided deeper insights into the role of phenol additives in modulating **GII** stability and electronic properties. Distinct ATR-FTIR and UV-Vis spectral features, particularly metal-ligand charge transfer absorption peaks, revealed critical interaction mechanisms. The dissociation of the phosphine ligand and subsequent formation of active species (**GII^{A}** and **GII^{AS}**) were shown to depend on the electronic nature of phenol substituents. A correlation was observed between the Hammett constant (σ_R) and catalyst transformation rate constant (k'_{obs}), with electron-donating substituents facilitating faster phosphine dissociation via enhanced hydrogen bonding between the -OH group and the chloride ligand of **GII**. This interaction destabilized the Ru-PCy_3 bond, accelerating catalyst activation. Conversely, electron-withdrawing groups exhibited distinct dissociation behaviour, indicating additional influencing factors beyond electronic effects alone. Notably, **GII-NP** displayed unique behaviour attributed to zwitterionic interactions, ultimately leading to catalyst decomposition.

Electrochemical analysis via cyclic voltammetry demonstrated that most **GII**-phenol adducts exhibited reversible redox behaviour, except for **GII-BP** and **GII-TFP**, which displayed quasi-reversible characteristics. The Ru^{II}/Ru^{III} redox potential was significantly influenced by phenol additives, reinforcing the importance of electronic effects. Catalytic testing confirmed that phenol

additives affected metathesis efficiency, particularly CM product yield. Additives with stronger electron-donating groups (higher pK_a) enhanced Ru electrophilicity, improving catalytic performance. However, no clear correlation was established between activation rate and product selectivity, suggesting that multiple factors influence overall catalytic efficiency.

In conclusion, this study provides valuable mechanistic insights into metathesis catalysis and highlights critical parameters for optimizing **GII**-based systems. The impact of phenol additives, solvent choice, and reaction conditions on catalyst performance underscores the complexity of metathesis chemistry. Future work should focus on further refining non-structural modifications of **GII** to enhance selectivity and efficiency in industrial applications.

6.2 Future Perspective

This study has established that non-structural modification of the commercially available olefin metathesis catalyst is better and cheaper route to improve catalyst efficiency and selectivity for metathesis reaction. The following should however be investigated further:

1. The investigation of the effect phenol derivatives has on metathesis reaction catalysed by other commercially available Grubbs and Hoveyda-Grubbs catalysts and the results compared to those obtained in this study.
2. A catalyst transformation study aimed at the investigation of dimer formation and/or catalyst decomposition.
3. Further NMR product distribution/kinetic studies of Grubbs and Hoveyda-Grubbs catalysts in the presence of additives in comparison to the results obtained in this study.
4. The investigation of the metathesis reaction between allylbenzene with electron donating and electron withdrawing group and 1-hexene catalysed by second generation Grubbs catalyst with phenol derivatives compared to the results obtained from this study.
5. An electrochemical study investigation of other commercially Grubbs' and Hoveyda-Grubbs catalysts in the presence of additives.

CHAPTER 7
PUBLICATIONS AND CONFERENCE CONTRIBUTIONS

The aim of this chapter is to summarise the publications published and conference contributions already made during this study.

7.1 Publications

7.1.1 Metathesis reactions: Effect of additives as co-catalysts to Grubbs' or Schrock's catalyst

Published in: Tetrahedron 2024, 162, 134105

DOI: https://doi.org/10.1016/j.tet.2024.134105

Authors: Odewole, O.A., Swart, M.R., and Erasmus, E.

Authors Contribution:

OAO: Data curation, writing- original draft preparation.

MRS: Conceptualisation, visualisation, supervision, writing - review & editing.

EE: Conceptualisation, visualisation, supervision, writing - review & editing.

The above-mentioned work was done under the supervision of Prof. Elizabeth Erasmus and with the co-supervision of Dr Marthinus R. Swart.

7.1.2 En route investigation of reaction conditions' influence on cross-metathesis yields employing Grubbs 2nd generation–*p*-cresol catalyst derivative

Published in: European Journal of Inorganic Chemistry 2025, 28, e202400085

DOI: https://doi.org/10.1002/ejic.202400085

Authors: Odewole, O.A., Swart, M.R., and Erasmus, E.

Authors Contribution:

OAO: Conducting the research, writing—original draft preparation.

MRS: Conceptualisation, writing—review and editing.

EE: Conceptualisation, writing—review and editing.

The above-mentioned work was done under the supervision of Prof. Elizabeth Erasmus and with the co-supervision of Dr Marthinus R. Swart.

7.1.3 Spectroscopic Exploration of Catalyst Dynamics and Electrochemical Properties of Grubbs Second Generation in Different solvent.

Published in: European Journal of Inorganic Chemistry 2025, e202400356

DOI: https://doi.org/10.1002/ejic.202400356

Authors: O. Abiola Odewole, Martinus Rudi Swart, and Elizabeth Erasmus

Authors Contribution:

OAO: Conducting the research, writing—original draft preparation.

MRS: Conceptualisation, writing—review and editing.

EE: Conceptualisation, writing—review and editing.

The above-mentioned work was done under the supervision of Prof. Elizabeth Erasmus and with the co-supervision of Dr Marthinus R. Swart.

7.1.4 Unveiling the power of additives: Enhancing Grubbs' catalyst performance with phenol derivatives

Published in: Inorganica Chimica Acta 578 (2025) 122519

DOI: https://doi.org/10.1016/j.ica.2024.122519

Authors: Odewole, O.A., Swart, M.R., and Erasmus, E.

Authors Contribution:

OAO: Conducting the research, writing—original draft preparation.

MRS: Conceptualisation, writing—review and editing.

EE: Conceptualisation, writing—review and editing.

The above-mentioned work was done under the supervision of Prof. Elizabeth Erasmus and with the co-supervision of Dr Marthinus R. Swart.

7.2 Conferences

7.2.1 Oral Presentations

Odewole O.A., Swart M.R., Erasmus E. Optimization of the metathesis reaction between *trans*-1-methoxy-4-(1-propenyl)benzene and 2-Ethylhexyl acrylate employing Grubbs 2nd Generation Catalyst. FreeStatePhyChem Symposium, University of the Free State, South Africa 18th November 2022

7.2.2 Poster Presentations

Odewole O.A., Swart M.R., Erasmus E. Co-catalyst route to enhance product distribution of Grubb's second-generation mediated olefin metathesis. ACS Spring, New Orleans Ernest N. Morial Convention Centre, New Orleans 2024

Odewole O.A., Swart M.R., Erasmus E. Influence of phenol derivatives on the metathesis reaction between *trans*-1-methoxy-4-(1-propenyl)benzene and 2-ethylhexyl acrylate employing Grubbs 2nd Generation Catalyst. ACS Spring, Indiana Convention Centre, Indianapolis 2023

Odewole O.A., Swart M.R., Erasmus E., Boosting metathesis: Phenol derivatives as co-catalyst in 2-ethyl acrylate and trans-anrethole reactions with Grubbs' catalyst. 2024 6th Internaional FreeStatePhyChem 2024 Symposium, Bloemfontein, 12 November 2024

APPENDICES

APPENDIX A: SUPPLEMENTARY INFORMATION FOR CHAPTER 3

En route investigation of reaction conditions' influence on cross-metathesis yields employing Grubbs 2nd generation–*p*-cresol catalyst derivative – Part 1

Odewole, O.A., Swart, M.R., and Erasmus, E.

SUPPLEMENTARY INFORMATION

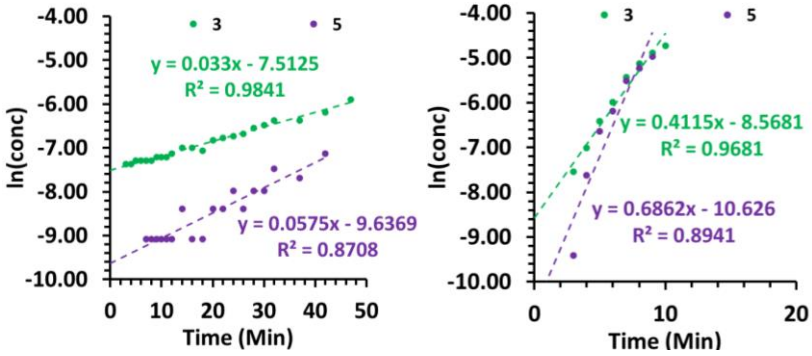

Figure S 3.1: The kinetic plots of the appearance of **3** (green) and **5** (purple) at (A) 25 °C and (B) 35 °C for the metathesis reactions that leads to the apparent observed first order rate constant k'_{obs}.

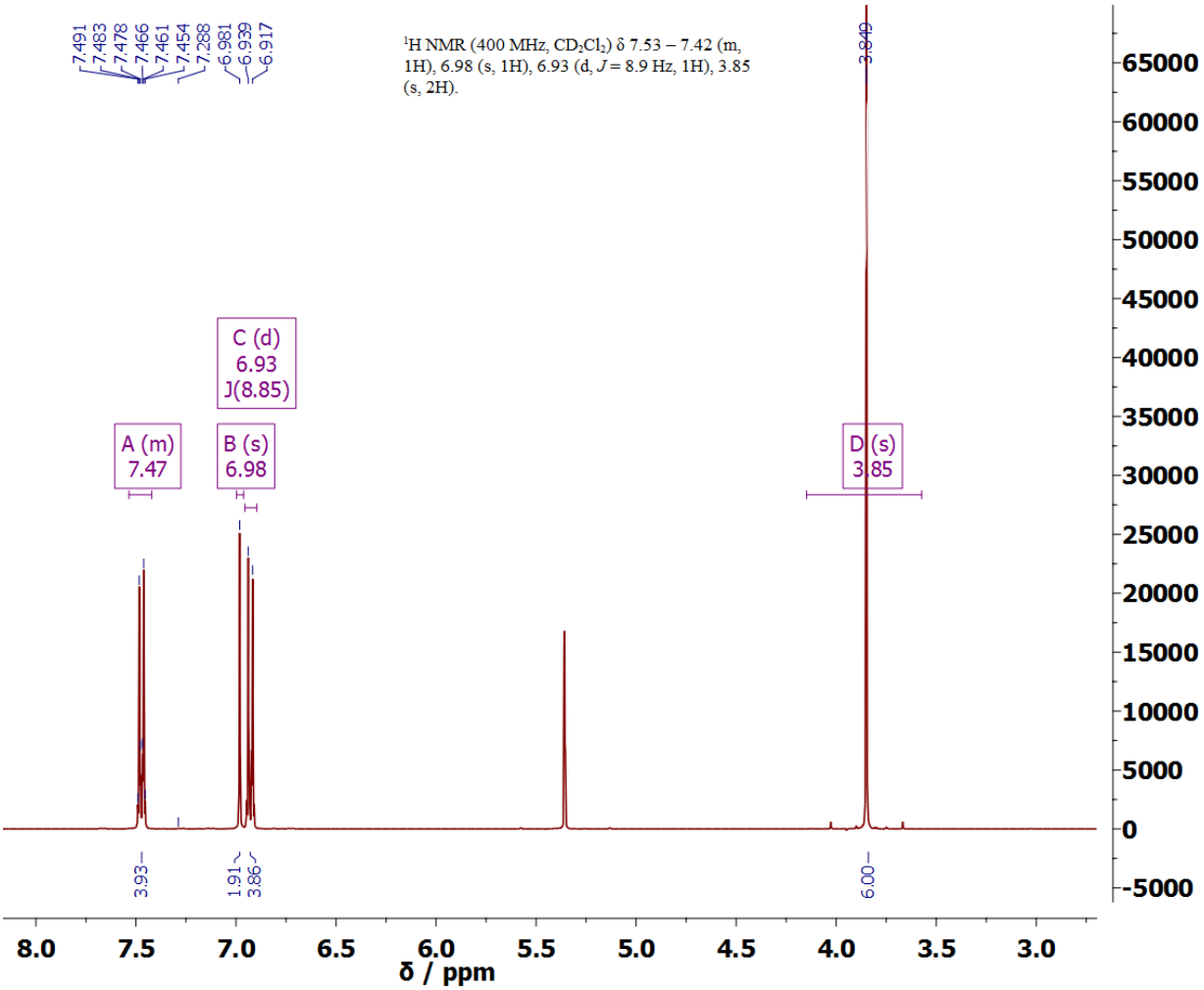

Figure S 3.2: The ^{1}H NMR data of (*E*)-1,2-bis(4-methoxyphenyl) ethene (**3**)

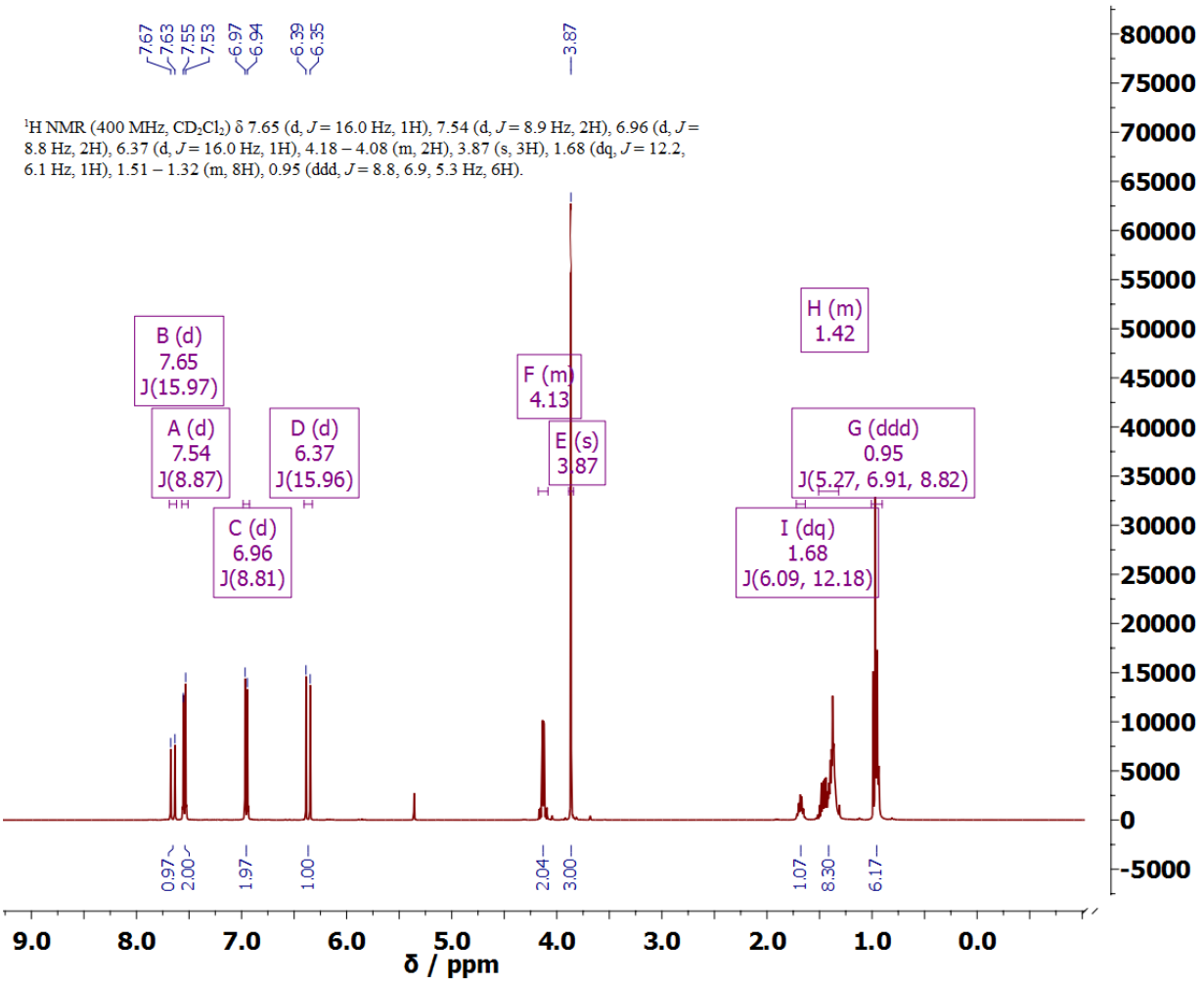

Figure S 3.3: The ^{1}H NMR data of (*E*)-2-ethylhexyl-3-(4-methoxyphenyl)acrylate (**5**)

Table S 3.1: Summarised data results of the *p*-cresol equivalent (*vs* GII eq.), resulting the isolated product yield of the self-metathesis product, and the ratio between the CM and SM product (for the reaction refluxed in CH_2Cl_2 under Ar and X_1 = 0.33).

Entry no	*p*-cresol eq.	CM yield %	SM yield %	CM: SM ratio
1	0	15	82	1.0: 5.5
2	0.5	21	8	2.6: 1.0
3	1	23	2	11.5: 1.0
4	2.5	25	28	0.9: 1.0
5	5.0	27	38	0.7: 1.0
6	10	28	6	4.7: 1.0
7	25	34	24	1.0: 0.7
8	50	43	34	1.0: 0.8
9	100	46	40	1.0: 0.9
10	150	46	24	1.0: 0.5
11	200	41	8	5.1: 1.0
12	300	34	40	0.9: 1.0

Table S 3.2: Table showing moles of reagent, mole fraction of 1, mole ratios, self-metathesis yield and the ratio between the CM and SM product.

Entry no	Mole substrate		X_1	Substrate ratio		SM yield %	CM: SM
	1	2		1	2	3	
	(mmol)	(mmol)					
1	13	1.3	0.91	10	1	70	1.0 : 70
2	6.5	1.3	0.83	5	1	66	1.0 : 8.3
3	4.55	1.3	0.78	3.5	1	50	1.0 : 8.3
4	2.6	1.3	0.67	2	1	42	1.0 : 2.5
5	1.3	1.3	0.50	1	1	34	1.0 : 0.9
6	1.3	2.7	0.33	1	2	40	1.0 : 0.7
7	1.3	4.55	0.22	1	3.5	10	1.0 : 0.2
8	1.3	6.5	0.17	1	5	6	1.0 : 0.1
9	1.3	13	0.09	1	10	0	1.0 : 0.0

APPENDIX B: SUPPLEMENTARY INFORMATION FOR CHAPTER 4

Spectroscopic Exploration of Catalyst Dynamics and Electrochemical Properties of Grubbs Second Generation in Different solvent

O. Abiola Odewole, Martinus Rudi Swart, and Elizabeth Erasmus

Supporting Information

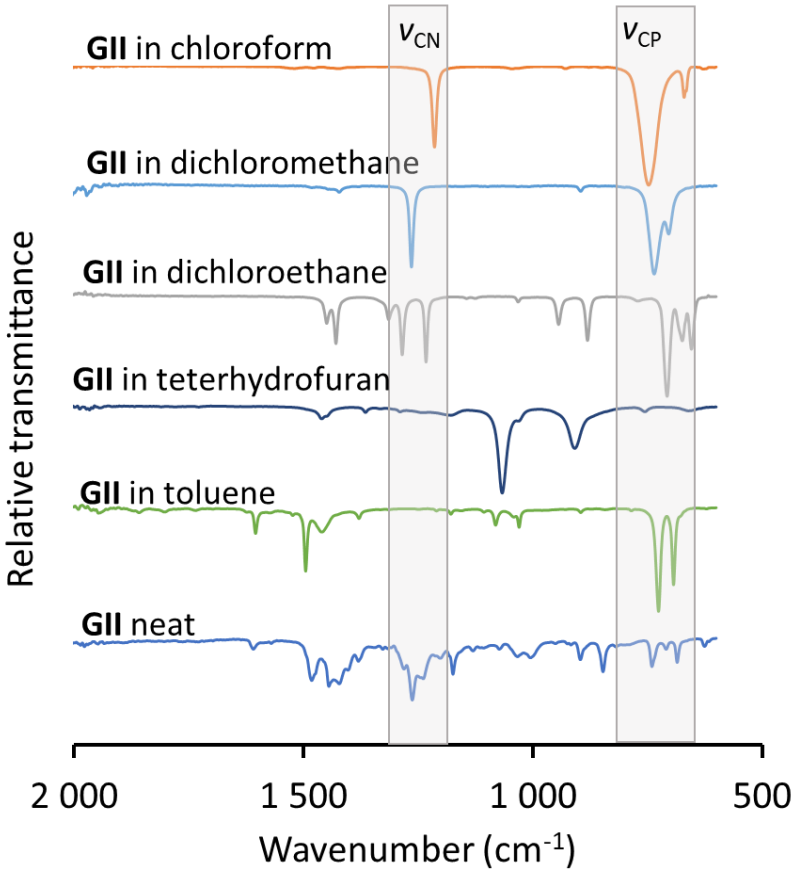

Figure S 3.1: The comparative ATR-FTIR spectra of **GII** dissolved in the different solvents (dichloromethane (DCM), chloroform (CLF), dichloroethane (DCE), tetrahydrofuran (THF), and toluene (TOL)).

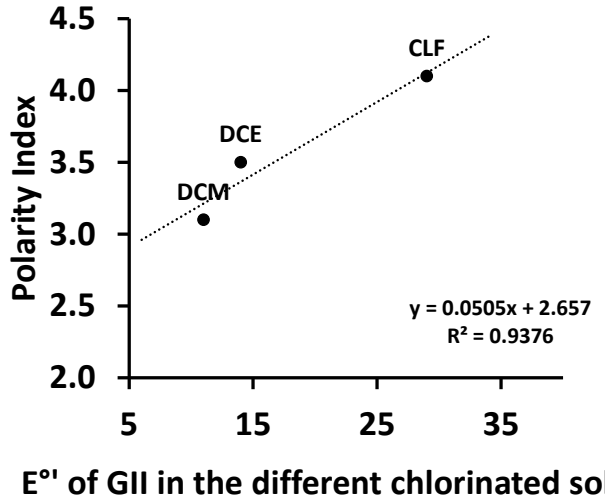

Figure S3.2: Graph showing the relationship between the E°' of **GII** in the different chlorinated solvents and the polarity index of the solvent.

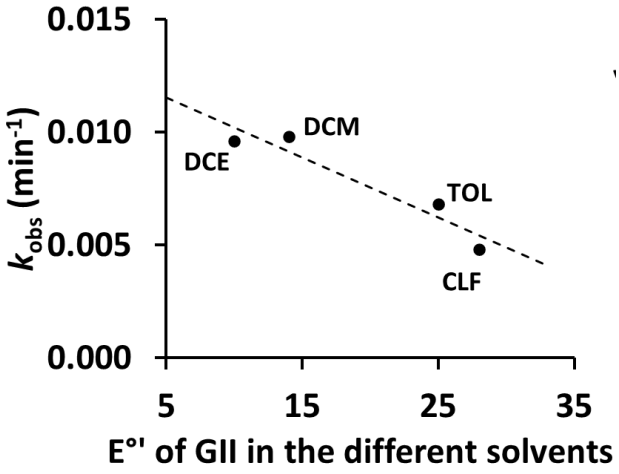

Figure S3.3: Graph showing the relationship between the E°' of **GII** and the k_{obs} (of the dissociation/association of the PCy_3) in the different solvents.

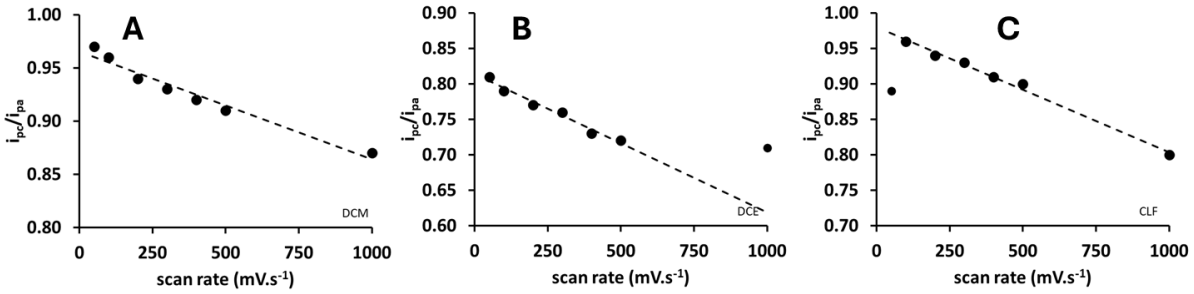

Figure S3.4: Graph showing the relationship between the scan rate and the chemical reversibility (i_{pc}/i_{pa}) of the redox process.

Optimised structure Information

Geometries for the GFN-xTB-optimised gas- and solution-phases (CH_2Cl_2) are also available for the visualisation of various Grubb catalysts, eg. GI, GII, Hoveyda (GI) and Hoveyda(HII). Also, other than the above POVRAY ray-traced image there are may other visualisation software that can also be used, including ORTEP.

Visualisation software: Cambridge Crystallographic Data Centre (CCDC) Mercury [Mercury 2022.1.0 (Build 343014)].[1]

Molecular modelling software, utilised for semi-empirical quantum mechanical, extended tight-binding GFN2-xTB model chemistry: xtb (version 6.5.1). The system was modelling with a closed shell electron configuration (spin multiplicity = 1) and a net formal charge of 0. The system was modelled in the gas phase (or in vacuo).[2]

[1] Mercury 4.0: from visualisation to analysis, design and prediction C. F. Macrae, I. Sovago, S. J. Cottrell, P. T. A. Galek, P. McCabe, E. Pidcock, M. Platings, G. P. Shields, J. S. Stevens, M. Towler and P. A. Wood, J. Appl. Cryst., **53**, 226-235, 2020 [DOI: 10.1107/S1600576719014092]

[2] For the xtb program:
C. Bannwarth, E. Caldeweyher, S. Ehlert, A. Hansen, P. Pracht, J. Seibert, S. Spicher, S. Grimme, WIREs Comput. Mol. Sci., 2020, 11, e01493. DOI: 10.1002/wcms.1493
For the GFN2-xTB method or model chemistry:
C. Bannwarth, S. Ehlert and S. Grimme., J. Chem. Theory Comput., 2019, 15, 1652-1671. DOI: 10.1021/acs.jctc.8b01176

APPENDIX C: SUPPLEMENTARY INFORMATION FOR CHAPTER 5

Unveiling the power of additives: Enhancing Grubbs' catalyst performance with phenol derivatives

Odewole, O.A., Swart, M.R., and Erasmus, E.

Supplementary Information

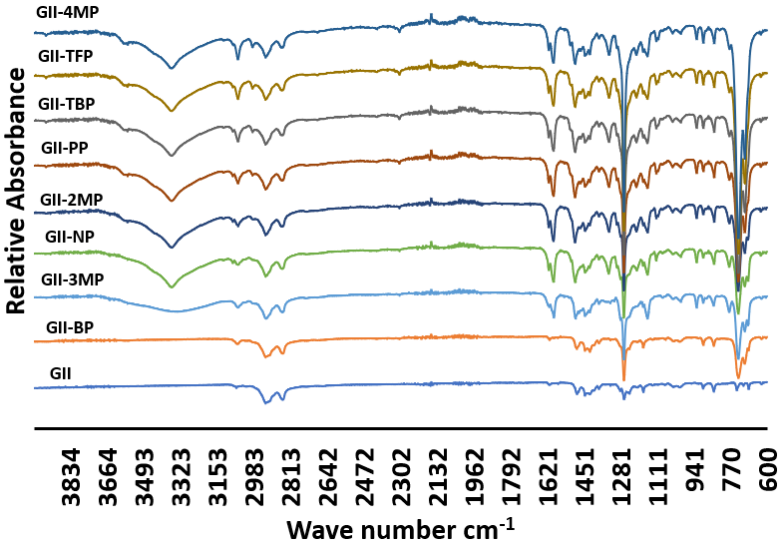

Figure S5.1.: ATR-FTIR of **GII** and the **GII**-phenol adducts.

ν /mVs^{-1}	E_{pa}/mV	$_{ipa}$/µA	E_{pa}/mV	E_{pc}/mV	E^0 /mV	$\triangle E_p$/mV	i_{pc}/i_{pa}	i_{pa}/µA	i_{pc}/µA	i_{Ru}/i_{phenol}
GII										
50			47	-27	10	74	1.00	3.29	3.29	
100			47	-27	10	74	1.00	4.34	4.34	
200			47	-27	10	74	0.98	6.18	6.05	
300			51	-33	9	84	0.97	7.89	7.63	
400			53	-37	8	90	0.96	8.82	8.42	
500			55	-38	9	93	0.95	9.74	9.21	
1000			59	-43	8	102	0.91	13.95	12.63	
GII-PC										
50	-60	3.66	47	-34	7	81	0.79	3.41	2.68	0.21

100	-27	4.02	48	-43	3	91	0.79	4.63	3.66	0.20
200	-9	5.00	55	-45	5	100	0.79	6.34	5.00	0.16
300	-2	6.59	56	-50	3	106	0.78	7.80	6.10	0.12
400	14	7.32	59	-50	5	109	0.77	9.51	7.32	0.11
500	22	10.98	61	-54	4	115	0.76	11.71	8.90	0.07
1000	42	10.98	71	-51	10	122	0.76	14.15	10.73	0.07
GII-2MP										
50	-219	4.76	41	-38	2	79	0.90	3.17	2.86	0.19
100	-218	8.89	39	-46	-4	85	0.75	5.08	3.81	0.08
200	-225	13.02	45	-42	2	87	0.70	7.30	5.08	0.05
300	-218	17.46	50	-42	4	92	0.64	9.37	6.03	0.04
400	-211	20.32	53	-34	10	87	0.60	11.11	6.67	0.03
500	-129	23.81	59	-67	-4	126	0.60	13.33	7.94	0.03
1000	-182	32.06	69	-49	10	118	0.57	17.78	10.16	0.02
GII-PP										
50	-176	3.33	55	-28	14	83	0.95	2.22	2.11	0.29
100	-175	5.56	47	-31	8	78	0.83	4.00	3.33	0.15
200	-173	6.22	52	-36	8	88	0.81	5.33	4.33	0.13
300	-169	8.67	57	-37	10	94	0.59	7.56	4.44	0.07
400	-164	9.78	58	-40	9	98	0.58	8.89	5.11	0.06
500	-178	8.89	64	-49	8	113	0.66	7.78	5.11	0.07
1000	-147	14.67	71	-45	13	116	0.57	12.89	7.33	0.04
GII-TBP										
50	-137	2.27	63	-13	25	76	0.92	2.73	2.50	0.40
100	-136	2.73	66	-15	26	81	0.85	4.55	3.86	0.31
200	-135	4.09	68	-23	23	91	0.81	6.14	5.00	0.20
300	-133	5.00	64	-30	17	94	0.76	7.73	5.91	0.15
400	-130	5.91	62	-38	12	100	0.76	8.64	6.59	0.13
500	-84	10.23	66	-38	14	104	0.72	10.68	7.73	0.07
1000	-121	9.09	80	-49	16	129	0.75	13.64	10.23	0.08
GII-3MP										
50	-81	2.63	71	-3	34	74	0.95	2.89	2.76	0.36
100	-107	7.89	54	-5	25	59	0.65	6.05	3.95	0.08
200	-109	11.84	56	-13	22	69	0.57	9.21	5.26	0.05
300	-111	15.26	58	-19	20	77	0.57	11.58	6.58	0.04
400	-113	16.84	58	-19	20	77	0.52	13.16	6.84	0.03
500	-25	23.68	58	-24	17	82	0.45	17.63	7.89	0.02
1000	-96	26.32	60	-24	18	84	0.44	23.16	10.26	0.02
GII-MOP										

50	-302	7.89	57	-23	17	80	1.00	2.89	2.89	0.13
100	-297	8.95	50	-26	12	76	1.00	4.21	4.21	0.11
200	-291	10.00	56	-28	14	84	1.00	6.05	6.05	0.10
300	-282	11.32	57	-28	15	85	1.00	7.37	7.37	0.09
400	-273	10.26	63	-28	18	91	1.10	7.63	8.42	0.11
500	-239	39.21	65	-28	19	93	0.80	12.89	10.26	0.02
1000	-232	41.58	76	-28	24	104	0.80	17.11	13.68	0.02
GII-P										
50	-23	3.16	64	-4	30	68	0.67	3.95	2.63	0.21
100	-40	6.58	57	-3	27	60	0.58	6.84	3.95	0.09
200	-59	11.05	58	-9	25	67	0.49	10.79	5.26	0.04
300	-63	15.26	61	-11	25	72	0.43	15.26	6.58	0.03
400	-62	17.63	66	-11	28	77	0.43	17.63	7.63	0.02
500	33	24.21	70	-6	32	76	0.36	21.05	7.63	0.01
1000	-28	28.68	71	-9	31	80	0.38	27.11	10.26	0.01
GII-BP										
50			21	-69	-24	90	0.27	7.33	2.00	
100			31	-70	-20	101	0.34	10.67	3.67	
200			52	-72	-10	124	0.34	15.17	5.17	
300			60	-81	-11	141	0.35	17.33	6.00	
400			70	-88	-9	158	0.36	20.33	7.33	
500			74	-88	-7	162	0.37	22.33	8.33	
1000			91	-88	2	179	0.39	28.33	11.00	
GII-TFP										
50	316	5.00	48	-51	-2	99	0.50	3.64	1.82	0.10
100	334	7.27	53	-49	2	102	0.58	5.45	3.18	0.08
200	372	8.18	70	-40	15	110	0.30	13.64	4.09	0.04
300	398	10.00	79	-39	20	118	0.27	18.64	5.00	0.03
400	409	10.45	80	-39	21	119	0.22	20.91	4.55	0.02
500	457	13.18	88	-39	25	127	0.18	33.64	5.91	0.01
1000	464	14.55	76	-50	13	126	0.19	34.09	6.36	0.01
GII-NP										
50	-113	0.88	84	-1	42	85	0.94	2.65	2.50	1.07
100	-109	1.62	84	-1	42	85	1.00	3.24	3.24	0.62
200	-99	2.35	84	-6	39	90	1.00	4.12	4.12	0.43
300	-91	3.38	84	-8	38	92	1.00	4.71	4.71	0.30
400	-81	4.26	86	-13	37	99	0.84	5.59	4.71	0.20
500	-67	5.88	86	-14	36	100	0.71	7.06	5.00	0.12
1000	-56	8.24	90	-14	38	104	0.71	8.24	5.88	0.09

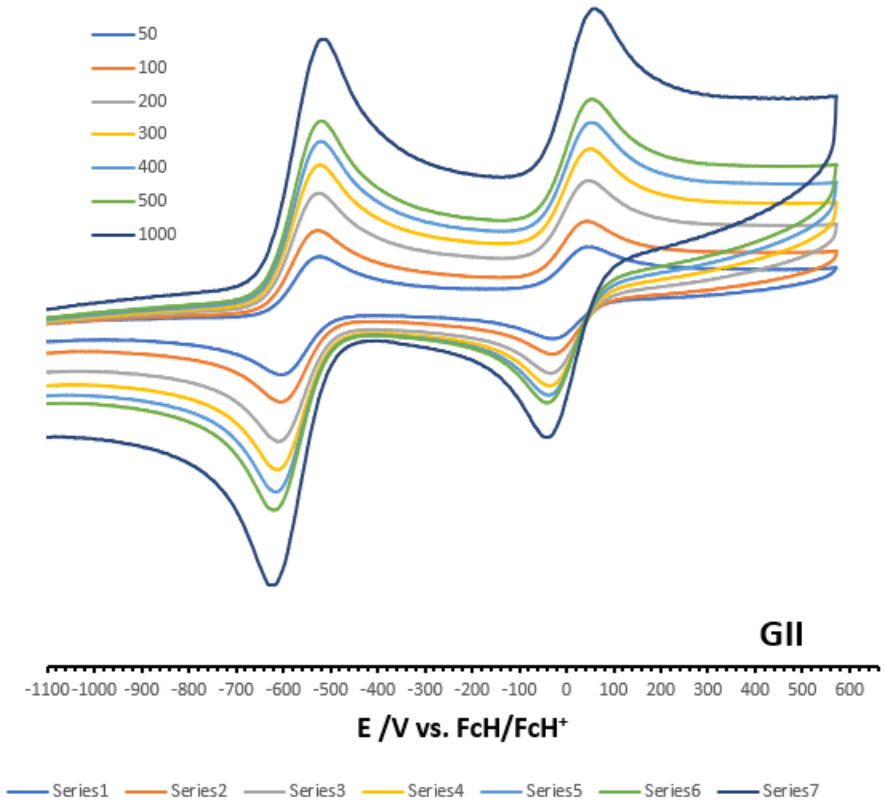
50
100
200
300
400
500
1000
GII
-1100 -1000 -900 -800 -700 -600 -500 -400 -300 -200 -100 0 100 200 300 400 500 600
E /V vs. FcH/FcH+
Series1 Series2 Series3 Series4 Series5 Series6 Series7

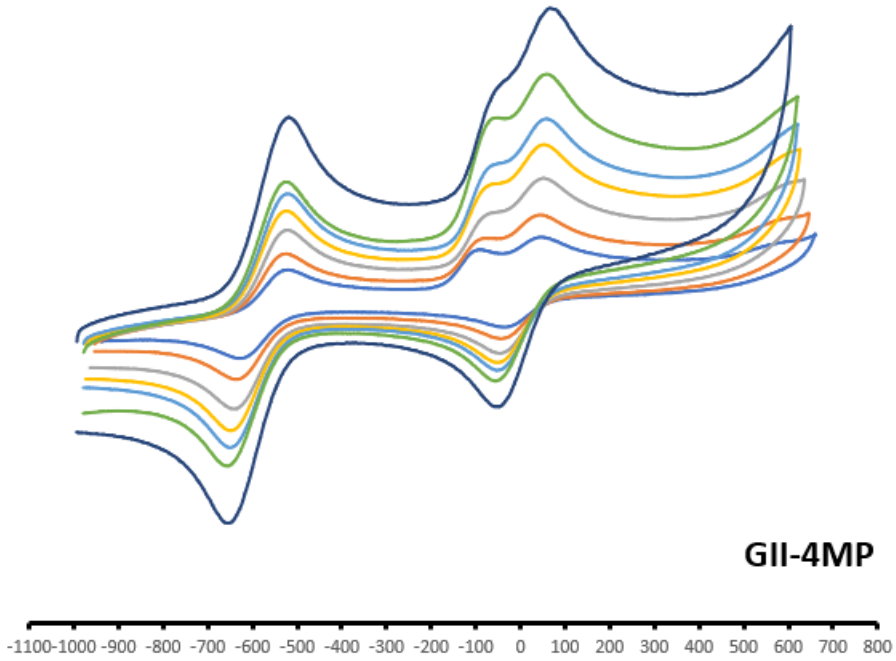
GII-4MP
-1100 -1000 -900 -800 -700 -600 -500 -400 -300 -200 -100 0 100 200 300 400 500 600 700 800

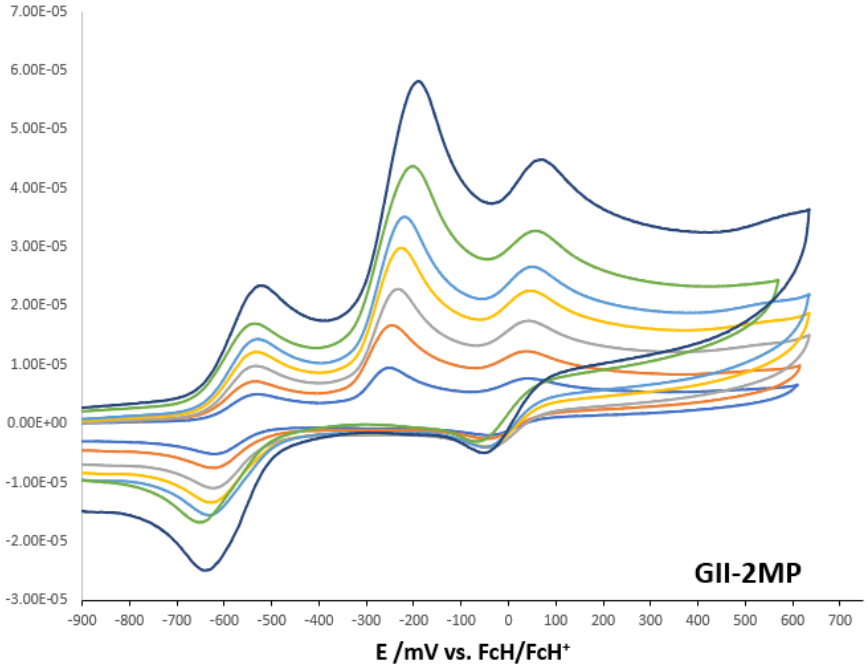
7.00E-05
6.00E-05
5.00E-05
4.00E-05
3.00E-05
2.00E-05
1.00E-05
0.00E+00
-1.00E-05
-2.00E-05
-3.00E-05
-900 -800 -700 -600 -500 -400 -300 -200 -100 0 100 200 300 400 500 600 700
GII-2MP
E /mV vs. FcH/FcH+

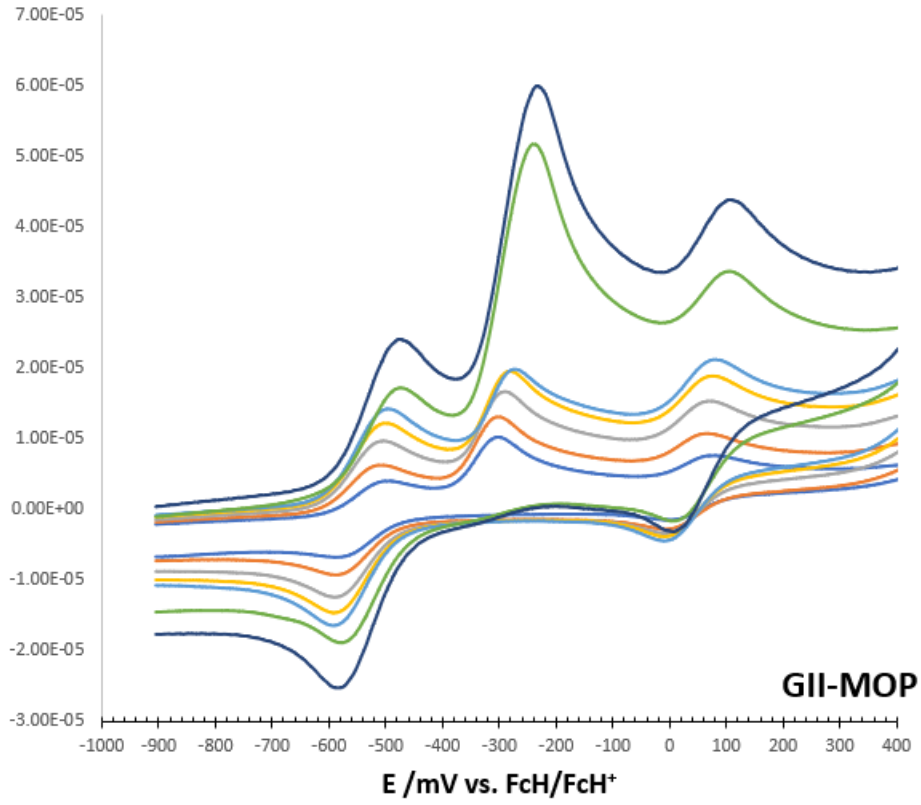
7.00E-05
6.00E-05
5.00E-05
4.00E-05
3.00E-05
2.00E-05
1.00E-05
0.00E+00
-1.00E-05
-2.00E-05
-3.00E-05
-1000 -900 -800 -700 -600 -500 -400 -300 -200 -100 0 100 200 300 400
GII-MOP
E /mV vs. FcH/FcH+

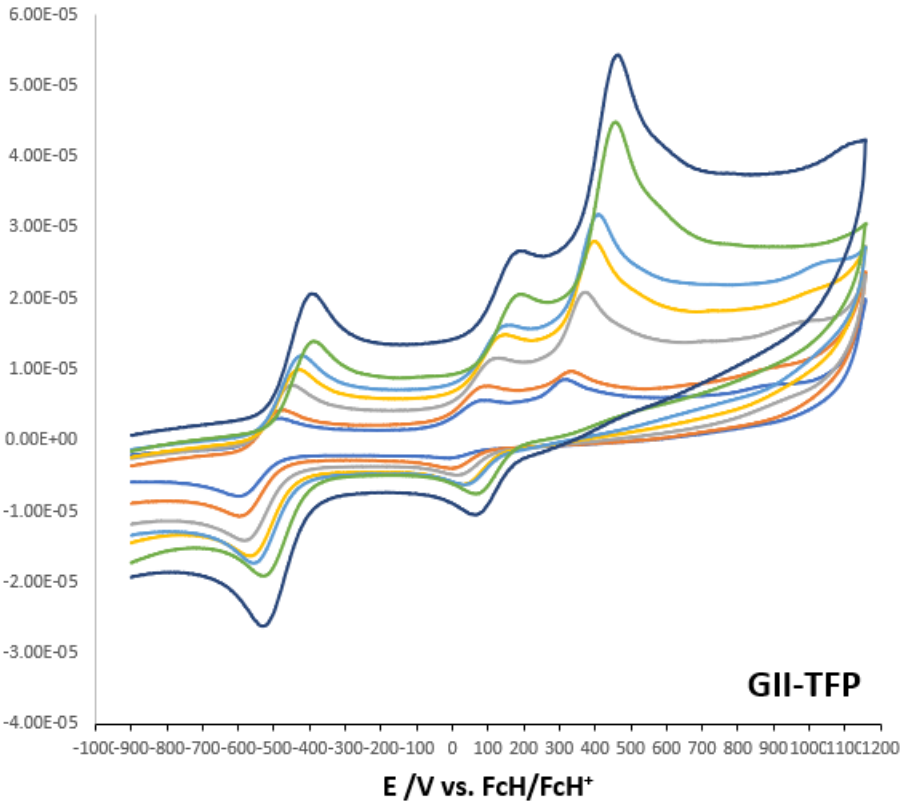
6.00E-05
5.00E-05
4.00E-05
3.00E-05
2.00E-05
1.00E-05
0.00E+00
-1.00E-05
-2.00E-05
-3.00E-05
-4.00E-05
-100(-900-800-700-600-500-400-300-200-100 0 100 200 300 400 500 600 700 800 900 100(110(1200
GII-TFP
E /V vs. FcH/FcH+

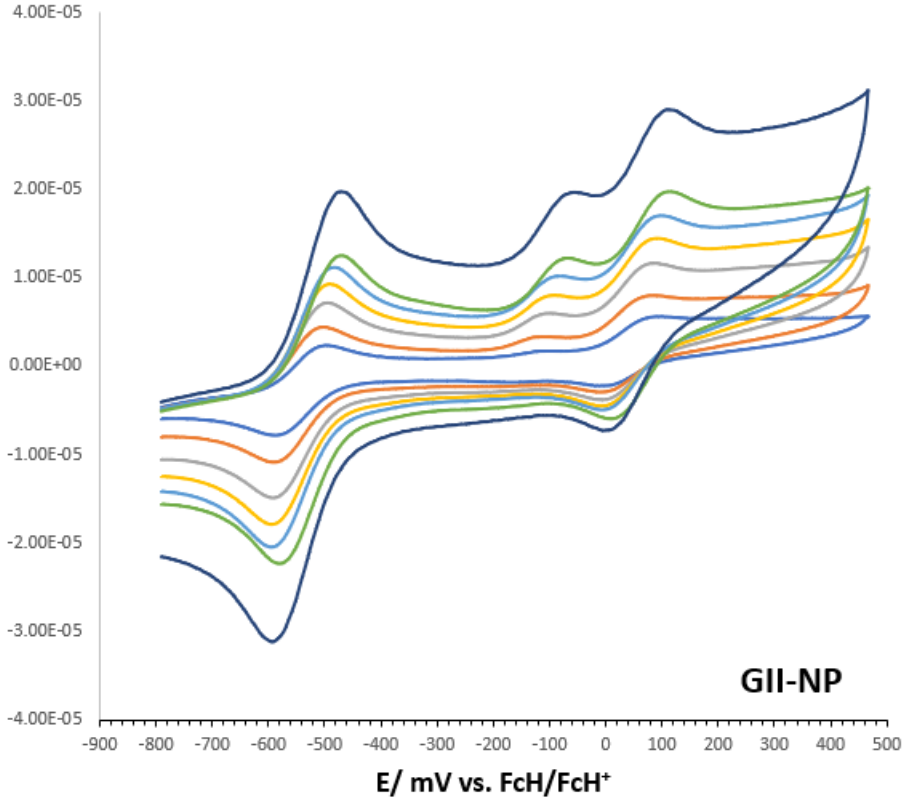
4.00E-05
3.00E-05
2.00E-05
1.00E-05
0.00E+00
-1.00E-05
-2.00E-05
-3.00E-05
-4.00E-05
-900 -800 -700 -600 -500 -400 -300 -200 -100 0 100 200 300 400 500
GII-NP
E/ mV vs. FcH/FcH+

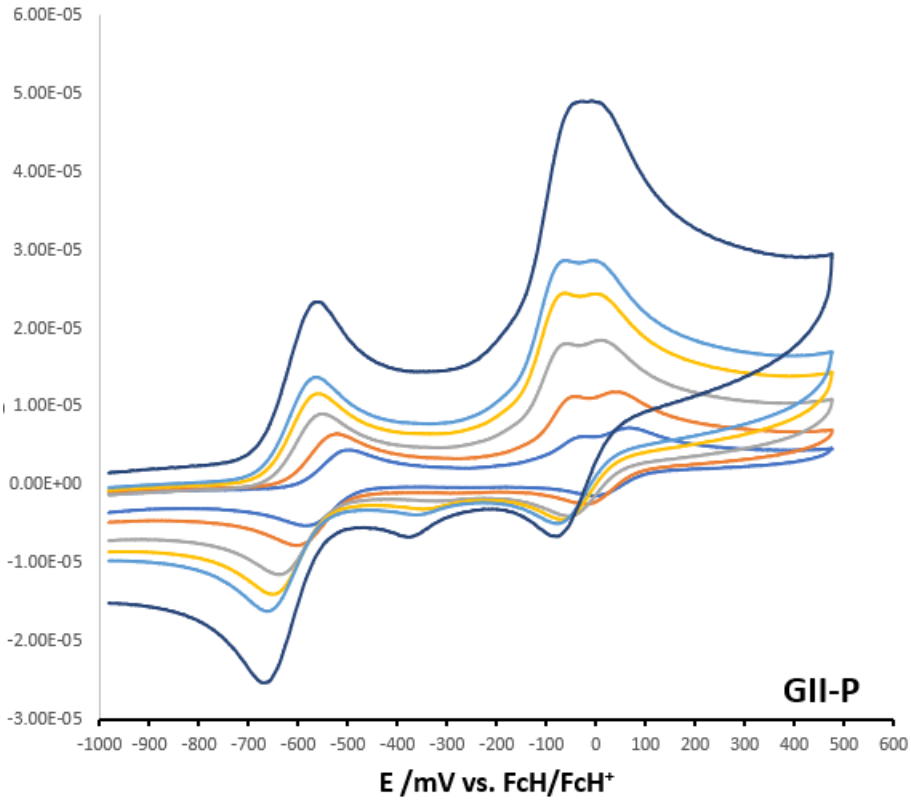
6.00E-05
5.00E-05
4.00E-05
3.00E-05
2.00E-05
1.00E-05
0.00E+00
-1.00E-05
-2.00E-05
-3.00E-05
-1000 -900 -800 -700 -600 -500 -400 -300 -200 -100 0 100 200 300 400 500 600
GII-P
E /mV vs. FcH/FcH+

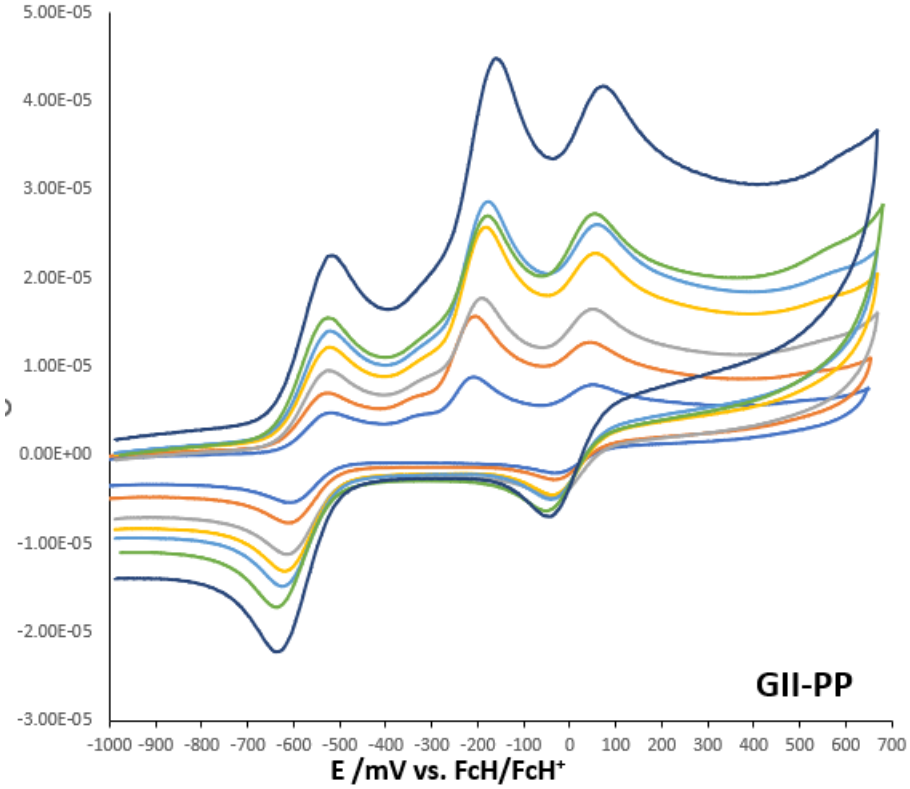
5.00E-05
4.00E-05
3.00E-05
2.00E-05
1.00E-05
0.00E+00
-1.00E-05
-2.00E-05
-3.00E-05
-1000 -900 -800 -700 -600 -500 -400 -300 -200 -100 0 100 200 300 400 500 600 700
E /mV vs. FcH/FcH+
GII-PP

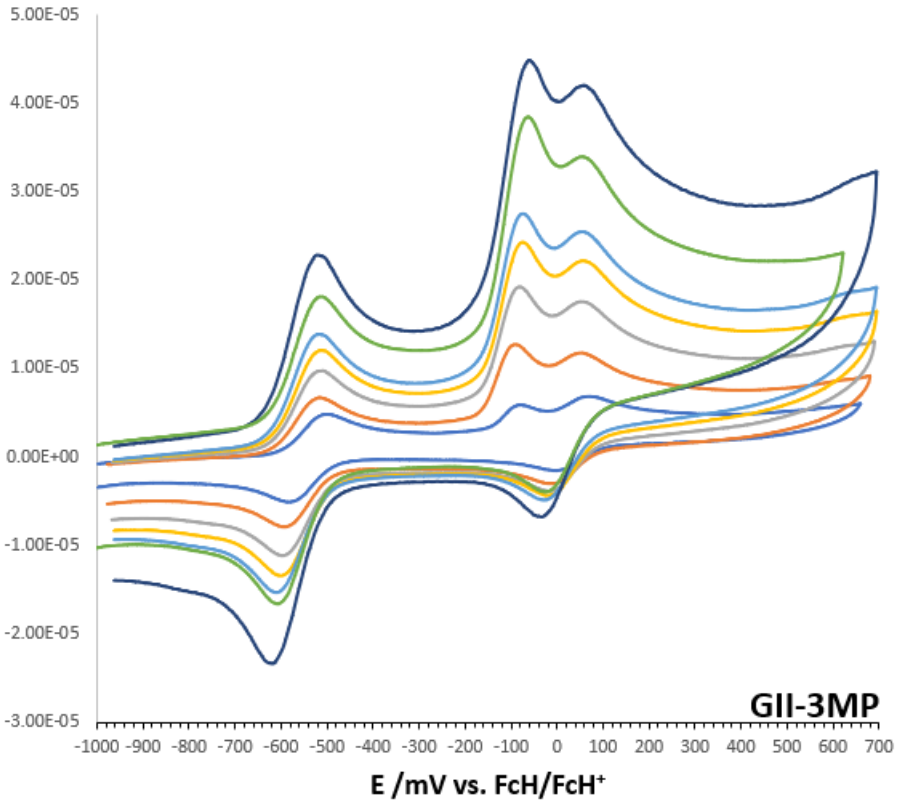
5.00E-05
4.00E-05
3.00E-05
2.00E-05
1.00E-05
0.00E+00
-1.00E-05
-2.00E-05
-3.00E-05
-1000 -900 -800 -700 -600 -500 -400 -300 -200 -100 0 100 200 300 400 500 600 700
E /mV vs. FcH/FcH+
GII-3MP

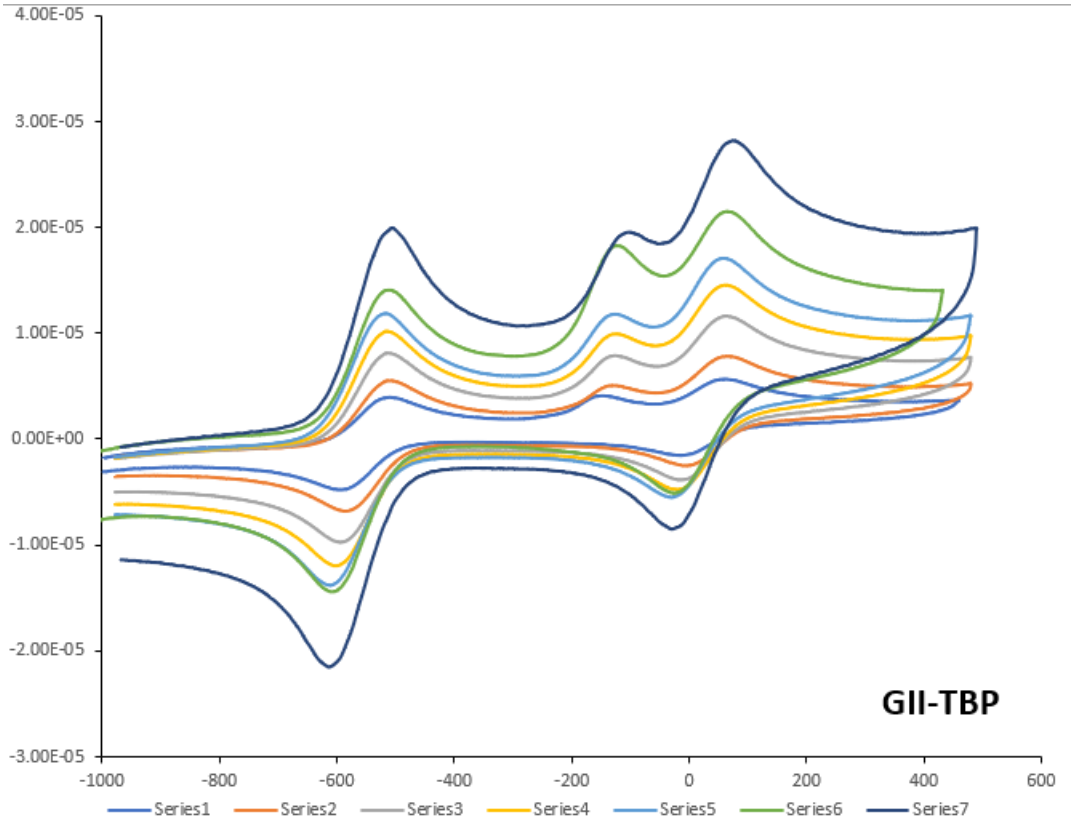
4.00E-05
3.00E-05
2.00E-05
1.00E-05
0.00E+00
-1.00E-05
-2.00E-05
-3.00E-05
-1000
-800
-600
-400
-200
0
200
400
600
Series1
Series2
Series3
Series4
Series5
Series6
Series7
GII-TBP

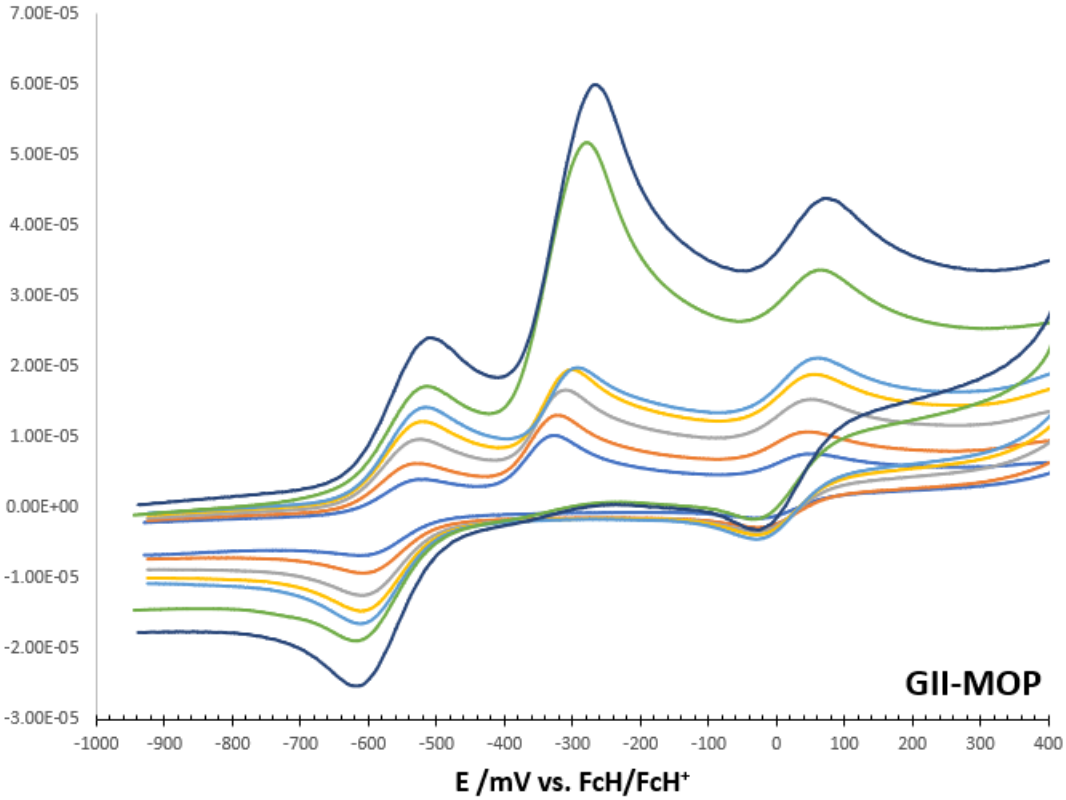
7.00E-05
6.00E-05
5.00E-05
4.00E-05
3.00E-05
2.00E-05
1.00E-05
0.00E+00
-1.00E-05
-2.00E-05
-3.00E-05
-1000
-900
-800
-700
-600
-500
-400
-300
-200
-100
0
100
200
300
400
GII-MOP
E /mV vs. FcH/FcH+

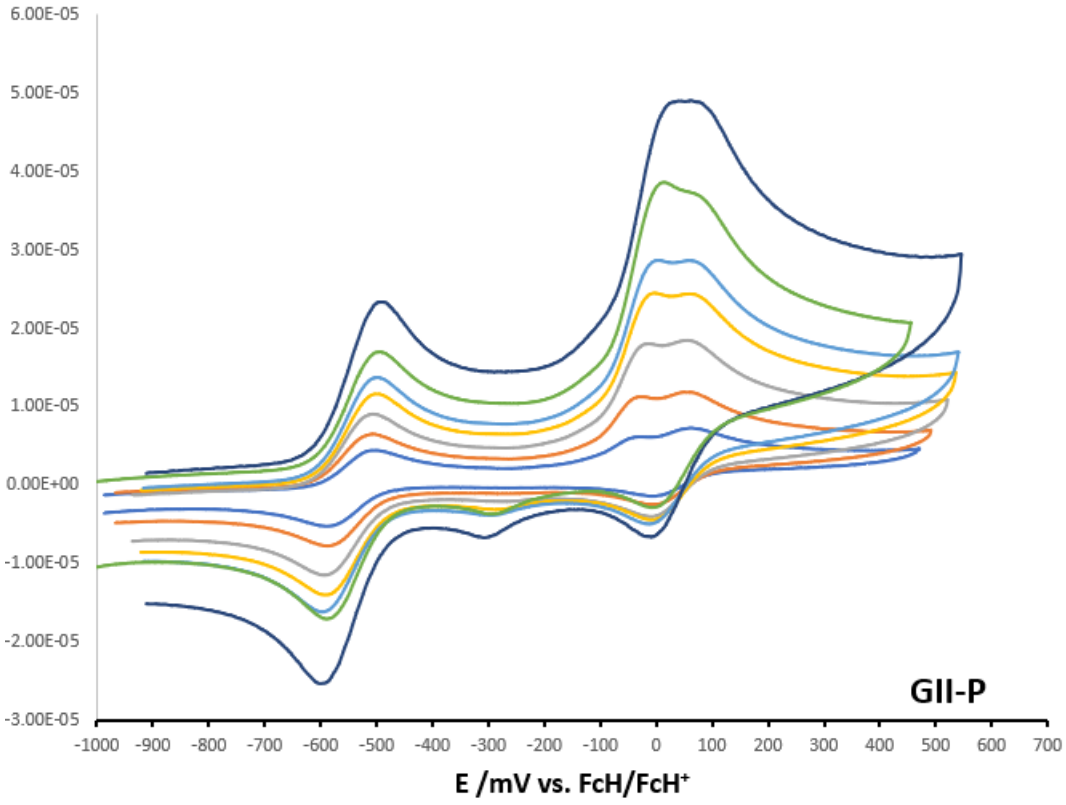
6.00E-05
5.00E-05
4.00E-05
3.00E-05
2.00E-05
1.00E-05
0.00E+00
-1.00E-05
-2.00E-05
-3.00E-05
-1000 -900 -800 -700 -600 -500 -400 -300 -200 -100 0 100 200 300 400 500 600 700
GII-P
E /mV vs. FcH/FcH+

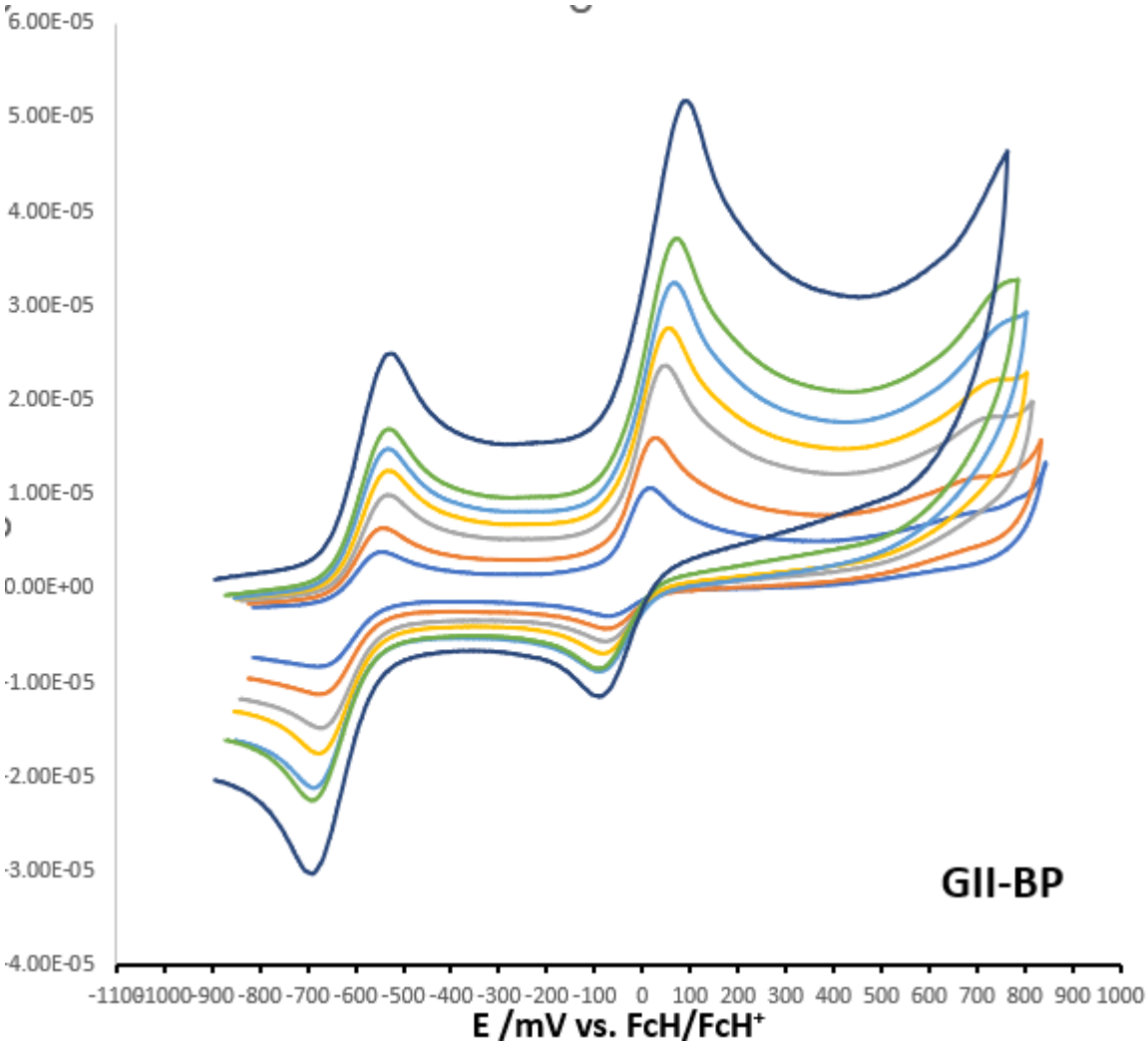
6.00E-05
5.00E-05
4.00E-05
3.00E-05
2.00E-05
1.00E-05
0.00E+00
-1.00E-05
-2.00E-05
-3.00E-05
-4.00E-05
-1100-1000-900 -800 -700 -600 -500 -400 -300 -200 -100 0 100 200 300 400 500 600 700 800 900 1000
E /mV vs. FcH/FcH+
GII-BP

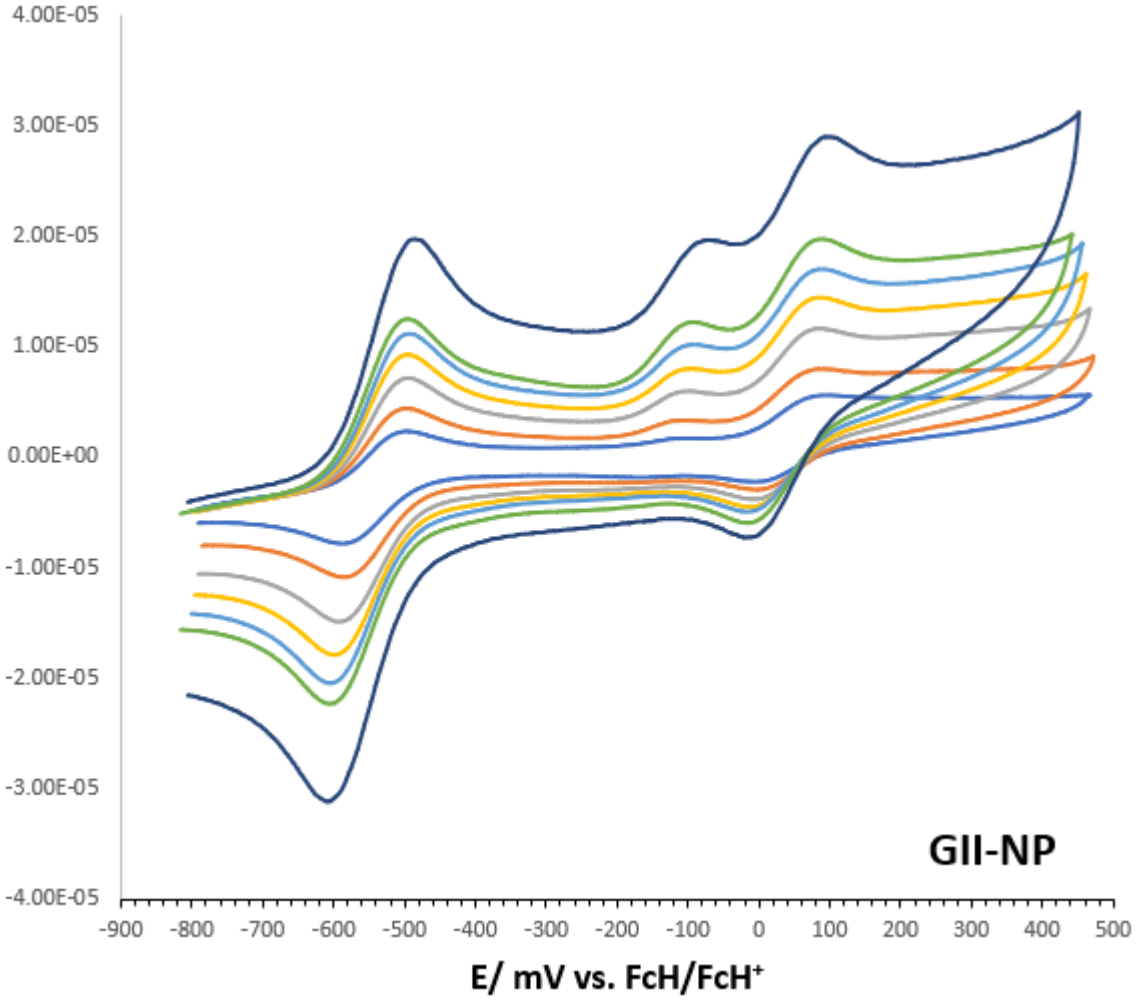

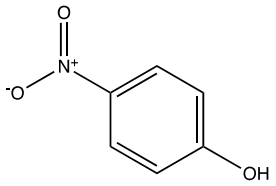

4-nitrophenol (NP)

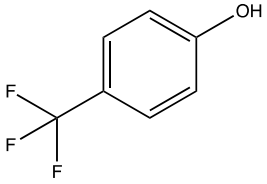

4-(trifluoromethyl)phenol (TFP)

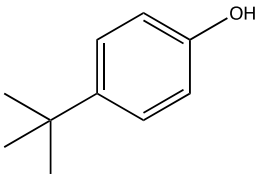

4-tertbutylphenol (TBP)

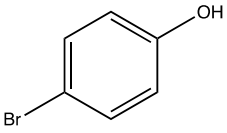

4-bromophenol (BP)

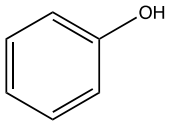

phenol (P)

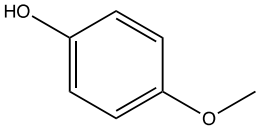

4-methoxyphenol (MOP)

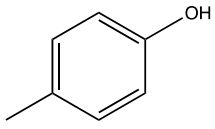

4-methylphenol (4MP)

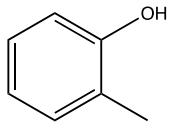

2-methylphenol (2MP)

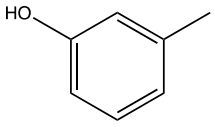

3-methylphenol (3MP)

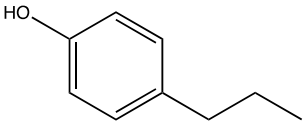

4-propylphenol (PP)